FIELD INVESTIGATIONS ON PERFORMANCE OF SHORT DRILLED SHAFT FOUNDATIONS UNDER INCLINED LOADING

by

RICHARD S. WILLIAMMEE, JR.

Presented to the Faculty of the Graduate School of

The University of Texas at Arlington

in Partial Fulfillment of the Requirements

for the Degree of

MASTER OF SCIENCE IN CIVIL ENGINEERING

THE UNIVERSITY OF TEXAS AT ARLINGTON

MAY 2010

ACKNOWLEDGEMENTS

This thesis is foremost dedicated to my Lord and Savior, Jesus Christ, through whom “all things are possible” (Matthew 19:26) and for His power, strength, and guidance (Philippians 4:13) to help me achieve this distinguished degree.

This thesis is next dedicated to my wife, Cheryl, and our daughters, Heidi and Kelly, who supported and encouraged me to attend classes and persevere with the coursework when I was not motivated. This is also dedicated to my father, Richard Sr., who instilled a the work ethic in me to work hard in all that I do.

This thesis is also dedicated to my Graduate Advisor, Dr. Anand Puppala, who convinced me to complete this degree after a 20 year sabbatical. He was also very encouraging when I felt that I was not keeping up with the other students and never wavered in his confidence in my abilities.

This thesis is dedicated to my fellow Civil Engineering Graduate students, especially my PhD Graduate Student, Thornchaya (Pomme) Wejrungsikul, who took me in as one of their own and worked side-by-side with me to help me pass my classes and perform the required work for this Thesis.

This thesis is finally dedicated to all of my co-workers and friends who supported me with technical assistance or with words of encouragement.

March 30, 2010

ABSTRACT

FIELD INVESTIGATIONS ON PERFORMANCE OF SHORT DRILLED SHAFT FOUNDATIONS UNDER INCLINED LOADING

Richard S. Williammee, Jr., M.S.

The University of Texas at Arlington, 2010

Supervising Professor: Anand Puppala

In the Kaufman County area within the Texas Department of Transportation's Dallas District, several short drilled shaft foundations supporting three-cable median barrier systems were observed to be distressed during severe winter storm conditions in late 2006 through early 2007. A research study was initiated at UT Arlington to determine and understand the mechanisms causing these shaft failures. The ends of the three-cable median barrier systems are fastened to a single drilled shaft foundation. In general, these shafts are short in depth and of the same dimensions, diameter, and depth. They are typically used in all soil conditions. This thesis presents the tasks of this study which includes the estimations of loads on the shafts and the design of reaction test piles for the application of inclined loads on test shafts of varying diameters and depths simulating the field construction of cable barrier systems. The application of inclined loading is a unique type of testing for which very little work has been published. Inclined load analyses results were utilized in the design of reaction shaft dimensions and spacings between reaction and test shafts. Salient details of analytical approaches used for load calculations are also included.

TABLE OF CONTENTS

LIST OF ILLUSTRATIONS

LIST OF TABLES

CHAPTER 1

INTRODUCTION

1.1 Introduction

Drilled shafts are structural members used to transfer loads to the foundation soil or resist lateral movements of structural objects. They are used to support many highway transportation structures such as bridges, retaining walls, buildings, overhead-sign structures, illumination towers, and roadway cable median barriers (CMB). Drilled shaft foundations were originally developed in order to support heavy buildings in many major U.S. cities (O'Neill and Reese, 1999). Drilled shafts were first used by the Texas Highway Department in 1950 to build a bridge in the San Angelo District (McClelland, 1996). Since then, drilled shafts have been extensively used as foundation and restraining systems throughout the highway system.

In Texas, two types of median barrier systems currently in use are concrete traffic and three-cable (3-cable) systems. This research focused on the failure of the drilled shaft foundations used to support the ends of the roadway cable barrier systems. Median barrier systems were developed by the cable manufacturing industry and have been used by the Texas Department of Transportation (TxDOT) to prevent cross-over collisions due to high traffic volumes, highway congestion, and driver error by capturing and maintaining errant vehicles in their direction of travel (Bligh et al., 2006; Albin et al., 2001). Many of the cable systems use a drilled shaft foundation for the end treatment to resist lateral movement due to 1) acting forces from vehicle impacts and 2) tension of the cables from stresses developed during the installation process and later from on-going thermal changes. The drilled shaft foundation provides an anchor point to which the three cables are attached. This allows the cables to be tightened to provide the manufacturers' tension requirements. In certain barrier systems, each

cable is connected to its' own individual drilled shaft. In the present case where the failures were discovered, all three cables were connected to a single shaft (see Figure A.1). It was theorized that the single drilled shaft foundation system did not function satisfactorily in an expansive soil environment due to several factors such as foundation upheaval caused by the loss of contact between the drilled shaft concrete and the adjacent soil. This could have been exacerbated from previous shrink/swell cycles during the previous 3 years prior to failure. In Kaufman County, east of Dallas, where two of these cable median barrier foundation failures were observed, the site surroundings had experienced low temperatures, including a few ice storms, from December 2006 to February 2007. When the expansive clayey soil was hydrated with water and subjected to cold temperature conditions, it was hypothesized that the short drilled shafts lifted in a vertical direction. This was due to uplift forces from the cold temperature conditions in the soils and also from an increase in the inclined loading created by an increase in the cable tension. The cable tension increase was a result of a decrease in ambient temperature conditions 15°-19°F (-9.4° to -7.2°C) as shown in Figure 1.1. All three cables used in the barrier systems contracted, which in combination, resulted in a significant tensile stress increase in the cables.

(a) (b)

Figure 1.1. Typical Foundation Failures on IH 20 Westbound (a) Sta. 903+00, Plan Sheet 61 and (b) Sta. 973+44, Plan Sheet 45 for CSJ: 0495-01-052

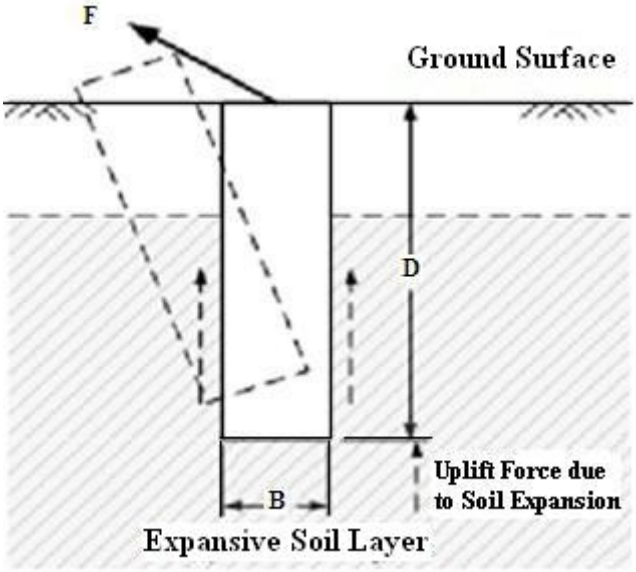

Figure 1.2. Failure Mechanism of 3-Cable Median Barriers
Built in Expansive Soil

The behavior of drilled shafts in nonexpansive and expansive soil is different. Figure 1.2 presents a hypothetical failure mechanism that may have occurred in the present site in an expansive soil environment; this corresponds well with the observed field distressed shaft foundations. The excessive vertical movement is the result from a combination of uplift force due to soil expansion and oblique pulling force from the cable.

Principally, lateral load influenced drilled shafts originated from earth pressures, current forces from flowing water, wind loads, and wave forces in some unusual instances (O'Neil and Reese, 1999). Examples of the structures where lateral forces have an effect on the drilled shafts are bridge abutments, offshore platforms, and transmission towers (Reese and Allen, 1977). Additionally, cable median barriers are required to be supported on drilled shaft foundations.

In this study, the drilled shafts supporting three-cable median barriers were considered for inclined load design. The lateral loads taken into account were derived from the sustained pretension lateral load due to anchorage of the cables, thermal stresses in the cable due to temperature fluctuations (expansion and contraction), and other loads coming from vehicular

impacts. Uplift loads from soil provide vertical loading forces acting on the shaft. Both lateral and uplift forces together constitute inclined loads that contributed to the failure of the shafts in the real field condition.

Drilled shafts were determined to be more advantageous than pile foundations and were selected for this research project as described below:

1. Drilled shafts provide significantly less ground vibrations and potential damage to nearby structures.
2. A bell shaped tip at the bottom of the drilled shaft can resist uplift pressures.
3. Drilled shafts have high resistance to both axial and lateral loads.
4. Drilled shafts are economical when avoiding the use of heavy pile caps.

Typical drilled shaft design by a specific manufacturer recommends the use of short drilled shafts of 8 ft (2.44 m) depth for all soil types (see Figure A.1). However, in this case, drilled shafts for the barrier systems are located in a highly expansive soil area of north Texas. Expansive soils in this region exhibit considerable swell and shrink volume changes due to moisture fluctuations and these soils pose several problems to civil engineering infrastructure including roads and foundations (Nelson and Miller, 1992). Considering the depths of the shafts being shorter than the active depths of moisture fluctuations, failures may occur in this soil environment. One such occurrence was noted in 2007 and details of these drilled shaft distresses are presented.

1.2 Research Objectives

The failure of the three-cable barrier systems constructed in the expansive soil area as shown in Figure 1.1 was affecting the safety measure of the barrier systems because they are used to mitigate cross-over collisions elevated by high traffic volumes and congestion. It is imperative to understand the cause of failures of laterally loaded drilled shafts, which leads to practical foundation systems on high PI clays without experiencing failures. In order to understand the cause(s) of the failures, the research covers the following objectives:

1. To identify the most significant soil parameters directly related to the volume changes and subsequent movements of the expansive and high-plasticity soils.
2. To investigate the failure mechanisms of inclined loaded drilled shafts in high-plasticity clay environments.
3. To quantify the impact of environmental-related and site-related parameters detrimental to the systems, especially the foundations.
4. To design and construct test drilled shafts with various diameters and depths and subject them to loading similar to the one that might have contributed to the failure under a similar field environment.
5. To determine the validity of the research approach based upon a comparison of the summer and winter condition field data.

1.3 Organization of the Thesis

This thesis consists of seven chapters.

Chapter 1 provides an introduction with background history explaining the significance of the project, research objectives, and organization to provide a framework of the completed research.

Chapter 2 presents a literature review on expansive soil behaviors, properties, and their swell/shrinkage prediction models. Several available load test methods are discussed.

Chapter 3 covers the site selection and laboratory testing used to determine the soil properties required for the design, construction, and testing of the drilled shaft system. The testing includes basic soil properties tests, physical, and laboratory engineering tests. A summary of the laboratory procedures and equipment used are presented in this chapter.

Chapter 4 discusses the analysis of the laboratory results. It also includes the predictions of the degree of the shrinking and swelling of the soils. Statistical analysis is also introduced as a simple technique to identify and predict the volume changes.

Chapter 5 presents the design and construction of the drilled shaft test setups.

Chapter 6 presents the results of the summer and winter condition field data acquisition. This data includes the loading increments, strain gauge readings, inclinometer and MEMS-SAA values, and elevation and dial gauge numbers at each test shaft. Additional data is presented for the inclinometer readings taken between the reaction and test shafts.

Chapter 7 presents a summary of the laboratory test results, designed shaft dimensions, and the field test results. It also presents the important conclusions of the design and analyzed drill shaft results, the interaction analysis between the soil-concrete and the drill shaft foundation-cable, and future recommendations.

CHAPTER 2

LITERATURE REVIEW

2.1 Introduction

In this chapter, a comprehensive review of the available literature on cable median barriers, drilled shafts and soil interaction, and temperature effects on the soils and cable are covered.

2.2 Cable Median Barrier System

2.2.1. Cable Median Barrier System

The Cable Median Barrier (CMB) System is an engineered product used by transportation officials to prevent opposing traffic from cross-over collisions that result in property damage, vehicle occupant physical injury, or even death. These systems came into the market in the 1960s but did not really gain attention until the 1980s. The Texas Department of Transportation (TxDOT) developed their specification (Cable Barrier System) for these systems in 2004, updated them in 2006 (TxDOT, 2006), and added many miles across the state in the past six (6) years. These have saved many lives, are actually more aesthetically pleasing than the concrete traffic barrier, and less costly to purchase, install, and maintain. In Texas, cable type barriers are used when medians are wider than 25 feet (7.6 m). Otherwise, rigid concrete barriers are used. The barrier system itself consists of stranded wire cable, vertical supports (posts), and end foundations for anchoring the cables. In general there are six major types of barriers that have been used in the U.S. as shown in Figure 2.1 below.

- US Generic Low Tension
- Safence
- Brifen (Wire Rope Safety Fence-WRSF)
- Gibraltar (Cable Barrier System)
- Nucor Marion (U. S. High Tension)
- Trinity (Cable Safety System-CASS)

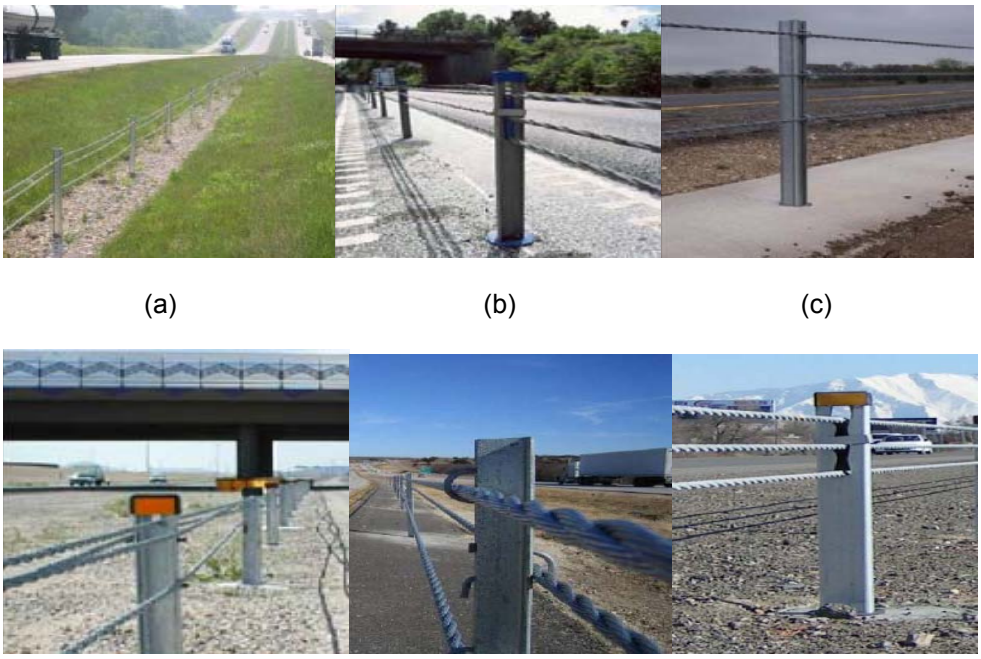

(a) (b) (c)

(d) (e) (f)

Figure 2.1. Photographs of Various Barriers by (a) US Generic Low Tension, (b) Safence, (c) Gibraltar Cable Barrier, (d) Brifen Safety Fence, (e) Nucor Marion, and (f) Trinity Cable Safety Systems used in Texas and in the USA (Alberson, 2006)

With the exception of the US Generic Low Tension System, the others are classified in the high tension cable group. In Texas, most of these systems have been used. Each system has its' own unique post design, cable placement, and end treatment (Alberson, 2006).

2.2.1.1 Cable

The cable part of the barrier system consists of 3/4 in. (19 mm) stranded galvanized wire or rope. These are supplied in 3- or 4-strand systems called TL-3 or TL-4 as set by National Cooperative Highway Research Program (NCHRP) Report 350, Recommended Procedures for the Safety Performance Evaluation of Highway Features (Ross et al., 1993). The cables are tightened with intermediate tensioners to strengths from 2000 psi – 9000 psi (13,790 kPa – 62,050 kPa) dependent upon the ambient temperature at the time of installation. These are anchored to foundations at the end of each run.

2.2.1.2 Posts

Posts are used to support the tensioned cables. These posts are made of galvanized steel and notched at a set distance from the bottom to readily shear when impacted. Most manufacturers have designed sockets that are set in concrete which then hold the posts vertically in position. The concrete used to hold the sockets is low strength to provide enough support from natural forces such as wind and soil movement but not too strong to jeopardize the shearing ability. TxDOT usually requires a concrete pad about 3 ft (1 m) wide and 5 in. (127 mm) to support the sockets and provide a mowing strip for vegetative management (Cooner, 2008).

2.2.1.3 End Foundations

Concrete drilled shafts are the primary engineered structure used as the anchor for the cable system due to their high resistance against the lateral loads coming from the tension mobilized in these cables. All 3 or 4 cables (TL-3 and TL-4 system types) are attached to one (1) or up to four (4) individual drilled shaft foundations. These foundations have been designed by the individual cable system manufacturers and are shown in their engineering drawings (Figure 2.2). The foundations function satisfactorily in nonexpansive subgrades; however, foundation failures have occurred in expansive soils by loss of contact with the soil and foundation uplifting. It has not been determined from the manufacturers' literature if these

foundations have been designed to all, a limited range, or a few certain soil types. But based on several failures around the state, this aspect has to be determined, analyzed, and corrected to eliminate TxDOT's liability against slack cables and failure to contain cross-over collisions.

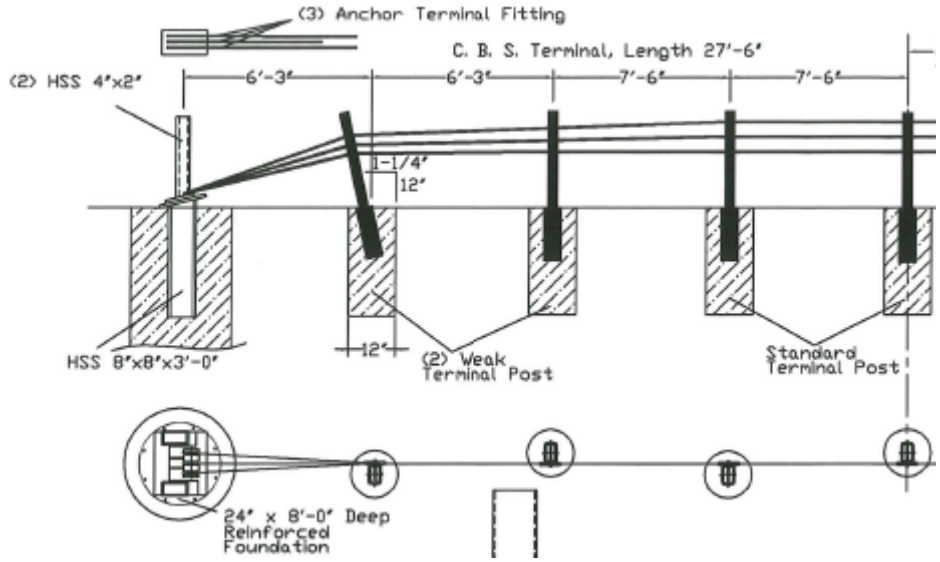

Figure 2.2. Connection Details of Cables to Drilled Shaft for TL-3 of Gibraltar Barrier

2.2.2 System Safety

2.2.2.1 National Level Standard

National Cooperative Highway Research Program Report (NCHRP) 350 (Ross et al., 1993) was developed to standardize the manner in which different safety systems are tested and measured for effectiveness. The Texas Transportation Institute (TTI) located in College Station, Texas performs these very valuable tests for DOTs before they can be used on any National Highway System (NHS) (Cooner ,2008). The cables and posts, as well as the complete system, are tested against 3 factors (Ross et al., 1993):

- Structural Adequacy: the system must contain and redirect the vehicle with no underriding, overriding, or penetration.

- Occupant Risk: fragments of the system cannot penetrate the vehicle compartment, the vehicle must remain upright during and after the collision, and the occupant(s) must not undergo excessive impact or deceleration.

- Vehicle Trajectory: after the impact, the vehicle should not intrude into adjacent traffic lanes nor should it exit the system at an angle greater than 60% of the entry angle.

2.2.2.1.1 Test levels

From NCHRP Report 350, six (6) test levels (TL) representing different vehicles, impact angles, and speeds were developed. Test levels three (TL-3) and four (TL-4) are the two levels used by the cable barrier system manufacturers for highway traffic. The TL-4 systems have successfully contained semi-trailer trucks.

2.2.2.1.2 Geographic Limits

Cable barrier systems are designed to be used on 6:1 (16.1°) or flatter slopes. The 6:1 requirement is determined from computer modeling and full-scale crash testing. In field applications, placement on steeper slopes is common (Cooner, 2008).

Since these systems are flexible, they can deflect as much as 8 ft (2.4 m) to 12 ft (3.7 m) upon impact. In Texas, cable barrier systems approved for use must pass NCHRP Report 350 of the test level specified (TL-3, TL-4, etc.) with a maximum deflection of 8 ft (2.4 m) (TxDOT, 2008). The highway design engineer must take this into account when determining the adequacy of placing this system between opposing directions of traffic.

2.2.2.1.3 Defective Installation, Repair, and Impacts

Incorrect installation of these systems from manufacturer plans can seriously mitigate the systems' effectiveness when impacted. Improper maintenance, replacement with incorrect parts, or no replacement of broken or damaged parts can mitigate their effectiveness. Installation below design grade can allow a car to jump the top of a barrier and be exposed to a

cross-over collision (KPHO, CBS 5, 2008). One wrongful death suit resulted in a one million dollar settlement with the state of Arizona (WSDOT, 2007; Wikipedia, 2009).

2.2.2.1.4 Impact to Other Vehicle Types

The installation of these median barrier systems has concerned motorcyclists. Researchers in the United Kingdom found little difference between crashes into cable median barriers and other barrier types. They found that most riders are separated from their motorcycles soon after leaving the pavement and are sliding on the ground by the time they reached the barrier. The data also did not show that cable barriers cause extraordinary injuries.

2.2.3 System Uses

2.2.3.1 National Level Usage

States such as Arizona, Colorado, North Carolina, Ohio, Oklahoma, Oregon, South Carolina, Utah, Texas, and Washington State are installing many miles of cable barrier systems in medians (WSDOT, 2007). Texas has installed 33,958 linear feet / 6.43 linear miles (10,350 linear meters / 10.35 linear kilometers) during 2009 alone with approximately 500 total miles (805 km) placed from 2004-2009 (Simms, 2010).

2.2.3.2 State Level Collision Results

New data demonstrates that cable median barriers are effective for preventing fatal and disabling collisions.

- In Washington State, annual cross-over fatalities have dropped almost ten-fold from 3.00 to 0.33 fatalities per 100-million miles (160,934,400 km) of vehicle travel with annual disabling accidents significantly declining from 3.60 to 1.76.
- In Iowa from 1990 to 1999, 2.4 percent of all interstate collisions were cross-over related yet they resulted in 32.7 percent of all of their interstate fatalities. This demonstrates the severity of these events.
- In South Carolina in one year from 1999 to 2000, more than 70 people died in 57 separate interstate cross-over collisions. From August 2000 through July 2003, the

cable median system was hit 3,000 times with only 15 vehicles penetrating the cables.

- In North Carolina, the DOT found cross-over collisions to be three times more deadly than other freeway types of collisions.
- The North Carolina and Oregon DOTs completed detailed in-service evaluation reports of cable barrier systems and found that the systems were nearly 100 percent effective in preventing deadly crossover collisions on freeways.
- Texas has invested approximately 157 million dollars on this cable barrier system technology.

2.2.3.3 Benefits

- CMB Systems cost approximately $70,000 per mile compared to $300,000 per mile of concrete traffic barriers (CTBs).
- The overall cost savings in lives and property were calculated to be $420,000 per mile annually in Washington State.
- Financial resources can be saved if crews at State DOTs develop the skills to rapidly repair cable median barriers. TxDOT's Fort Worth District has restricted the installation of the available systems to 3 manufacturers due to inventory costs for rapid repair of damaged systems. This could be opened if the manufacturers are willing to assist with more local storage to allow quick access to parts for rapid restoration of the individual systems (Easterling, 2010).

2.3 Focus on Load Testing on Drilled Shafts

2.3.1 Foundation Failures

Failure of the anchor foundations at the ends of each run causes the cables to go slack. This totally eliminates the effectiveness of the system. This is not acceptable as it places direct liability on the transportation agency should a cross-over incident occur. Therefore, it is imperative that these foundations be designed and installed to withstand any type of failure. The

foundation must have the proper steel reinforcement grade, quantity, and spacing. The concrete must be strong enough to resist stresses developed from impacts and attacks from the soil such as sulfates. The anchors must be properly set to be restrained within the concrete foundation upon direct or indirect impact. And the foundation must be able to completely resist uplift forces, usually oblique or inclined, from the cable system or soil conditions such as wet or dry, sandy or clay, thawed or frozen, or other site specific conditions.

2.3.1.1 Texas System Failures

In 2004, TxDOT installed its' first cable barrier system (Cooner, 2008). Currently, over 500 total miles (805 km) have been added to their highways. Failures were not recorded until 2007 when they were first observed in north Texas. Recent inquiries have uncovered at least one failure in the Austin area and one in the Fort Worth area. The conditions for failure are unknown.

2.3.1.2 North Texas System Failures

TxDOT extensively used the TL-3 median barriers along Interstate Highway 20 (IH 20) and US Highways 80 and 175 (US 80 and US 175) in Dallas and Kaufman Counties in north Texas. Construction of these barriers occurred between July 2006 and February 2007. TxDOT later observed failures in the anchored drilled shaft foundations supporting these cable barriers. Figure 1.1 above shows some of the typical failures observed in the field. The pictures were taken from systems on IH 20 and show excessive lateral movements and uproot of the drilled shaft foundation. A review of the causes of these failures yielded the following observations (Heady, 2007):

- Kaufman County, where the drilled shaft foundation failures were recorded, had experienced low temperatures, including a few ice storms, during the months of December 2006, January 2007, and February 2007.

- Two other barrier systems, CASS and SAFE Roads LLC, were designed and constructed such that each of the three wire rope cables was connected to an individual drilled shaft of 18 in. (0.46 m) diameter by 5 ft (1.52 m) depth.
- Two additional barrier systems that were used, Brifen USA and Gibraltar Inc., were designed and connected to two different drilled shafts of 48 in. (1.2 m) diameter by 3 ft (0.9 m) depth and 24 in. (0.6 m) diameter by 6 ft (1.8 m) depth, respectively.

2.3.2 Drilled Shafts

Drilled shafts are the main foundation type installed throughout Texas. Sometimes driven piles may be used in coastal or soft soil conditions. This research focuses on the drilled shaft foundations that have failed in north Texas. As shown in Figure 1.1, uplift forces from expansive soils and freezing conditions creating high cable stresses are theorized as the failure mechanisms, either individually or in combination. This research focuses on studies on both of these conditions to analyze and then establish the potential contributors to failures in the field.

2.4 Soils

2.4.1 High-Plasticity Clays

The soil-concrete interface is of extreme importance to the success or failure of the foundations. Clay soils exhibiting an expansive, cohesive, and high-plasticity nature are significant in their engineering behavior and subsequent actions upon structures. According to the Unified Soil Classification System (USCS) (ASTM D2487-10), the particle size of a fine-grained soil smaller than $8x10^{-5}$ in. (0.002 mm) is classified as clay. In this research, the focus is directed at the expansive soils found in the areas where the failures occurred. Expansive soils exhibit swell-shrink characteristics due to moisture fluctuations and have been a problem to civil engineering infrastructures including roads and foundations from ancient times (Nelson and Miller, 1992). In the United States, expansive soils are abundant in the states of Texas, Colorado, Wyoming, and California (Chen, 1988). In the United States, damage from the swell and shrink behavior of clay soils cost owners about 6 to 11 billion dollars per year

(Nuhfer et al., 1993). An earlier National Science Foundation (NSF) study reported that the damage to structures caused by expansive soils, particularly to light buildings and pavements, is more than any other natural disaster; including earthquakes and floods (Jones and Holtz, 1973). Petry and Armstrong (1989) noted that it is always advisable to stabilize expansive clay soils during construction of a facility than leaving the soils unstable which will need future remediation. It is more economical to address the problem at the present time than to delay for remedial treatments later.

Soils are formed from the natural combination of many minerals. The type or amount of clay minerals can significantly influence their properties such as swelling, shrinkage, and plasticity. Examples of expansive clays include high-plasticity index (high-PI) clays, over-consolidated (OC) clays rich with Montmorillonite minerals, and Shales. Soils containing significant quantities of the minerals such as Montmorillonite, Illite, and Attapulgite are characterized by strong swell or shrinkage properties. Kaolinite is relatively nonexpansive (Johnson and Stroman, 1976). The mineral, Montmorillonite, has an expanding lattice and can undergo large amounts of swelling when hydrated or shrinkage when dried. Soils rich with these minerals can be found in many areas around the world especially in the arid and semi-arid regions (Hussein, 2001). A simplified method was developed by Mitchell (1976) and Holtz and Kovacs (1981) to estimate the type of mineral in the soil using the soil's plasticity and liquid limit as shown in Figure 2.3. However, this technique is not accurate enough due to the fact that soil can consist of many clay minerals.

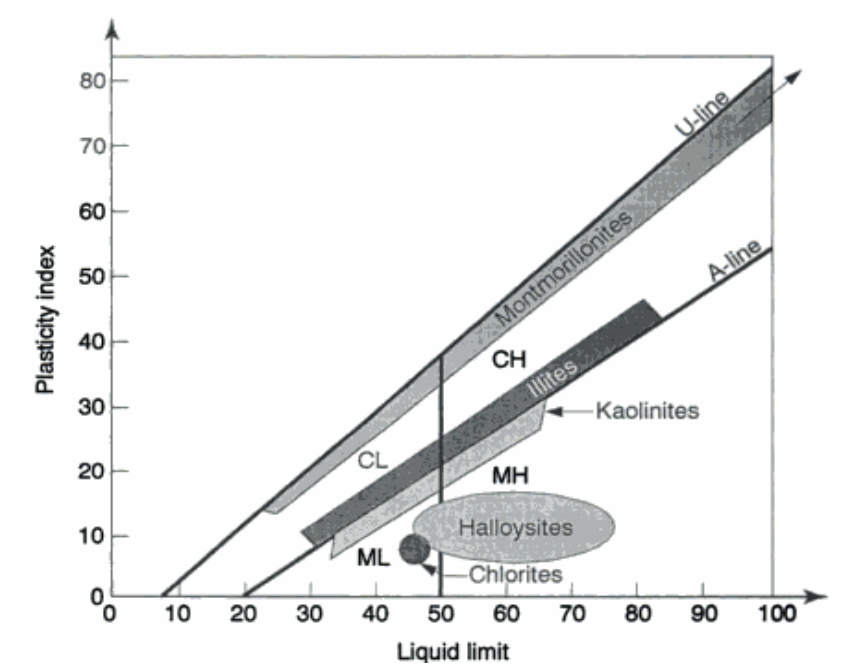

Figure 2.3. Plasticity Chart for Indicating Minerals in Soil
(Mitchell, 1976; Holtz and Kovacs, 1981)

According to Wiseman et al. (1985) the following factors can be used to classify a soil as problematic or not:

1) Soil type that exhibits considerable volume change with changes of moisture content.
2) Climatic conditions such as extended wet or dry seasons.
3) Changes in moisture content (climatic, man-made, or vegetation).
4) Light structures that are very sensitive to differential movement.

A summary of various methods for identifying the expansive nature of soils can be found in Puppala et al. (2004). Expansive soils can be identified by using the following plasticity-based index tests and the magnitudes of their test results as shown in Table 2.1.

Table 2.1. Expansive Soils Identification (Wiseman et al., 1985)

Index Test	Nonproblematic	Problematic
Plasticity Index	<20	>32
Shrinkage Limit	>13	<10
Free Swell (%)	<50	>100

Foundations to support civil infrastructure often extend beyond the active depths of these clay layers. In Texas, active clay depths range from 2 ft (0.6 m) to 30 ft (9.1 m) or more. Deep foundations, in particular drilled shafts or piles, are often used through these clay layers to support various structures including median barriers.

2.4.2 Temperature Effect

In Texas, the extreme temperatures recorded have been -23° F (-30.6° C) in the winter and 120° F (48.9° C) in the summer which is considered to be a very wide range. As previously discussed, the failure of the drilled shaft foundations occurred during low temperatures in the winter. Low temperatures contract the steel used for the cables which cause thermal stresses. High temperatures expand the steel allowing them to sag. These temperatures also create ice lens with the moisture in the ground which cause frost heaves and uplift. Moisture in the ground evaporates quickly with high temperatures and gusty winds cause shrinkage.

2.4.2.1 Cables

A change in temperature causes material expansion or contraction. Temperature can significantly influence material properties such as yield strength and modulus of elasticity (Craig, 1999). Generally, expansion or contraction of homogeneous materials is linearly related to the temperature increase or decrease in all directions (Hibbeler, 2008). Thermal strain is expressed with the following equation;

$$\epsilon_x = \epsilon_y = \epsilon_z = \alpha\Delta T \quad (2.1)$$

where $\epsilon_{x,y,z}$ is the thermal strain,

α is the coefficient of thermal expansion, and

ΔT is the change in temperature.

The elongation in a member has been identified as:

$$\Delta T_{xT} = (\alpha\Delta T)L_x,\ \Delta T_{yT} = (\alpha\Delta T)L_y,\ \Delta T_{zT} = (\alpha\Delta T)L_z \quad (2.2)$$

where $\Delta T_{xT,yT,zT}$ is the elongation in the x, y, and z directions, respectively.

The Coefficient of Thermal Expansion (CoTE) (α) identifies the thermal property of a material. The CoTE is determined by measuring the change in material dimensions before and after applying a temperature change. The CoTE is expressed in strain per degree of temperature unit (e.g., 1/°F, 1/°C, or 1/K). For determining the contraction of materials due to temperature decrease, the change in temperature (ΔT) in Eq. 2.2 is negative.

2.4.2.2 Soils

The temperature variation in soils cause moisture content fluctuations. These moisture fluctuations cause a swell-shrink behavior if the given soil is expansive in nature. During summer (high temperature) periods, a soil's moisture content evaporates leading to shrinkage of the soil. To the contrary, rainy seasons add moisture leading to swelling of these expansive soils. Studies on the effects of frost and heaving, which can cause damage to pavement and foundations, has been studied by many researchers such as Casagrande (1932b), Kaplar (1970), Penner and Bern (1970), and Yong and Warkentin (1975). In the expansion of water when it freezes, there is almost a 10 percent increase in volume. Damage from frost in the soil is due to formation of ice lens leading to frost heave. Originally, frost heave was considered when freezing of water in soil occurs. However, the vertical displacement of the frost heaving phenomenon can be greater than the expansion that occurs when ice freezes. Day (2006) stated that there are many cases where damage or deterioration from water

expansion is not evidently shown until the frost is melted; therefore, it might be very difficult to summarize damages caused from frost heave. One report by Penner and Burn (1970) revealed that movements studied in the soil resulting from ice lens expansion can be transmitted to the structure as shown in Figure 2.4, a process called adfreezing. It was theorized by these authors that adfreeze strength studies could provide the exact uplift values for all foundation materials such as concrete, wood, and steel in various soil types but this was determined to be an incorrect theory. In this research, it is believed that the probability that frost heave can occur in Texas is very low since temperatures for extended periods must occur which is a rare event within the state.

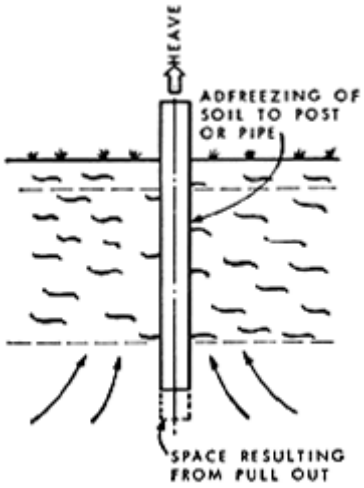

Figure 2.4. Behavior of Post in Frost Heaving (Penner and Burn, 1970)

2.5 Oblique Loading

2.5.1 Applicable Studies

An extensive investigation was performed looking for research applied using oblique loading on structural members installed in the ground. Very few reports exist. Of the few found, the focus was on piles in cohesionless soils. This research focuses on the drill shafts required for the cable systems in cohesive soils, especially very expansive, consolidated or overconsolidated clays.

2.5.1.1 Uplift Capacity of Deep Foundations in Cohesionless Soil Subjected to Inclined Loading

The primary function of a deep foundation system is to transfer axial, Q_u, and lateral, Q_h, loads from the superstructure to the foundation soil. In some cases, deep foundations are designed to resist uplift loads for tall structures such as illumination towers and foundations in expansive soils. The uplift capacity of foundations under vertical and inclined loads was studied by Meyerhof (1973a, b; 1980). He presented a semi-empirical relationship to estimate the ultimate uplift capacity of rigid piles in clay under inclined load as shown in Figure 2.5. The behavior of foundations under inclined loads is dependent upon the extent of the deformation characteristics of both the foundation and the soil. The failure mechanism becomes more complicated when considering the unsymmetrical and three-dimensional loadings.

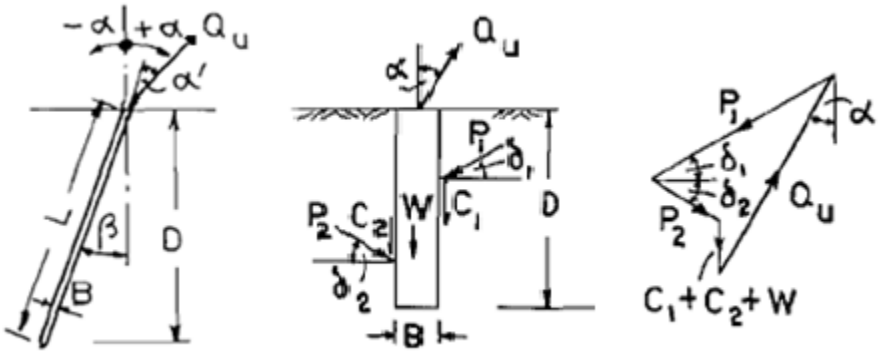

Figure 2.5. Forces of Anchors under Inclined Load (Meyerhof 1973a; 1980)

From Figure 2.5 above, the ultimate load can be estimated from the force using the following semi-empirical equation:

$$Q_u = \left(cK_c' D + \frac{\gamma D^2 K_b'}{2} \right) B + W \cos\alpha \qquad (2.3)$$

where Q_u is the net ultimate capacity of the piles,

D is the depth of the pile,

K'_b is the uplift coefficient based on the soil's angle of internal friction,

K'_c is the uplift coefficient given by $K_c^{'} = 1 + 0.08\frac{D}{B}$

with a maximum value of 3 for horizontal tension

(Meyerhof and Adams, 1968)

$K'_c = \pi$ in saturated clay ($\phi = 0°$)

W is the weight of the pile,

C is the cohesion force of the soil,

γ is the unit weight of the soil, and

B is the width of the pile.

Figure 2.6 can also be used to graphically determine the vertical and horizontal uplift coefficients.

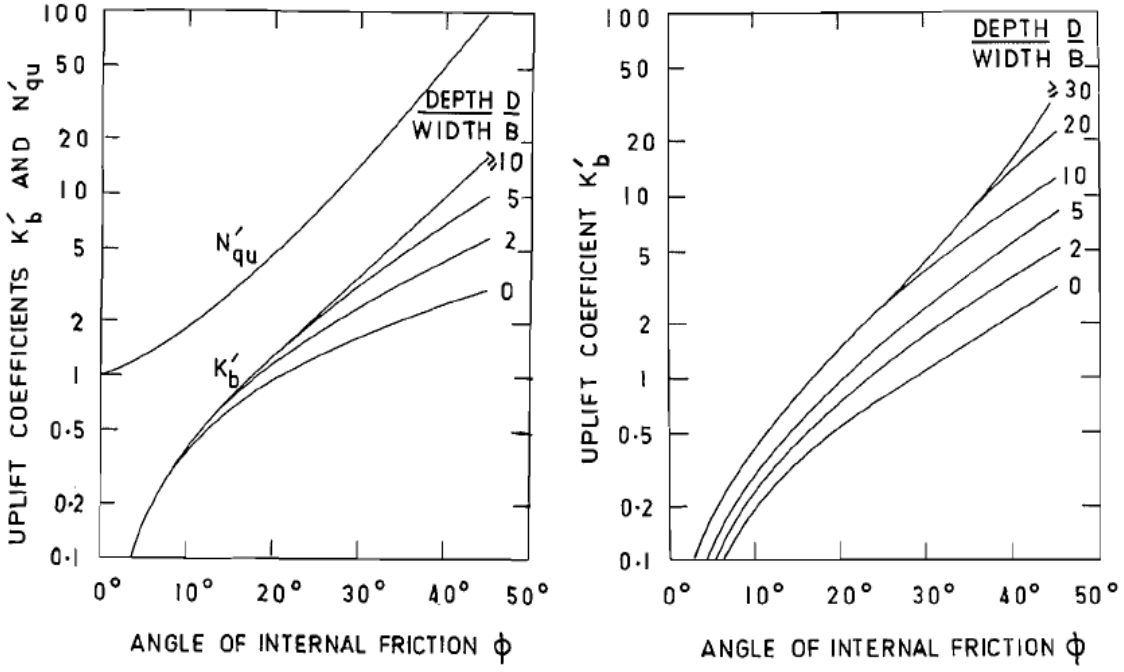

(a) (b)

Figure 2.6. Uplift Coefficients, (a) Vertical and (b) Horizontal for a Rigid Rough Pile (Meyerhof 1973a)

Meyerhof (1973a) developed the relation between vertical and horizontal pulling resistance, Q_v and Q_h, respectively through a series of model tests. The expression for the ultimate bearing capacity (Q_u) due to an obliquely loaded tension is shown below.

$$\left(\frac{Q_{u(\alpha)}\cos\alpha}{Q_v}\right)+\left(\frac{Q_{u(\alpha)}\sin\alpha}{Q_h}\right)^2 = 1 \qquad (2.4)$$

where Q_h is given by Eq. [zz] with α = 90°,

Q_v is given by Eq. [zz] with α = 0° , and

α is the angle of the inclined force with the horizontal axis (°)

In 1985, Ubanyionwu compared his study with Meyerhof's equation by using a laboratory model test in which a 1 in. (25.4 mm) diameter pile was installed in an 18 in. x 18 in. x 30 in. (457.2 x 457.2 x 762 mm) box compacted with clay. In these studies, the density of the compacted clay was maintained at 129.0 lb/ft^3 (20.25 kN/m^3) and the degree of saturation was equal to 97.9%; almost 100% saturated soil. The piles were extracted at different angles (0° – 90°). The results of this experiment agreed well with the semi-empirical equation developed by Meyerhof (1973a).

When considering inclined loading, Q_u decreases as the inclination of the load with the pile axis increases. Curves for various eccentricities, *e*, of the load are geometrically similar to those for a central load (Figure 2.7). Comparing the vertical component $Q_{uv} = Q_u \cos a$ of the eccentric inclined failure load Q_u with the ultimate value Q_m of a pile under an eccentric vertical load for different load inclinations, α, Figure 2.8 indicates that the decrease of the ratio Q_{uv}/Q_{ev} with an increase of α depends mainly on the relative density of the sand and to a smaller extent on the load eccentricity depth ratio, *e/D.* For shear strength purposes, dense sands are regarded as very similar to over-consolidated clays.

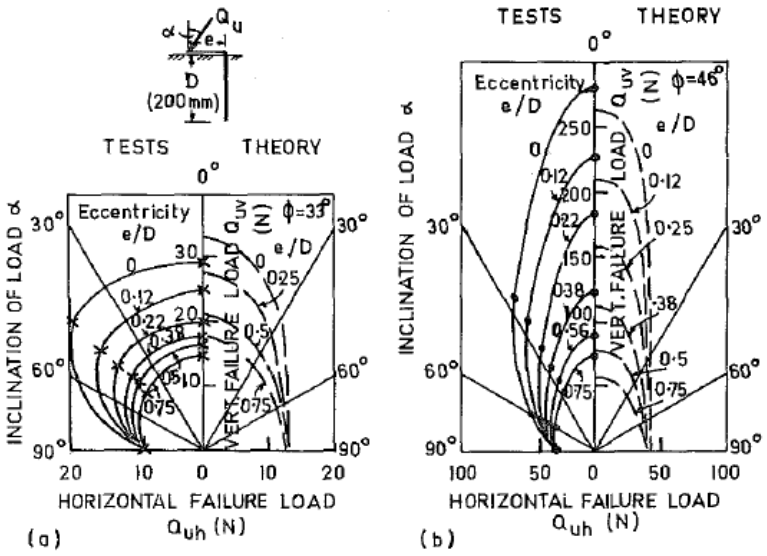

Figure 2.7. Polar Bearing Capacity Diagrams for Single Piles Under Eccentric Inclined Loads: (a) Loose Sand; (b) Dense Sand
(Meyerhof et al., 1983)

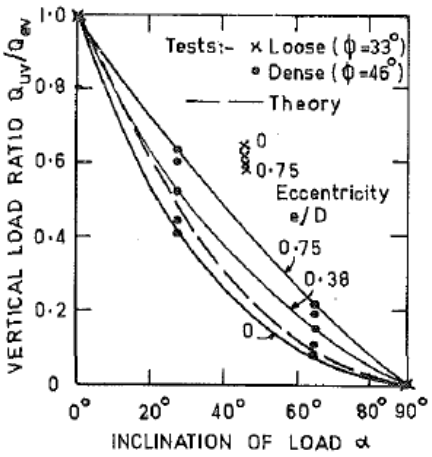

Figure 2.8. Effect of Load Inclination on Ultimate Bearing Capacity of Single Piles
(Meyerhof et al., 1983)

2.5.1.2 Uplift Capacity of Deep Foundations in Cohesive Soil

Subjected to Inclined Loading

Generally, capacity of piles or shafts is the combination of resistance from end bearing and skin friction. However, the design of deep foundations in cohesive, expansive soils is different than in noncohesive soils. Damage from the three-dimensional expansion of cohesive

soils can be very extensive and possibly completely destructive. When these movements are excessive, shafts can be lifted up as shown in Figure 2.9. Shaft uplift can occur when the uplift force from the soil swell pressure is higher than the skin friction resistance.

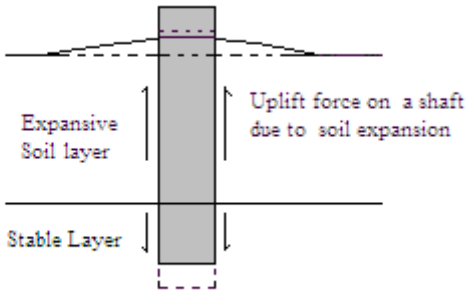

Figure 2.9. Deep Foundation Movements in Expansive Soil

Many researchers have studied the uplift capacity of piles from the view of temperature, moisture content, and active depth (Westman, 1993). O'Neill and Poormoayed (1980) developed an equation for computing the value of f_{max} in the zone of expansion as shown in Equation 2.5.

$$f_{\max} = \varphi \sigma'_{ho} \tan \delta_r \tag{2.5}$$

where φ is the correlation coefficient (recommended at 1.3),

σ'_{ho} is the horizontal swell pressure at the depth where f_{max} is computed,

δ_r is the effective residual of interface friction between the pile concrete and the expansive soil.

In this equation, it is assumed that the expansion process happens slowly resisting the development of excess positive or negative pore water pressures. Cameron and Walsh (1981) described a study of small diameter, timber piles driven to various depths in an expansive soil profile and monitored through several wet and dry seasons at an active depth of the expansive soil layer between 60 in. (1.5 m) and 78.7 in. (2.0 m). After monitoring for five years, they

observed maximum seasonal ground surface movements of 2.6 in. (65 mm). Piles driven into the active depth recorded movements between 15 – 32% of the movement at the ground surface. However, piles driven below the active depth to 78.7 in. (2 m) and 98.4 in. (2.5 m) were effective in resisting all movement at the ground surface. In 1984, Duffy and Charania developed a modified oedometer-type test to model the interaction between a pile and expansive clay when exposed to water. Additional numerical simulations of piles in expansive soils were performed by Justo et al. (1984), Mohamedzein et al. (1999), and Sinha and Poulos (1999). Westman (1993) studied different variables that affect pile uplift in expansive soil and formulated Equation 2.6 from 729 numerical models that measured the vertical displacement of the pile head where load was applied.

$$Y = \frac{e^{0.3575} T^{1.61}}{D^{1.17} L^{0.831} f_s^{0.760} C^{1.61}} \tag{2.6}$$

where Y is the vertical displacement of the pile head (ft.)

S is the swell pressure of the expansive soil (ksf)

T is the thickness of the expansive soil (ft.)

D is the depth to the center of the expansive soil (ft.)

L is the structural load applied to the pile head (ksf)

f_s is the interface friction between the pile and the soil, and

C is the cohesion of the expansive soil (ksf)

Al-Saoudi and Salim (1998) studied the movements of the heads of model piles embedded in expansive soils. The results showed that the movements of the pile heads were less than the movements at the ground surface. Chapel and Nelson (1998) conducted the test using bored concrete piles and helical screw plate anchors for lightweight construction in expansive soils and concluded that both of the piles and the anchors perform satisfactorily when installed below the active depth of the expansive soil layer.

2.5.2 Analysis Methods

The application of lateral load to a drilled shaft results in lateral deflection which causes a soil reaction. Lateral load which is greater than lateral resistance of the drilled shafts can lead to excessive deformation of the shafts, soil failure around the shafts, and structural failure of the overlying member. Factors such as maximum bending moment and shear force in the embedded drilled shaft are also important and are dependent to a large extent on the reaction provided by the soil. Consequently, the main objectives of designing the shaft are to determine the necessary penetration depth of the drilled shaft, diameter of the shaft, mechanical properties of the concrete to resist bending and shear, and determine the deformations or stiffness of the drilled shaft in order to assess the performance of the structure.

In the analysis of laterally loaded drilled shafts, there are many common design methods used such as “Broms”, “Equivalent Cantilever”, “Characteristic Load”, “p-y”, and “Strain Wedge”. These methods deal with the nonlinear system of soil response (Reese and Allen, 1977) which will be described later.

2.5.2.1 Broms Method

The lateral capacity of drilled shafts had been initially studied by Brinch Hansen (1961). Later Broms (1964a, 1964b, 1965) developed a test to determine the ultimate lateral capacity of deep foundations in purely cohesive and cohesionless, homogeneous soil deposits. Broms constituted the analysis by considering the distribution of shear resistance with depth, the short rigid piles, long flexible piles, and fixed- and free-head cases separately. In addition, he gave the criterion for dividing shafts into two groups which are short-rigid and long-flexible piles which is the ratio between embedded length of shafts and stiffness factor as given below:

Short-Rigid Pile: $\frac{L}{T}$ or $\frac{L}{R} \leq 2$ (2.7)

Long- Flexible Pile: $\frac{L}{T} \geq 4$ or $\frac{L}{R} \geq 3.5$ (2.8)

where T and R are the stiffness factors

These factors account for the pile elasticity modulus (E) and moment of inertia (I) of the pile and soil modulus (the compressibility of the soil) which are dependent upon the depth of the influence area, width of the pile, and the soil type. For normally consolidated (NC) clays and cohesionless soils, the subgrade modulus is assumed to increase with depth linearly, and the stiffness factor can be expressed as below:

$$T = \left[\frac{EI}{n_h}\right]^{\frac{1}{5}} \text{ in length units} \qquad (2.9)$$

where E is the modulus of elasticity of the pile material,

I is the moment of inertia of the pile section, and

n_h is the coefficient of modulus variation.

For normally consolidated clay, n_h = 350 to 750 kN/m^3

For soft organic silt, n_h = 150 kN/m^3

For granular soil, n_h can be seen in Table 2.2.

Table 2.2. Values of n_h for Cohesionless Soils (kN/m^3) (after Terzaghi 1955)

Type of Sand	Loose	Medium	Dense
Dry or moist sand	2500	7500	20,000
Submerged sand	1400	5000	12,000

For overconsolidated clays, the modulus is assumed to be constant with the depth, so the stiffness factor is:

$$R = \left[\frac{EI}{KD} \right]^{\frac{1}{5}} \quad \text{in length units} \tag{2.10}$$

where D is the diameter or width of the pile,

K is $K_s/1.5$ and

K_s is Terzaghi's subgrade modulus reaction (kN/m^3), or

K is $n_h x/D$ if x, depth of the soil, is considered.

According to Terzaghi (1955), K_s values are listed in Table 2.3 below.

Table 2.3. Values of K_s for Cohesive Soils (kN/m^3)

Consistency	Stiff	Very Stiff	Hard
Unconfined Strength (kN/m^2)	10 - 20	20 – 40	≥40
Recommended K_s	27,000	54,000	108,000

In the case where short, free-headed piles in cohesive soils occur (3-cable median barriers), Equations 2.11, 2.12 and 2.13 apply as shown below. In addition, the schematic of deflected shape, passive soil reaction, and moment diagram in cohesive soil can be seen in Figure 2.10.

$$f_s = \frac{H_u}{9 c_u D} \tag{2.11}$$

where f_s is the pile length required to develop the passive soil reaction,

H_u is the ultimate lateral capacity of the pile,

c_u is the undrained cohesion of the soil, and

D is the diameter or width of the pile.

$$M = H_u\left(e + 1.5B + 0.5f\right) \tag{2.12}$$

where M is the moment in the pile at the point of fixity, and

e is the unsupported length of the pile.

$$2.25Dc_u\left[L - \frac{H_u}{9c_uD}\right]^2 = H_u\left[e + 1.5D + \frac{H_u}{18c_uD}\right] \tag{2.13}$$

where L is the embedded length of the pile.

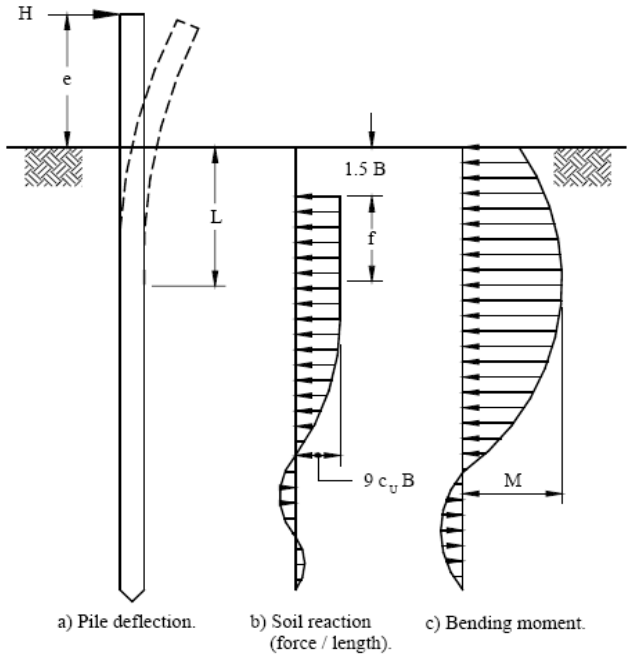

Figure 2.10. Schematic for a Laterally Loaded Pile in a Cohesive Soil (Broms, 1964a)

Equation 2.11 can be solved by trial and error for H_u. However, Broms simplified this method by using the following graph.

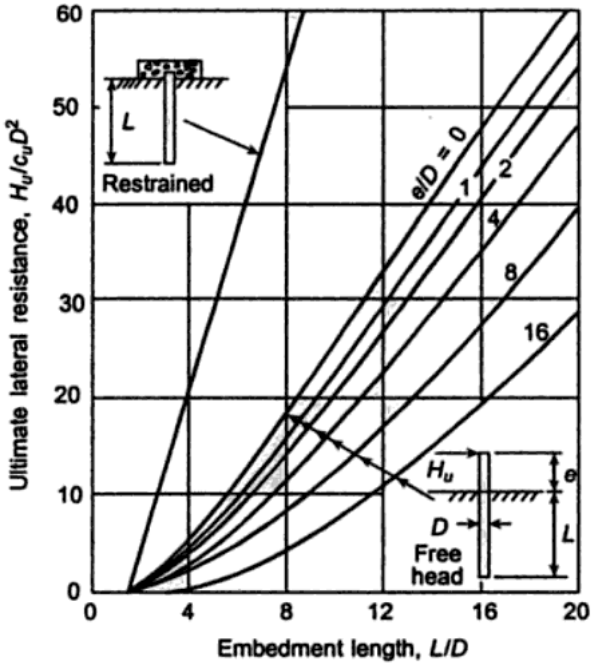

Figure 2.11. Design Chart for Short Piles in Cohesive Soils (Broms, 1964b)

2.5.2.2 Equivalent Cantilever Method

Davisson and Robinson (1965) determined the elastic forces and moments in piles using an equivalent cantilever method. Greimann et al. (1987) developed this design method based on Rankine's equation for inelastic buckling. Abendroth et al. (1989) evolved this method into designing piles of integral bridges to provide less conservative results. They idealized the piles through a cantilever model as shown in Figure 2.12. This method was based on analytical and finite element studies. The drilled shaft was replaced by an equivalent cantilever beam in order to simplify the analysis. However, Robinson et al. (2006) observed that the results from the analyses of the cantilevered columns with an "equivalent" length did not match the magnitudes of maximum moments, lateral pile top displacements, or buckling behavior from nonlinear lateral analysis.

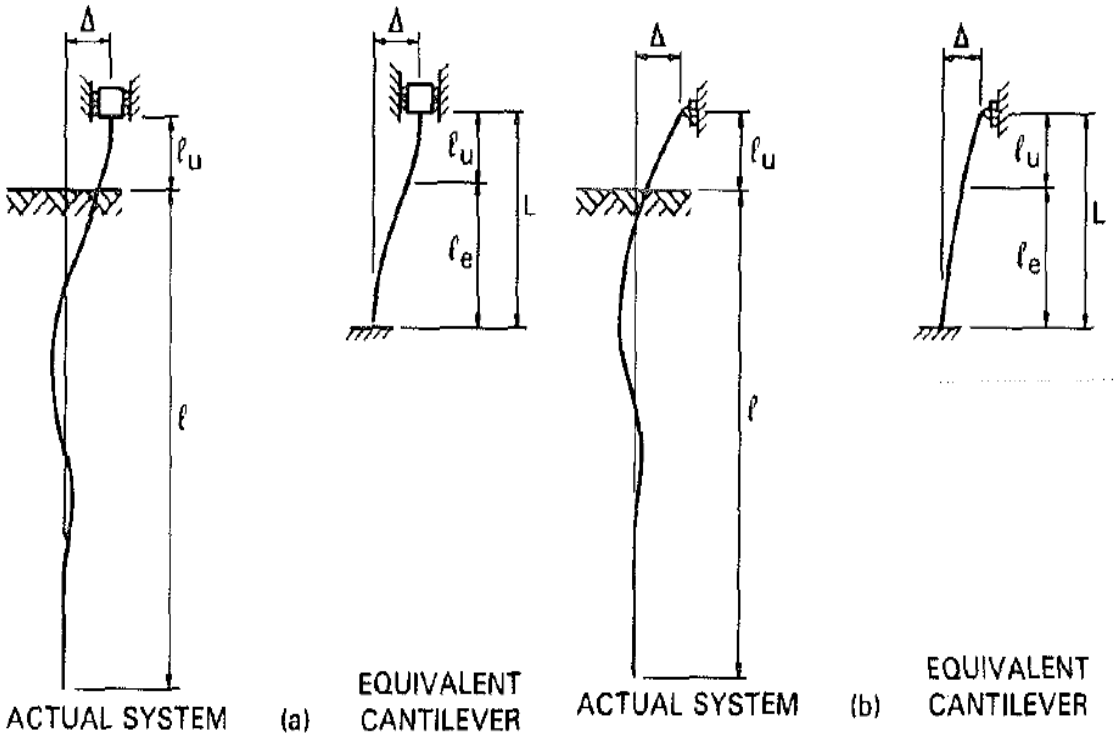

Figure 2.12. Cantilever Idealization of a Pile: (a) Fixed Head; (b) Pinned Head (Abendroth et al., 1989)

2.5.2.3 Characteristic Load Method (CLM)

Duncan et al. (1994) proposed a method based on parametric analysis of numerous p-y curves. The significance of this method over the equivalent cantilever method is that it can use nonlinearity of the soil behavior. The nonlinear behavior of pile foundations subjected to lateral loads is affected by two factors. The first factor is nonlinearity of the load-deflection behavior of the soil around the pile. The second factor is the load transfer from the upper part of the pile to greater depths resulting in an increase of the moment. In addition, the authors stated that this method can be used to determine:

1. Ground line deflections due to ground line shears for fixed shaft condition.
2. Ground line deflections due to moment applied at the ground line.
3. Maximum bending moment within the shaft.
4. Position of the maximum moment.

The relationships of the CLM were formed by using dimensionless variables to handle a wide range of soil properties as shown below:

For clay,

$$P_c = 7.34D^2\left(E_p R_I\right)\left[\frac{s_u}{E_p R_I}\right]^{0.68} \tag{2.12}$$

$$M_c = 3.86D^2\left(E_p R_I\right)\left[\frac{s_u}{E_p R_I}\right]^{0.46} \tag{2.13}$$

where P_c is the characteristic or normalizing shear load,

M_c is the characteristic or normalizing bending moment,

D is the width or diameter of pile or drilled shaft,

E_p is the modulus of elasticity of pile or drilled shaft,

R_I is the ratio of moment of inertia (I_p/I_r)

with I_p as the ratio of moment of inertia of the pile or drilled shaft, and

I_r as the moment of inertia of a solid circular cross section, and

S_u is the undrained shear strength of the undisturbed clay samples.

From the above equations, the moments and shear loads are determined at the groundline. After determining the variables, the solution parameters can be obtained with the help of various curves which are ground line shear- and moment-deflection curves as presented in Figure 2.13.

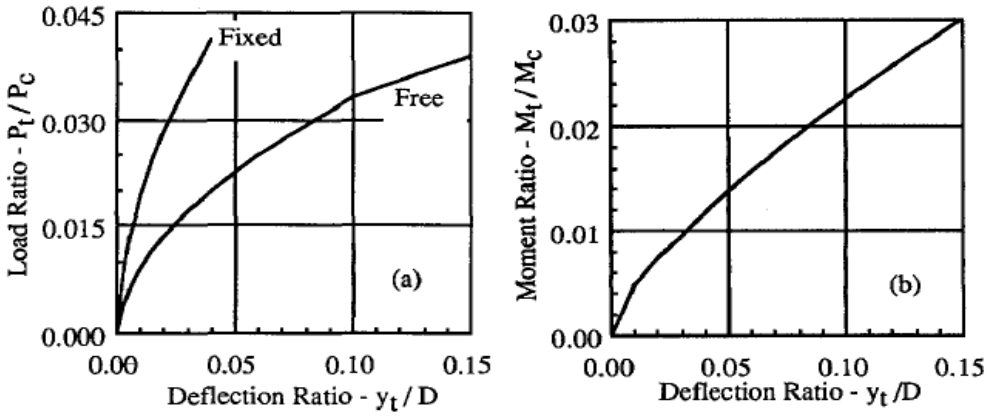

(a) (b)

(b)

Figure 2.13. Deflection Curves of (a) Groundline Shear and (b) Groundline Moment for Clay (Duncan et al., 1994)

In the computations, P_t and M_t are the load and moment, which will be divided by the characteristic shear load (P_c) and characteristic bending moment (M_c). The deflection ratios from the groundline shear load- and groundline moment-deflection curves are determined from Figure 2.13 (a) and (b). Next, the groundline shear (P_m) is determined by using the same deflection ratio from the groundline moment (M_m) while also being determined using the same deflection ratio from the groundline shear, of which both values can be determined from Figure 2.13 (a) and (b) for the second time. Then the ground deflection (y_{tpm}), caused by the summation of the actual load and the groundline shear ($P_t + P_m$), and the ground deflection (y_{tmp}), caused by summation of the actual moment and the groundline moment ($M_t + M_m$), are determined from Figure 2.13 (a) and (b) for the third time. Finally, computation of the lateral deflection ($y_{t\ combined}$) is performed by using the following equation:

$$y_{t(combined)} = 0.5\left(y_{tpm} + y_{tmp}\right) \tag{2.14}$$

In order to find the maximum moment in this method in a free- or fixed-head drilled shaft and if the only load applied is a groundline shear, Figure 2.14 can be used.

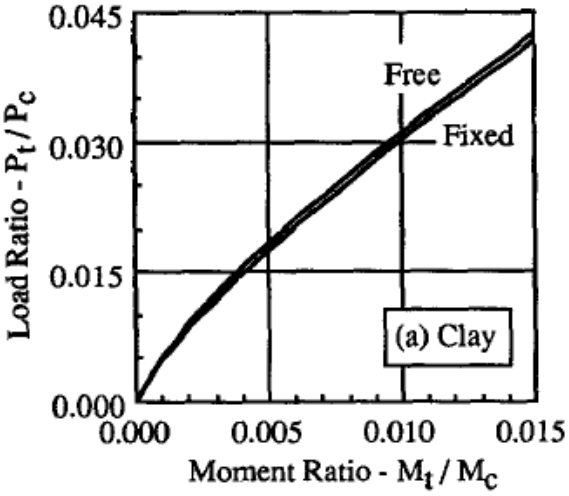

Figure 2.14. Load-Moment Curves (Duncan et al., 1994)

However, if the moment and shear are both applied, lateral deflection, $y_{t\ (combined)}$, is determined as mentioned above, and the characteristic length (T) is found from the following equation:

$$y_{t(combined)} = \frac{2.43P_t}{E_p I_p} T^3 + \frac{1.62M_t}{E_p I_p} T^2 \tag{2.15}$$

The next step is to calculate the bending moment of the drilled shaft by using the following equation:

$$M_z = A_m P_t T + B_m M_t \tag{2.16}$$

where M_z is the moment at depth z,

A_m, B_m is the dimensionless moment coefficient, which is obtainable from Figure 2.16 below,

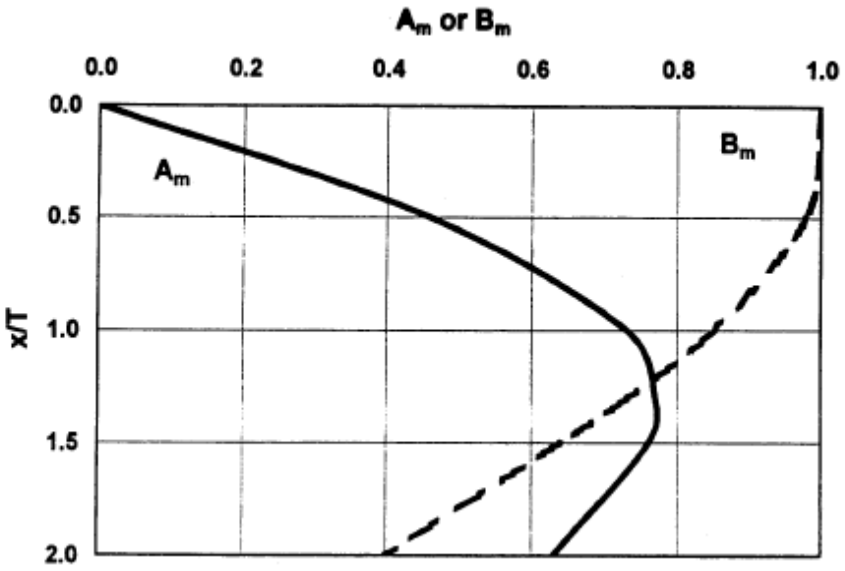

Figure 2.15. Parameters A_m and B_m (Matlock and Reese, 1961)

Although the characteristic load method was developed from the p-y method, it is not generally used as the p-y method. There are some limitations of the CLM (O'Neill and Reese, 1999) which are outlined below:

1) Piles and drilled shafts must be long enough so that the behavior is not affected to any significant degree by their depth, which depends on the relative thickness of the piles or shaft to stiffness of the soil. Thus, Duncan et al. (1994) provided the minimum drilled shaft penetrations to fit with this method. However, in case the shaft is shorter than the depth mentioned in Table 2.4, the groundline will be underestimated and the maximum bending moment will be overestimated. In addition, minimum penetration is affected by the cyclic loading and the presence of free water.
2) It is founded on a generally uniform soil condition; also, it has not been used with shafts in rock sockets.
3) The effect of axial loads on the bending moment is not taken into account.
4) The shear could not be analyzed directly.

5) The nonlinear bending in the drilled shaft is not considered in this method. Thus, if there are some cracks at the depth of maximum moment, the groundline deflection will be underestimated.

Table 2.4. Minimum Penetrations for Clay of Drilled Shaft for the Characteristic Load Method (Duncan et al., 1994)

Type of Soil	Criterion	Minimum Depth
Clay	E_pR_I/S_u = 100,000	6D
Clay	E_pR_I/S_u = 300,000	10D
Clay	E_pR_I/S_u = 1,000,000	14D
Clay	E_pR_I/S_u = 3,000,000	18D

2.5.2.4 'p-y' Method (Nonlinear Analysis)

This method is more generally used to analyze a drilled shaft subjected to lateral loading due to its' versatility for including the distributed load along the shaft caused by flowing water or creeping soil, nonlinear bending characteristics, cracked concrete pile sections, layered soils, and nonlinear soil response. This method is recommended for use with most critical foundations. The p-y model was first developed by using the response of a single shaft subjected to lateral loads (Reese and Matlock 1956). McClelland and Focht (1958) modified the p-y model based on the results of a lateral load test on a 24 in. (610 mm) diameter pile embedded 75 ft (23 m) into a normally consolidated (NC) clay from the Gulf of Mexico. More improvements to the method followed including Matlock and Ripperger (1958), Matlock (1970), Reese et al. (1975), Reese and Welch (1975), and Bhushan et al. (1979). Later, Reese (1984, 1986) reported the comprehensive information on laterally loaded piles and drilled shafts design in a Federal Highway Administration (FHWA) document which has been broadly accepted.

The fundamental portion of this method represents the p-y curves of the true behavior of soils by considering the nonlinearity of the soil modulus. This is based on a numerical solution of a physical model for the laterally-loaded deep foundation based on the soil along the unit length of the shafts, replaced with a series of mechanisms, as shown in Figure 2.16. At different depths of shaft, the resisting force per unit length of the shaft (soil reaction) (p) performs as the nonlinear function of the lateral deflection (y).

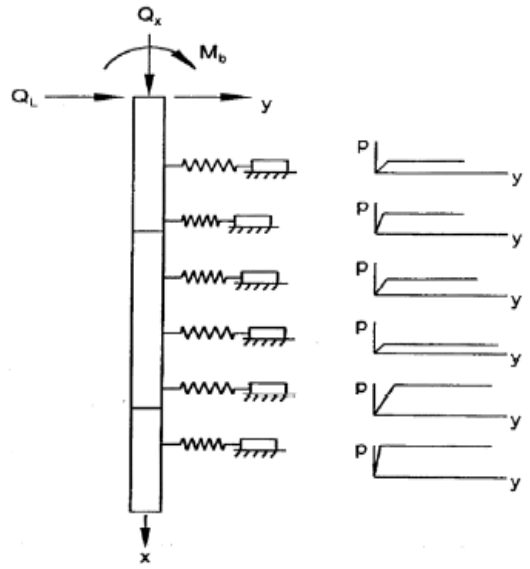

Figure 2.16. Physical Model of a Deep Foundation under Lateral Load
(Reese and Welch, 1975)

The method used to determine the p-y curves use the following equations.

$$EI\frac{d^4y}{dx^4} + Q\frac{d^2y}{dx^2} - p - w = 0 \qquad (2.17)$$

where Q is the axial load on the shaft,

y is the lateral deflection of the shaft at a point x along the length of the shaft,

p is the lateral soil reaction per unit length,

EI is the flexural rigidity of the drilled shaft, and

w is the distributed load along the length of the shaft.

In addition, the equations that are produced as derivatives are necessary in design as shown below.

The drilled shaft is treated as a beam column with lateral soil support. The general behavior of a drilled shaft under a combination of lateral and axial loading can be obtained by solving the differential equation given below (Hetenyi, 1946):

For transverse shear (V),

$$EI = \frac{d^3 y}{dx^3} + Q\frac{dy}{dx} = V \tag{2.18}$$

For bending moment in the drilled shaft (M),

$$EI\frac{d^2 y}{dx^2} = M \tag{2.19}$$

For the slope of the deflection diagram (S),

$$\frac{dy}{dx} = S \tag{2.20}$$

For the slope of secant to any p-y curve or soil modulus (E_s),

$$E_s = \frac{p}{y} \tag{2.21}$$

After substituting E_s (Eq. 2.21) into the main equation (Eq. 2.17), the results show that there are finite difference terms depending on a number of nodes along the drilled shafts, with the p value at each node equal to $E_s y$. Thus, y values are the unknown parameters in this problem. Generally, y values depend on soil stiffness which is increased by higher vertical stresses with deeper foundations. Also, the lateral movement from the piles will additionally increase the stresses in the soil.

Even though the bending moment, shear force, and other design aspects of the drilled shafts are computed from the finite difference forms of the equations, computer generated solutions using LPILE software programs are efficient, time saving, and create an opportunity for investigating the influence of a large number of parameters with minimum difficulty.

In the present project, the researchers propose to analyze the pile load test results using the 'Broms Method'. Other methods, including 'Characteristic Load Method' and 'p-y Method' based software, LPILE, will also be considered if the soil conditions at the test site location can match with the assumptions used in these methods.

2.5.2.5 Strain Wedge Model

The Strain Wedge (SW) Model, developed in 1996 by Ashour et al. (1998), improved upon Reese's (1977) Beam on Elastic Foundation (BEF) pile response parameters and his realization of limitations of the p-y curves (1983) for soil continuity and pile properties. The SW method added the capability to analyze piles in multiple soil layers to include sand and clay. Additionally, the method allowed the effect of pile head conditions (free- or fixed-head) to be included in the analysis.

The method uses a 3-D passive soil wedge that is formed in front of a laterally loaded pile that accounts for stress-strain-strength parameters. The SW model is interdependent upon the BEF model through the horizontal soil strain, ε, the horizontal soil stress change, $\Delta\sigma_h$, and the nonlinear variation in the Young's modulus, E.

A diagram of the soil wedge is shown in Figure 2.17. The deflection pattern of the pile is assumed to be linear and is shown in Figure 2.18. Each layer's soil properties encountered in the field can be applied in this model and used to more accurately determine the effect to the soils from lateral loading on the pile.

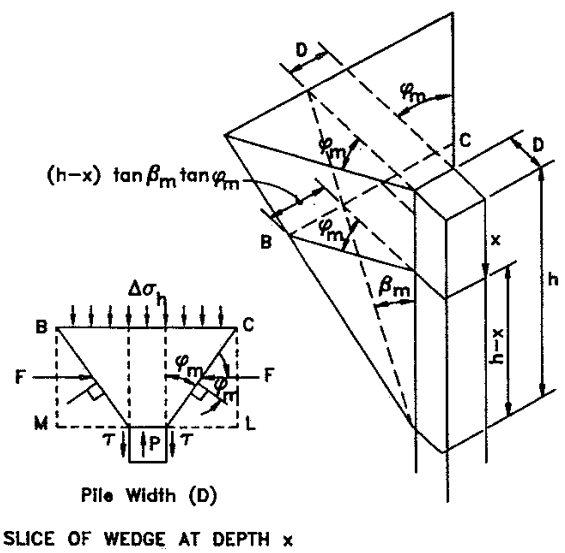

Figure 2.17. Basic Strain Wedge in Uniform Soil
(Ashour et. al, 1998)

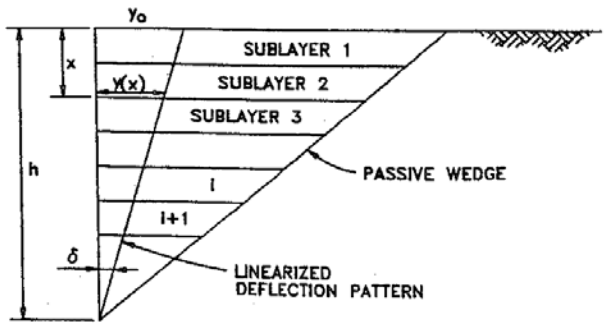

Figure 2.18. Linearized Deflection Pattern
(Ashour et al., 1998)

The horizontal strain in the soil is the most influential parameter in the model. In normally consolidated clay, the effective unit weight, the Plasticity Index, effective friction angle, undrained shear strength, and soil strain at 50% stress level are used in the calculation of the modulus of subgrade reaction, *E*, and representing the secant slope at any point on the p-y curve.

Wedge thicknesses are created based upon soil types. But additional wedges can be created if a soil layer is determined to be too thick and possibly affect the calculations.

Additionally, a wedge can be created for a fixed-head pile and included in the calculations. This greatly assists in replacing the conditions in such programs as COM624 and LPILE that consider p-y curves to be unique. Soil and pile variations have a dramatic effect upon the response of soils and their p-y curves as shown by actual field tests in Figure 2.19.

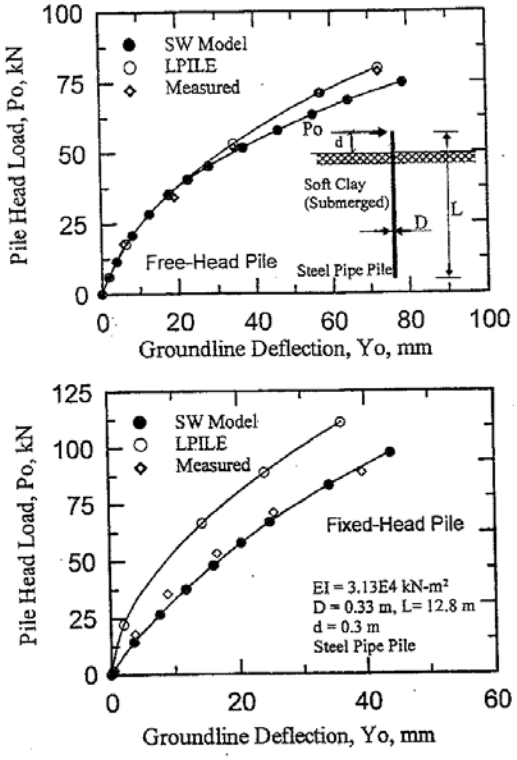

Figure 2.19. Comparison of SW, LPILE, and Field Data for Free- and Fixed-Head Piles in Clays at the Sabine River (Ashour et al., 2002)

2.5.2.6 Comparison of Lateral Load Analysis (Broms method and p-y method)

Klaiber et al. (2004) compared the results between the Broms method (the linear method) and the p-y method (nonlinear method) and reported that the p-y method can be used in more complex soil conditions thus providing more accurate results of the moment distribution along the depth of the piles. The Broms method does not take the redistribution of loads below the point of fixity. They also compared both methods by using different soils which are stiff clay (SPT blow count of N = 25), soft clay (SPT blow count of N = 2), and cohesionless soil (SPT blow count of N = 25) with different magnitudes of lateral loads by changing the backwall

height. As shown in Figure 2.20, the Broms method is more conservative in predicting stiff clays than the p-y method. As shown in Figure 2.21, the Broms method is less conservative in predicting soft clays than the p-y method. As shown in Figure 2.22, both methods yield the same results in predicting cohesionless soils.

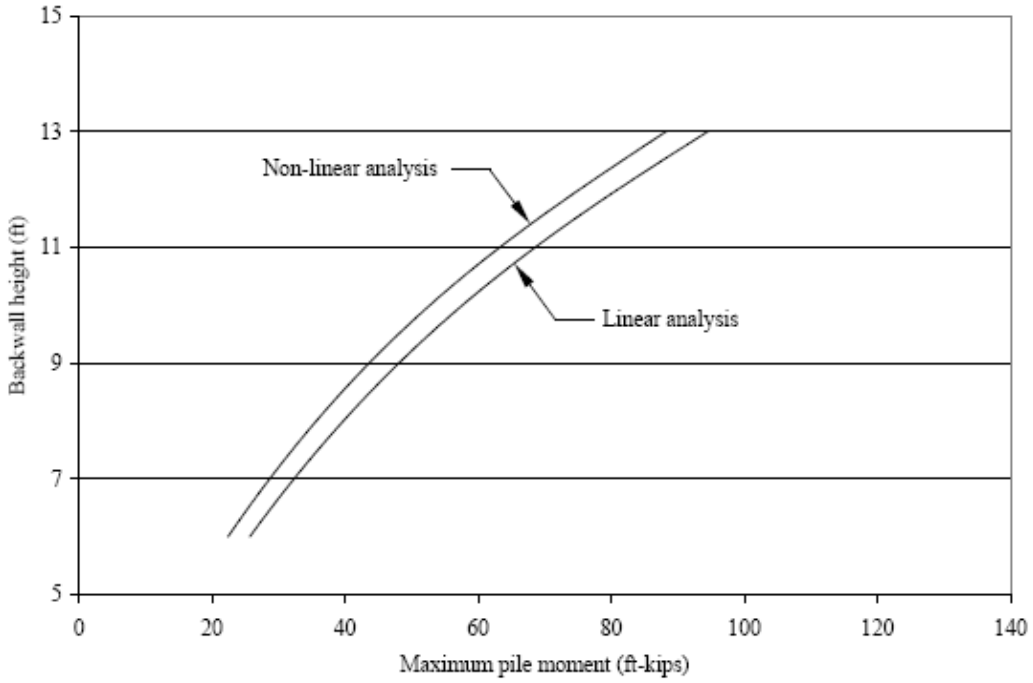

Figure 2.20. Comparison of Lateral Load Analysis in Stiff Clay (Klaiber et al., 2004)

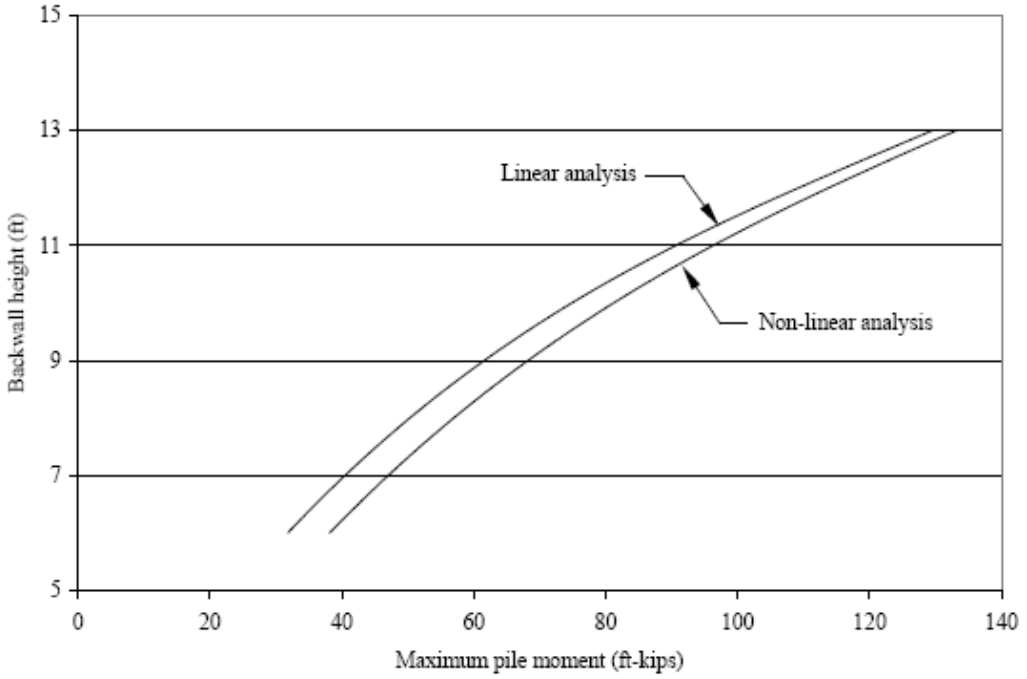

Figure 2.21. Comparison of Lateral Load Analysis in Soft Clay (Klaiber et al., 2004)

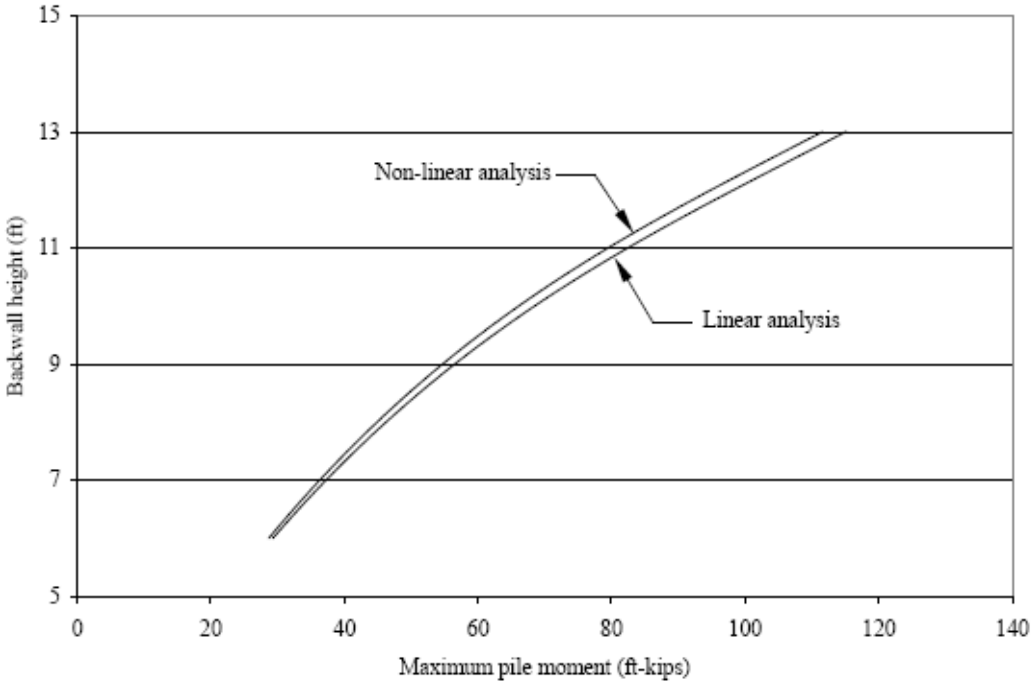

Figure 2.22. Comparison of Lateral Load Analysis in Cohesionless Soil (Klaiber et al., 2004)

2.5.2.7 Comparison of Lateral Load Analysis (Broms method and Allpile method)

Moayed et al. (2008) analyzed a single pile's bearing capacity in cohesive soils when subjected to lateral loading only. Using Broms method, they found the following advantages to this theory:

1. It is applicable for short and long piles.

2. It considers both cohesive and cohesionless soils.

3. It considers both free-head and fixed-head piles.

The theory does have the following disadvantages:

1. It does not apply in a layered soil system.

2. It does not consider c – ϕ soils.

As shown in Figure 2.23, Matlock (1970) used Broms (1964) equation of $p_u = 9c_ub$ for the magnitude of the shear at the pile's hinge point. Moayed's test results showed that the soils they used collapsed well before the p_u value was obtained.

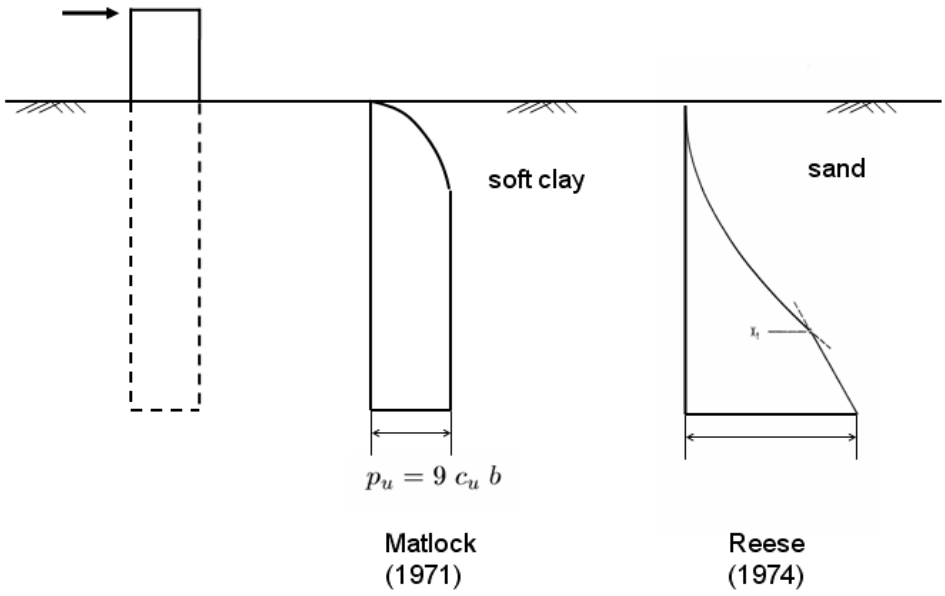

Figure 2.23. Comparison of Ultimate Soil Resistance of Soft Clay (Matlock, 1970) and Sand (Reese et al., 1975)

Broms developed the curves found in Figures 2.24, 2.25, and 2.26 which the Federal Highway Administration (FHWA) has adopted in their pile capacity manual.

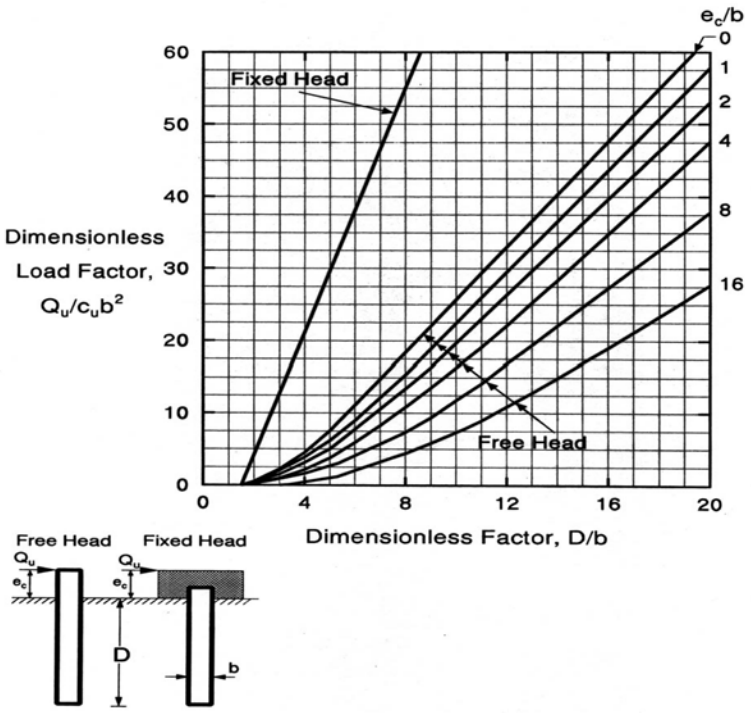

Figure 2.24. Ultimate Lateral Load Capacity of Short Piles in Cohesive Soils (FHWA-HI-97-013, 1998)

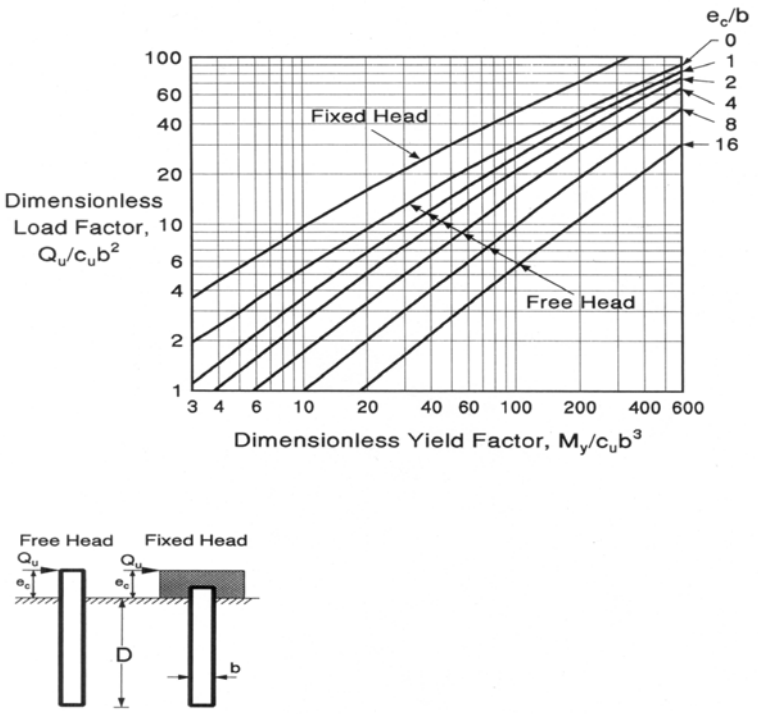

Figure 2.25. Ultimate Lateral Load Capacity of Long Piles in Cohesive Soils (FHWA-HI-97-013, 1998)

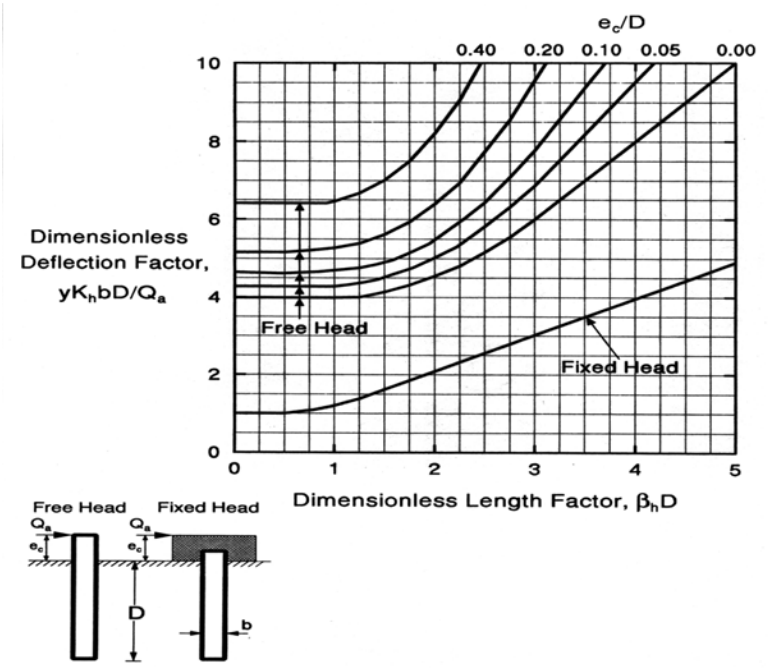

Figure 2.26. Lateral Deflection at Ground Surface of Piles in Cohesive Soils (FHWA-HI-97-013, 1998)

Moayed also reported that the pile diameter does not significantly change the normalized ultimate lateral bearing capacity.

The AllPile finite difference program was used for comparison to the Broms method. AllPile is another software program that is similar to LPILE, both based on COM624, which was used to compute the p-y curves. Both programs handle all types of piles and drilled shafts. By integration of lateral pressure, shear, moment, rotation, and deflection, the pile and soil interaction and behavior are analyzed. AllPile performs lateral analysis under different head-load boundary conditions. It calculates compression (with settlement), uplift, lateral capacity, and group analysis. AllPile determines the Point of Fixity and Stiffness, k, of the pile for rotation, lateral, and vertical deflections.

The AllPile program results matched those from Dunnavant and O'Neill (1985) in which they field tested steel pipe piles in overconsolidated Texas clays at the University of Houston (see Table 2.5). These results can be considered very valuable due to the proximity of the University of Houston tests compared to the failure sites that occurred in Kaufmann County.

Table 2.5. Comparison Between Measured Ultimate Lateral Bearing Capacity of Pile and Full Scale Test

Test Location	Q_{ult} (kN)		
	Full Scale Test	Broms Method	AllPile Finite Difference Program
Houston, Texas, USA	1330	3644	1786

These results demonstrate the conservative nature based on the disadvantages listed above of the Broms method when compared to the AllPile results.

2.6 Lateral Load Tests on Drilled Shafts

Since the main intent of this research was to perform load tests in the field and then identify the causes of the failures, an attempt was made to collect recent field lateral load test information. Information by Anderson (2005), FHWA (1997), Johnson et al. (2007),

KDOT (2007), and Tensar (2001, 2007) was thoroughly reviewed and used in the test setup design.

2.6.1 Field Tests

The performance of drilled shafts in different soil types and the derivation of p-y curves were evaluated by using different types of tests leading to more accurate design of drilled shafts (O'Neill and Reese, 1999). Standard lateral load tests for drilled shafts are described by FHWA IP-84-11 and ASTM D 3966-07. The most common types of lateral load tests that are conducted on drilled shafts are Conventional Load, Osterberg Cell, and Statnamic Load. A brief description of each test method is provided in the following sections.

2.6.1.1 Conventional Load Test

In the Conventional Load test, a test shaft of known diameter is placed between two reaction shafts which are connected by a reaction frame. The load is gradually applied by the reaction frame to the test shaft. Hydraulic jacks are placed on the test shaft on a leveled steel plate. A typical test setup is shown in Figure 2.27.

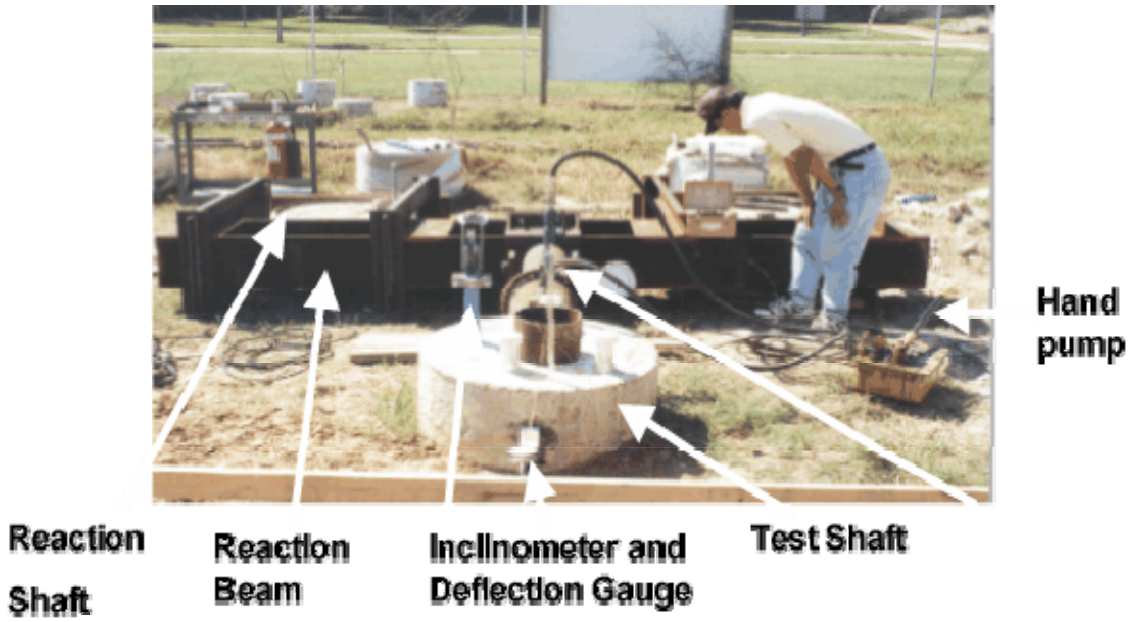

Figure 2.27. Setup for a Conventional Load Test
(Source: http://www.fhwa.dot.gov/infrastructure/tccc/tutorial/shafts/fhcha10.htm)

In this test, the test shaft is pulled away from the two reaction shafts and the readings are taken using the dial gauge fitted to the test shaft. The inclinometer casing cast into the drilled shafts along the centroidal axis is used to measure the deflection of the shafts. As a result, the p-y curves can be obtained directly from the load tests if the bending moment is considered as a function of the lateral loads and the depth (Welch and Reese, 1972; Dunnavant and O'Neill, 1989). The disadvantage of this method is that it is very expensive compared to other testing methods. However, several reaction piles can be installed with a single I-beam framework bolted to the reaction piles and the number of test shafts can be increased since they will be of a smaller magnitude and depth in comparison to the reaction piles.

2.6.1.2 Osterberg Cell Test

The Osterberg Cell, or O-cell, named after its inventor, Dr. Jorj O. Osterberg, has radically changed the way foundation load tests are designed, performed, and interpreted. This test can be performed on high capacity piles at low costs unlike the Conventional Load test. In this method, the Osterberg cell is installed within the drilled shaft during construction as shown in Figure 2.28. The cell is mounted on a reaction socket which is made of two plates. These plates are then hydraulically jacked apart to mimic the effect of lateral loading. Lateral displacement is measured using Linear Variable Displacement Transducers (LVDTs) connected between the plates. The lateral load applied can be calculated by dividing the load in the cell by the length of the socket.

Figure 2.28. Setup for an Osterberg Cell Test
(Source: http://www.loadtest.co.uk/Loadtest%20Ltd/downloads.htm)

2.6.1.3 Statnamic Load Test

Drilled shafts are also tested in the lateral direction by placing Statnamic devices transversely to the shaft (O'Neill et al., 1990; Rollins et al., 1997). In this test, lateral loads are instantly applied to the shaft with the help of a propellant accelerated to generate heavy forces (Figure 2.29). This type of test is more economical when there are no reaction frames. Also the type of loading that is applied is impact loading. McVay (2003) conducted a study to collect a database of Statnamic and conventional tests on drilled shafts and driven piles in different soil and rock conditions to establish resistance factors for Load Resistance Factors Design (LRFD) used to design bridge supports.

Figure 2.29. Setup for a Statnamic Test
(Source: http://www.fhwa.dot.gov/infrastructure/tccc/tutorial/shafts/fhcha10.htm)

Lateral load tests were conducted by several researchers in nonexpansive soils and a few of these results are discussed in tasks outlined in the work plan. Houston et. al (2004) conducted lateral load tests to assess the performance of drilled shafts installed in cemented sands. In the case of high-plasticity clays, limited test results are available but a recent one is included here.

Greis and Muchard (2009) conducted tests for Northgate Constructors, Inc. for TxDOT's DFW Connector Design-Build project. Vertical and lateral load tests were performed on drilled shafts in stiff and lean clays to determine whether the LRFD curves could be adjusted to reduce column diameters and depths for bridge structures. The stiff clays consisted of soils created from the Eagle Ford formation and the lean clays consisted of soils created from the Woodbine formation. These tests were conducted in soils similar to those used in this research.

2.6.1.4 Load Testing of Drilled Shafts in an MSE Wall (KDOT)

A research project performed under the purview of the Kansas DOT investigated the capacity of laterally loaded shafts behind an MSE block wall (Pierson et al., 2009).

2.6.1.4.1. Design and Field Details

Eight (8) drill shafts were constructed in the select fill behind the modular block wall face. Geogrid was used as the reinforcement in the fill for the blocks as shown in Figure 2.30.

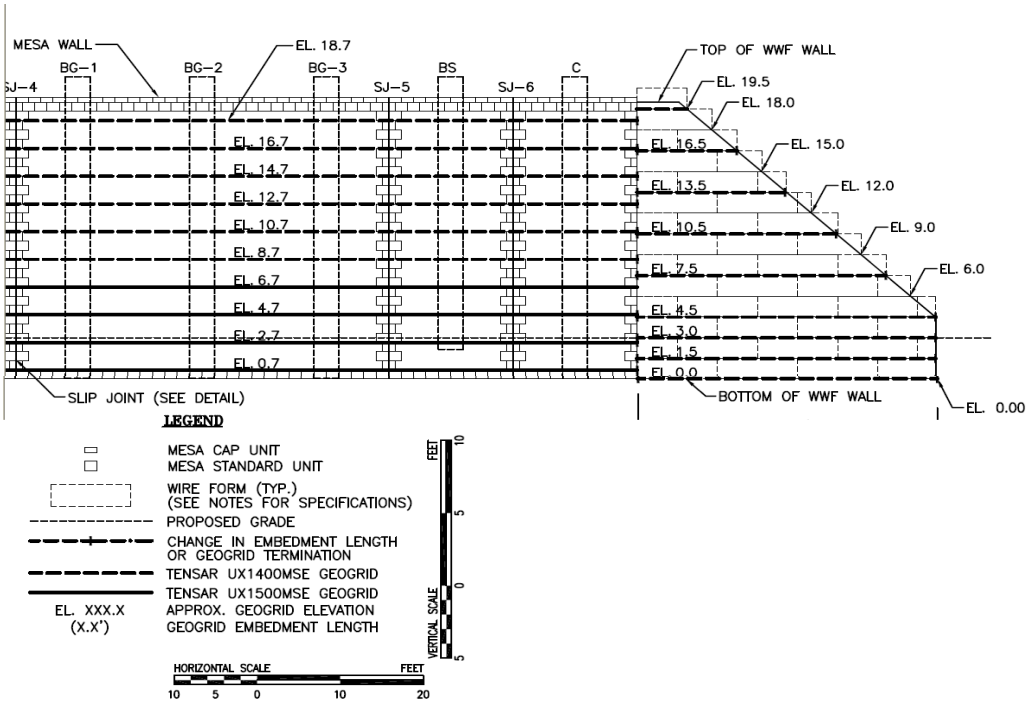

Figure 2.30. Wall and Drill Shaft Layout (Tensar, 2007)

The researchers used load cells and LVDTs to measure the movements of the shafts and wall face. Inclinometer readings were taken frequently to record horizontal movements. The inclinometer casings can be seen in Figure 2.31 below as blue with red caps attached to the face of the wall.

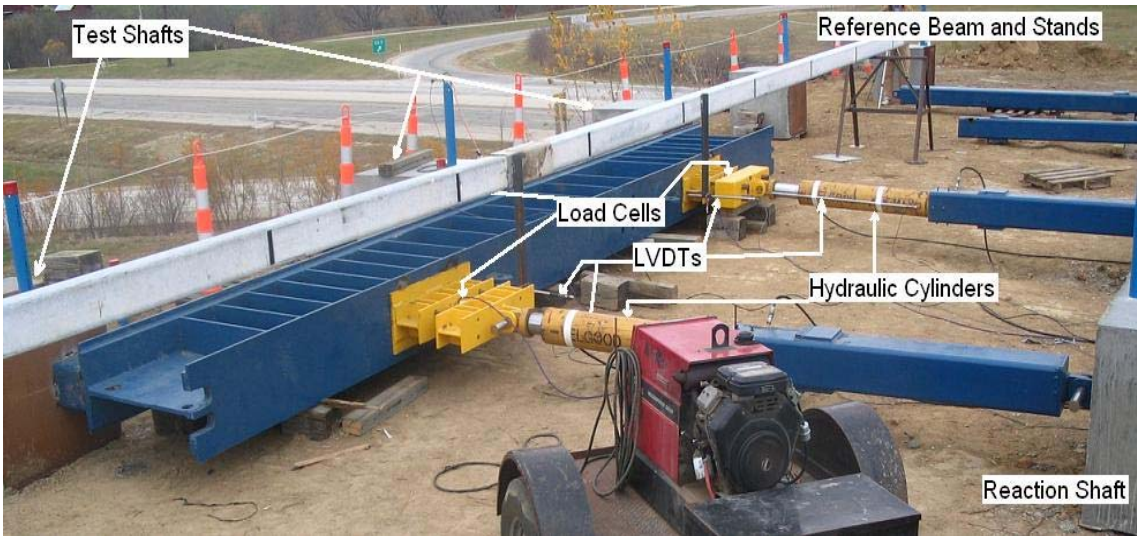

Figure 2.31. View of Instrumentation (Pierson et al., 2009)

Figure 2.32 shows a typical load graph of a single test shaft. The peaks represent final loading for each increment and the low points show unloading prior to the next load increment application. The LVDT results show an increase upon loading and a flat line for the 5 minute holds in order to take inclinometer readings.

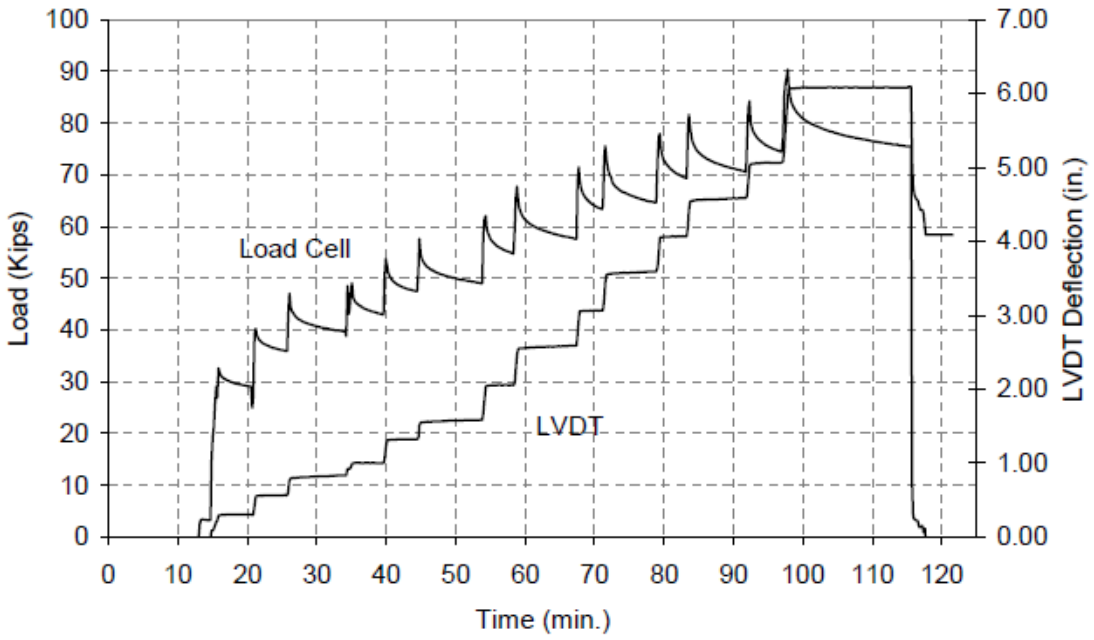

Figure 2.32. Typical Graph Showing Loading and Deflections (Pierson et al., 2009)

2.6.1.4.2 Physical Results

The topsoil cover cracked during the testing process. All of the shafts had cracks form behind the shafts due to caving and from the sides at a diagonal toward the wall facing as a result of shaft movement. Figure 2.33 shows typical cracks that formed directly behind each shaft and cracks that formed at a diagonal to the sides of the shaft.

Figure 2.33. Typical Cracks After Testing (Pierson et al., 2009)

2.7 Summary

In this chapter, many different research efforts allowed the universities to develop and test many different types of analysis theories. Most are in use today, either still directly applied or used as the base for the framework of advanced computer software programs designed to introduce many variables once considered tedious to run due to the sheer volume of computations required. Today's computers can run many trials in a relatively short time with great accuracy allowing designers to run multiple trials in order to select the best method.

CHAPTER 3

SITE SELECTION AND LABORATORY TESTING

3.1 Introduction

This chapter describes the site that was selected for the field test setups. It also describes the laboratory tests in detail that were performed on the soils collected from the site.

3.2 Site Selection

3.2.1 Site Location

During the site selection process, two sites were proposed. The first site was Interstate Highway (IH) 20 at Rose Hill Road and the second one was IH 20 at FM 2578, both in Kaufman County. Several criteria, such as high-plasticity characteristics of the CH soil at Site 1 or cable barrier foundations that experienced distress problems at Site 2, were considered in the selection process but the most important criterion was if the area would have enough space to allow the installation of the field test setups. Site 2 was excluded due to the lack of available area between the right-of-way (ROW) line and the roadway for the construction of the test setups. This was a safety concern for the workers, testers, and the travelling public. Comparing the two sites, the first location met the criteria much better than the second one. Therefore, the test site located on IH 20 and Rose Hill Road was selected as shown in Figure 3.1.

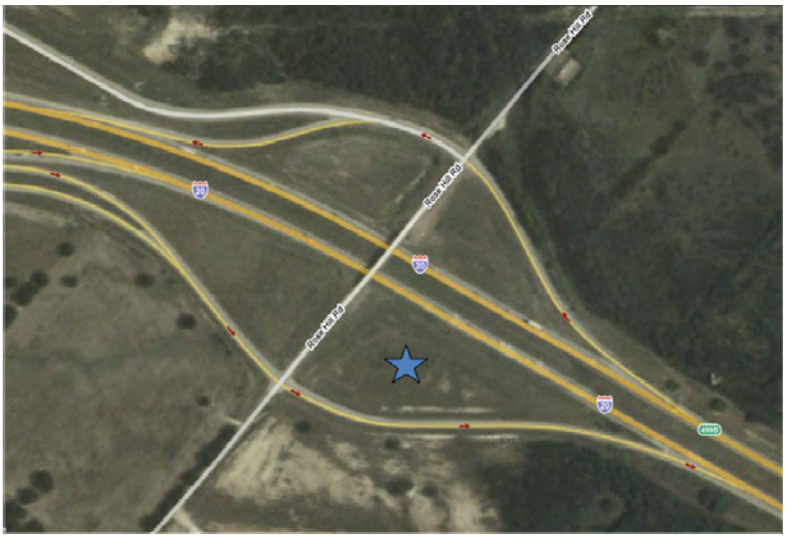

Figure 3.1. Test Site Located on IH 20 and Rose Hill Road
(Source: http://maps.google.com/maps. January 2008)

3.2.2 Soil Sampling

For identifying properties of the in-situ soil, a backhoe was used to excavate the soil to expose the different soil layers. A total of five (5) soil layers were found within the test shaft maximum design depth of 14 ft (4.3 m). Representative samples of the different soil types found in each layer were taken for laboratory testing. A nuclear density gauge was used to determine the field density in each soil layer. These two operations can be seen in Figure 3.2.

Figure 3.2. Soil Sampling and Field Density Measurement by Using a Nuclear Density Gauge

3.3 Laboratory Testing

All of the physical and engineering tests were performed at the UTA Laboratory with the exception of the field tests. The test methods used and additional comments regarding each are included in the following sections. All results and summaries of each are included in Chapter 4.

3.3.1. Physical Tests

The soil samples collected in the five (5) different soil layers were subjected to a variety of laboratory physical tests including specific gravity, Atterberg limits (ASTM Test Method D4318-10), and linear shrinkage bar tests (TxDOT Test Method Tex-107-E). These tests were necessary to classify the soils in accordance with the Unified Soil Classification System (USCS) method (ASTM Test Method D2487-10). All of the soils were classified as fine-grained since more than 50% of the particles passed through the No. 200 sieve.

3.3.2. Engineering Tests

3.3.2.1 Standard Proctor Compaction Test

Standard Proctor Compaction tests were performed using ASTM Test Method D698-07, "Standard Test Methods for Laboratory Compaction Characteristics of Soil Using Standard Effort (12,400 ft-lbf/ft^3 (600 kN-m/m^3))" to establish moisture-density relationships. The purpose was to determine the optimum moisture content (OMC) at the maximum dry density of the soil. Water contents at 95% of the maximum dry density conditions representing dry of OMC and wet of OMC were selected for testing as shown in Figure 3.3.

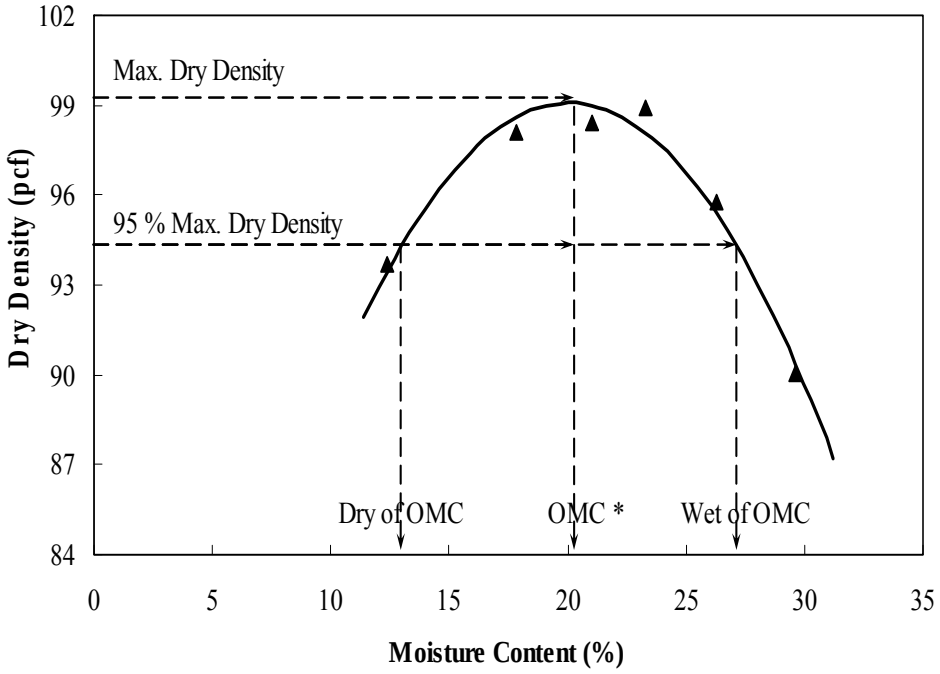

Figure 3.3. Typical Standard Compaction Curve for a Clay or Sand

3.3.2.2 Direct Shear Test

The Direct Shear test employs a simple method for finding the shear stress and friction angle of soils. This test was performed using ASTM Test Method D3080-04, "Standard Test Method for Direct Shear Test of Soils Under Consolidated Drained Conditions". The soil specimen can be cubical or cylindrical. The shape used in this test was cylindrical. Normal forces used for the Direct Shear test were 2000, 4000, and 8000 psf (95.8, 191.5, and 383 kN/m^2). The specimen tested was the silty sand located in the first layer (0 – 3 ft (0-1 m)). The other four (4) layers were predominantly classified as lean or fat clay; therefore, this test was not applicable to these soils. Three (3) identical specimens were prepared and tested at the same moisture content and dry density as measured in the field; 19% moisture content and 92.7 pcf (14.85 kN/m^3) dry density. The equipment and a typical soil specimen used in the test are shown in Figure 3.4 below.

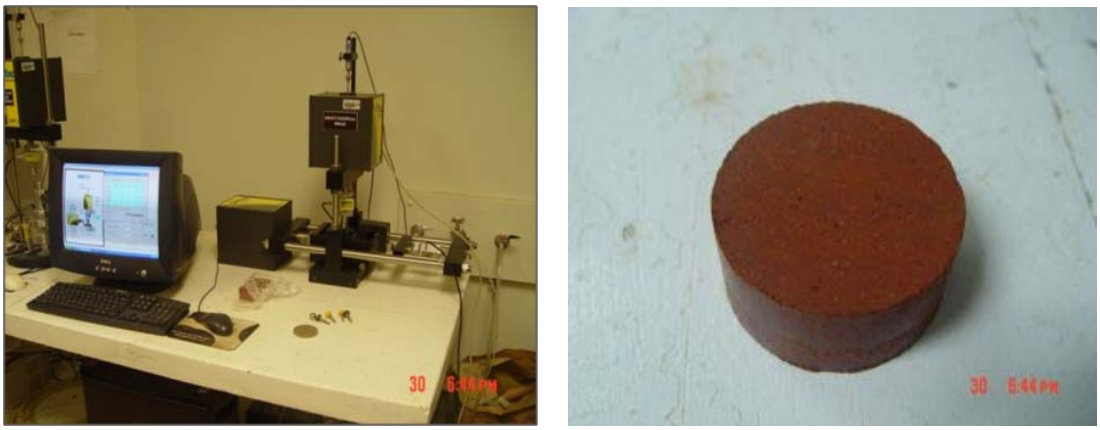

Figure 3.4. The Direct Shear Test Setup and Compacted Silty Sand Used in the Test

3.3.2.3. Unconsolidated-Undrained (UU) Triaxial Test

The unconsolidated-undrained test is used to find the shear strength parameters (c and ϕ). This test is performed using ASTM Test Method D2850-03a, "Standard Test Method for Unconsolidated-Undrained Triaxial Compression Test on Cohesive Soils." The test method is performed by placing a cylindrical soil specimen, sealed by a rubber membrane, in the triaxial chamber. A lateral confining pressure is applied disallowing porewater to dissipate from the specimen. Finally, an axial load is continuously applied down from the top of the soil specimen thereby increasing the vertical stress until the specimen fails in shear. A typical failed soil specimen from the UU test due to shearing is shown in Figure 3.5 below. In the Figure, it appears that the specimen failed due to bulging but the shear actually caused the specimen to become larger than it's original shape.

Figure 3.5. Typical Failed Triaxial Specimen

UU tests were performed on the soils in an unsaturated and saturated condition. For the unsaturated condition, all soil specimens were approximately prepared to the same moisture content and density as that determined in the field from the nuclear density test. The soil specimens were then subjected to UU testing. For the saturated condition, all soil specimens were prepared at the same moisture content and density and then saturated by soaking totally submerged under water for two to four weeks.

3.3.2.4 One-Dimensional (1-D) Swell Pressure Test

Swell pressure tests were conducted on all soil samples using ASTM Test Method D4546-08, “Standard Test Methods for One-Dimensional Swell or Settlement Potential of Cohesive Soils”. Figure 3.6 shows the test setup used for this method. These results were used in the estimation of uplift forces on the cable barrier system foundation drill shafts. According to Sridharan et al. (1986) and Fredlund and Rahardjo (1993), the swell pressure tests are

performed by determining the maximum loads or pressures that soils can withstand while maintaining their original volume. When a soil stops expanding in the presence of excess water, the pressure at that time is considered the maximum swell pressure. Soils tested at wet of OMC usually reveal low pressures while soils tested at dry of OMC usually reveal high pressures. This is exhibited by soils in the field being in the dry of OMC phase created by extended drought periods and then exposed to heavy rainfall periods. The resultant swells are evidenced by vertical movement of structures. Three (3) soil specimens were compacted to the same moisture content and density as that determined in the field from the nuclear density test. The specimens were then placed in a controlled moisture room for a minimum of 24 hours to equalize the moisture content before testing.

Figure 3.6. One-Dimensional (1-D) Swell Pressure Test Setup

3.3.2.5. Three-Dimensional (3-D) Free Swell Test

The three-dimensional (3-D) free swell test provides a reasonable representation of the soil's maximum volumetric swell potential (Punthutaecha et al., 2006). The 3-D swell tests were

conducted to investigate the maximum vertical, radial, and volumetric swell potential of the field soils at various depths. Three (3) specimens were prepared at three (3) different moisture contents (dry of optimum, optimum, and wet of optimum moisture content) for each soil layer. In addition, one specimen was prepared at the field moisture content and density. The majority of the swell strains were observed within the first eight (8) hours with subsequent swell strains continuously recorded until no further swell movement was measured.

All of the specimens were prepared to a 4.0 in. (101.6 mm) diameter by 4.6 in. (116.8 mm) height, placed between two porous stones (Figure 3.7a), wrapped in a rubber membrane, and subjected to soaking by inundating with water from both ends. A typical test setup is shown in Figure 3.7b. Measurements were taken at the top, middle, and bottom circumferences of the samples and averaged at a frequency similar to the Consolidation Test. This was done until the soil stopped swelling in the presence of water.

(a)

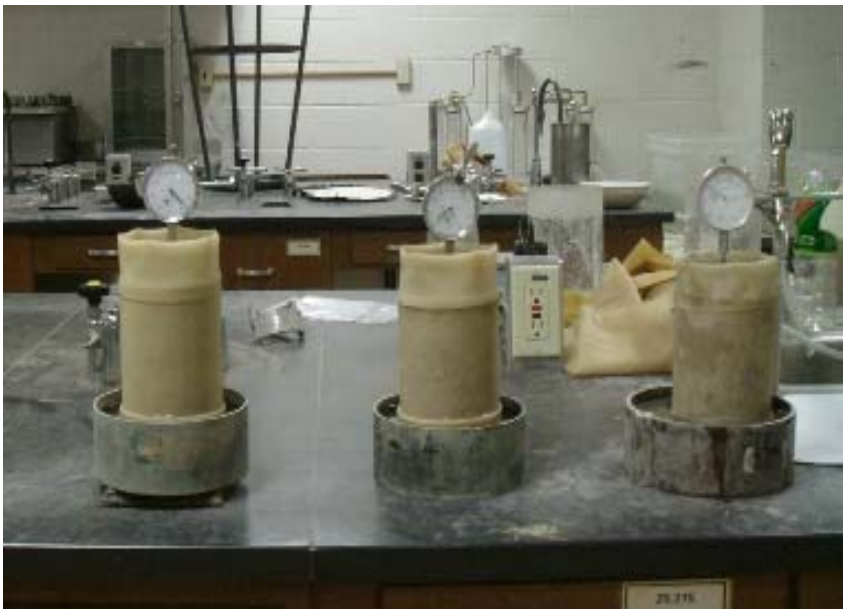

(b)

Figure 3.7. Three-Dimensional (3-D) Swell Test with (a) Radial Strain Measurement and (b) Test Setup of 3-D Swell test (Dry of OMC, OMC and Wet of OMC (left to right)) in Progress

3.3.2.6. Three-Dimensional (3-D) Shrinkage Test

This test was developed at UTA due to limitations in the linear bar shrinkage test (TxDOT Test Method Tex-107-E). This test method was published in an ASTM geotechnical testing journal (Puppala et al., 2004) signifying the importance of it as a potential replacement for the linear bar shrinkage test once accepted by peer researchers and practitioners. There are several advantages of the volumetric shrinkage test over the conventional linear bar shrinkage test such as reduced friction at the mold surfaces with the soil, a greater amount of soil can be tested allowing for a better representative sample, and better simulation of the compaction states of the moisture content - dry density conditions.

Volumetric shrinkage tests were conducted to measure the decrease in the total volume of the soil specimens, due to the loss of moisture from the predetermined initial moisture content, to a completely dry state. Three (3) different initial moisture contents (dry of optimum, optimum, and wet of optimum) were used as the initial compaction conditions. Specimens were prepared by mixing the air-dried clay with an appropriate amount of water added to achieve the design water contents, compacting the soil specimens in 2.26 in. (57 mm) diameter by 5 in. (127 mm) high molds, and measuring the initial height and radial dimensions of the specimens. The specimens were cured in the molds at room temperature for 12 hours. They were transferred to an oven at a temperature of 220° F (104° C) and dried for 24 hours. Upon removal from the oven, the average height and radial dimensions of the dried soil specimens were manually measured. The volumetric shrinkage strain was calculated from these measurements. Figure 3.8 shows a typical example of the specimens just after molding and after drying.

(a)

(b) (c)

Figure 3.8. Typical Three-Dimensional (3-D) Shrinkage (a) Sample Preparation and Resultant Specimens (b) Before Testing and (c) After Testing

3.4. Summary

The test methods discussed were critical to the understanding and design of the reaction and test shafts used in this research. Since five (5) different soil types were uncovered at the field test site, a thorough knowledge of the properties was paramount to a proper design and expected positive field test results. As many of these tests are advanced, an experienced person was required to ensure proper test protocol in running each test and diligence to details to reduce equipment variability for precision and accuracy of the results.

CHAPTER 4

SUMMARY OF LABORATORY TEST RESULTS

4.1 Introduction

This chapter summarizes the physical and engineering test results that were performed on the soil samples from the five (5) layers collected in the field. Important results culminating from the testing are noted in each section.

4.2 Laboratory Testing

The laboratory test results shown in this chapter were measured based on the test methods performed as described in Chapter 3.

4.2.1. Physical Tests

The soil samples collected in the five (5) different soil layers were subjected to Atterberg limit and linear shrinkage bar tests according to those listed in Section 3.3.1. The obtained test results are shown here in Table 4.1.

Table 4.1. Basic Soil Properties

Layer Number	Depth, ft (m)	LL	PL	PI	SL	% Linear Shrinkage	USCS Classification
1	0.0 – 1.0 (0.0 – 0.3)	N.A.	N.A.	N.A.	N.A.	0.00	Silty Sand
2	1.0 – 3.0 (0.3 – 0.9)	77	18	59	10	12.07	CH
3	3.0 – 5.0 (0.9 – 1.5)	47	20	28	14	8.40	CL
4	5.0 – 10.0 (1.5 – 3.0)	41	20	21	15	2.62	CL
5	> 10.0 (> 3.0)	33	21	12	17	2.10	CL

As seen from the PI and Classification columns, the soils in this area consist of a thin sandy layer, followed by a thicker, lower permeable, highly plastic clay layer, and then underlain by a less thick, more permeable, less plastic clay layer.

Focusing on the PI and % Linear Shrinkage results, it is observed that the Layer 2 and 3 soils are potentially problematic with elevated values compared to the Layer 1, 4, and 5 soils. Any % Linear Shrinkage values greater than 5% are considered high. The lower PI values indicate the potential for drill shaft failure based upon skin friction.

4.2.2. Engineering Tests

4.2.2.1 Standard Proctor Compaction Test

The Standard Proctor Compaction test, as described in Section 3.3.2.1, was conducted on the soils sampled from Layers 2 and 3, respectively. For this test, seven (7) specimens ("points") were compacted for the soil obtained from Soil Layer 2 and six (6) specimens ("points") were compacted for the soil obtained from Soil Layer 3. The number of specimens compacted were required to provide at least two (2) "points" on the wet side and two (2) "points" on the dry side of the estimated optimum moisture content (OMC). This allows a "best-fit" curve to be drawn to establish the actual percent moisture content and dry density for each soil. The percent moisture content and the dry density determined for each "point" are plotted for each soil layer and are shown in Figures 4.1 and 4.2. The dry densities achieved from the soils in the field by the Nuclear Gauge are also shown on these figures as a yellow dot. It should be noted here that there is no correlation between the natural field densities and the laboratory compaction tests as the laboratory tests were merely conducted without any specific intent.

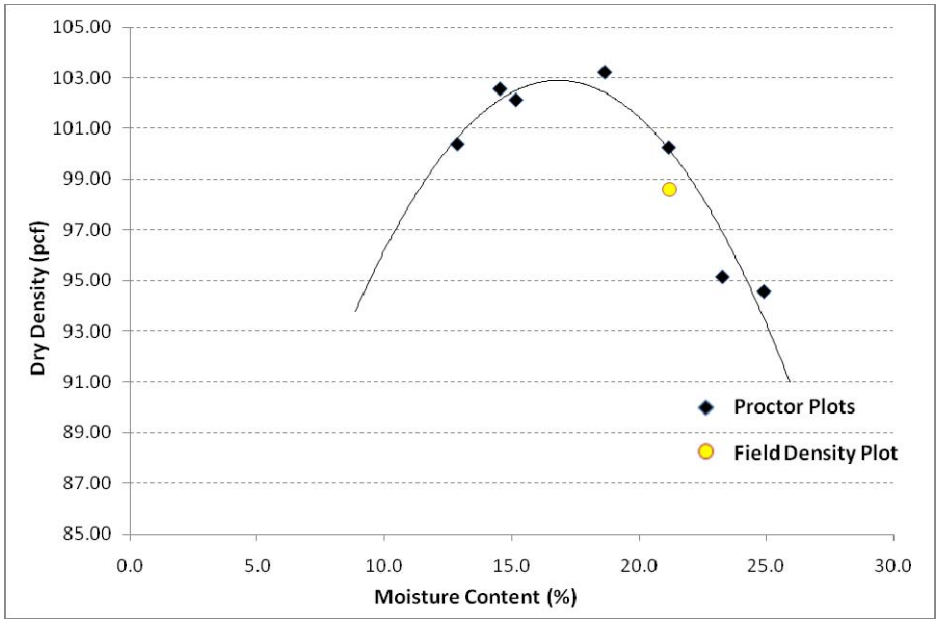

Figure 4.1. Standard Compaction Curve and Point of Field Density of Soil Layer 2

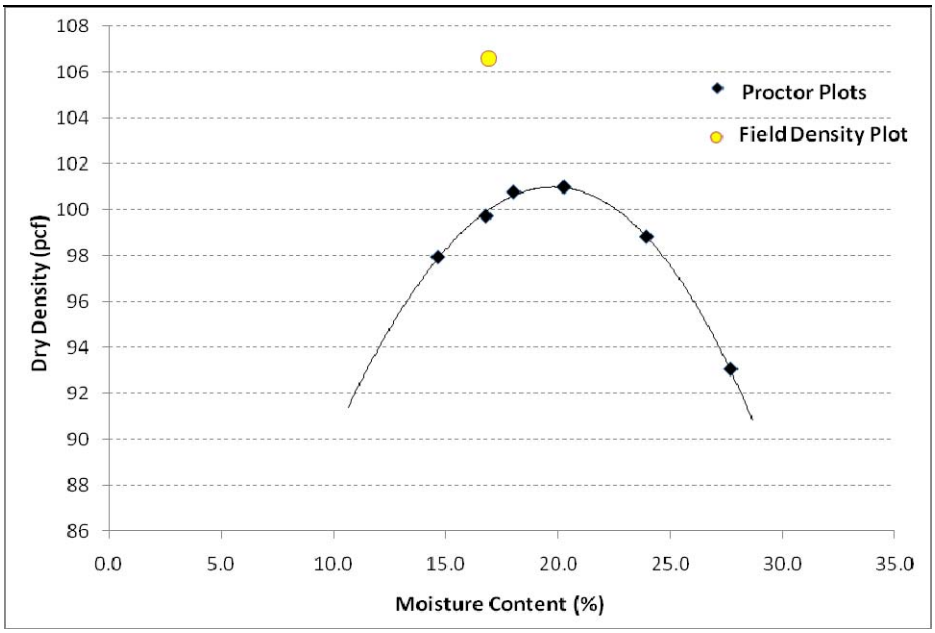

Figure 4.2. Standard Compaction Curve and Point of Field Density of Soil Layer 3

Table 4.2 summarizes the results of the tests run at dry of OMC, OMC, and wet of OMC. It is noted that all three compaction moisture content conditions are used as reference moisture contents for other engineering tests performed in this research.

Table 4.2. Standard Proctor Compaction Test Results

Property	Moisture Condition	Layer 2 1.0 - 3.0 ft (0.3 – 0.9 m)	Layer 3 3.0 - 5.0 ft (0.9 – 1.5 m)
Moisture Content (%)	Dry OMC	10.91	13.02
	OMC	16.80	19.80
	Wet OMC	22.80	26.05
Dry Density, pcf (kN/m^3)	Dry OMC	97.76 (15.7)	95.95 (15.4)
	OMC	102.90 (16.5)	101.00 (16.2)
	Wet OMC	97.76 (15.7)	95.95 (15.4)

Note: OMC – Optimum Moisture Content in %

Soils in the field undergo moisture content fluctuations during the seasonal changes and hence it is important to determine the properties of soils over a wide range of moisture contents anticipated in the field. These properties were used for the numerical modeling of the field load tests on the drilled shafts as a part of the analysis task detailed in Chapter 6.

4.2.2.2 Direct Shear Test

The Direct Shear Test, as described in Section 3.3.2.2, was only performed on the silty sand (Soil Layer 1) due to its' natural density condition. The confining pressures used in the test are plotted and shown in Figure 4.3. The resultant plot from these three (3) pressures is shown in Figure 4.4 which provided a cohesion intercept, c, equal to 0 psf (0 kPa) and an internal friction angle, ϕ, equal to 26.2°.

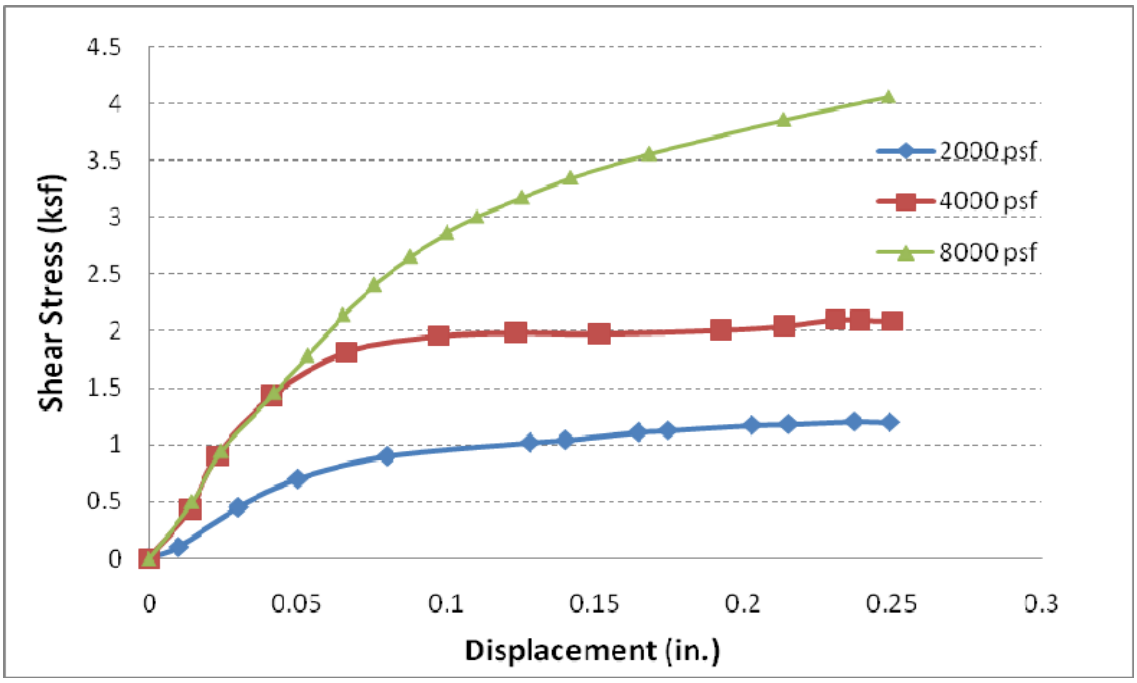

Figure 4.3. Shear Stress versus Horizontal Displacement for the Silty Sand

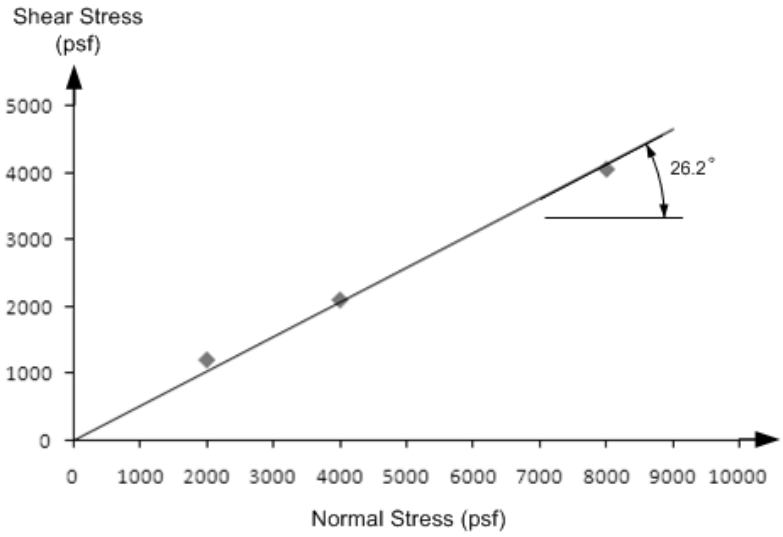

Figure 4.4. Shear Strength versus Effective Normal Stress for the Silty Sand

4.2.2.3. Unconsolidated-Undrained (UU) Triaxial Test

The Unconsolidated-Undrained Triaxial test, described in Section 3.3.2.3, describes the procedure used for performing theses tests on the clay soils; both the high-plasticity CH clay in

Soil Layer 2 and the lean CL clay in Soil Layers 3 through 5. The tests were performed on remolded samples rather than undisturbed due to the unavailability of a drilling rig to secure undisturbed samples. These tests provided the cohesion intercept, c, and the internal friction angle, ϕ, of the different clays in both the unsaturated and fully saturated conditions. The UU results obtained at different confining pressures, σ_3, and the typical shear failure envelope plots are shown in Figures 4.5 through 4.8. Actual numeric test values are shown in Tables 4.3 and 4.4.

4.2.2.3.1 Unsaturated Condition

The unsaturated condition describes the soil at a degree of saturation less than 100%. Air and water is contained within the pores of the soil structure. If the soil's moisture content is 0%, air has completely replaced all of the water. As shown in Tables 4.3 and 4.4, the water content changes between each soil type in the different clay layers. Three (3) unconsolidated-undrained triaxial tests were conducted on each of the clay soils from Soil Layers 2 through 5 in the unsaturated condition. Figures 4.5 and 4.6 present these test results. The various levels of unsaturated soil are shown per the moisture content, w, in Table 4.3.

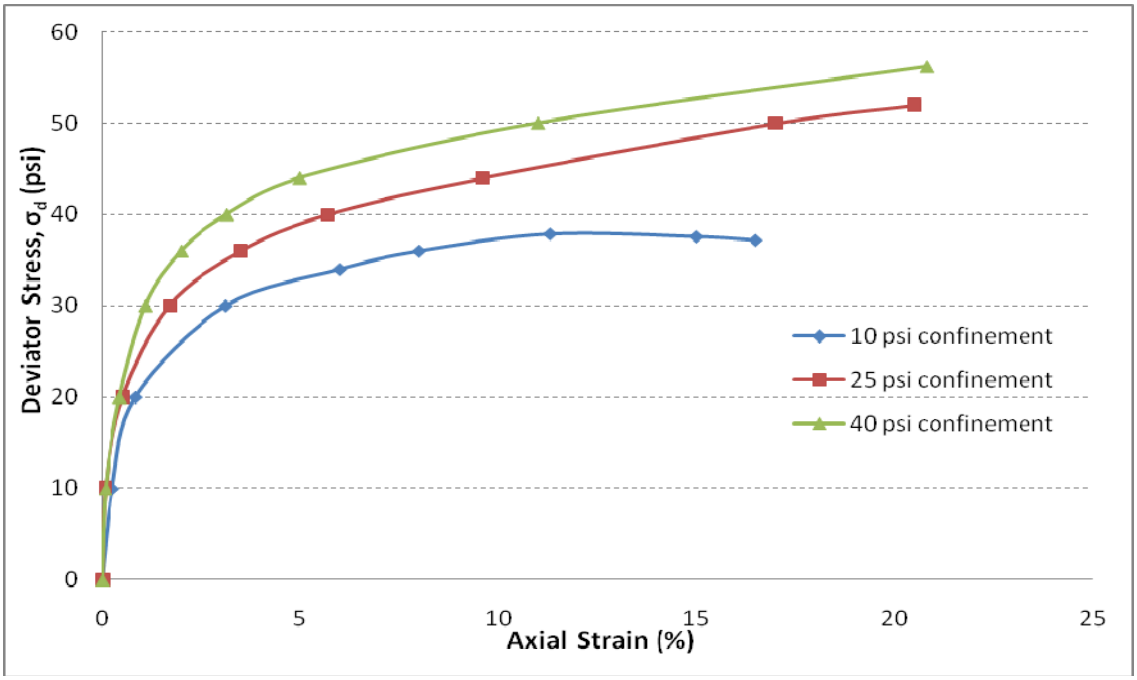

Figure 4.5. UU Test Results for Unsaturated Soil Layer 3

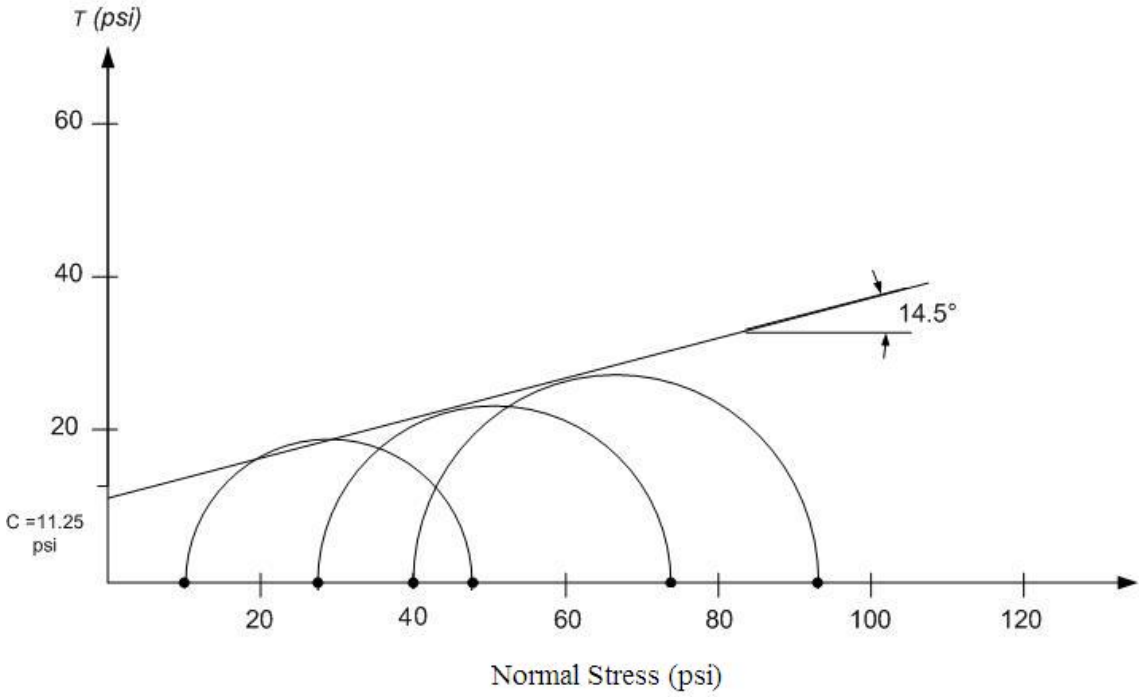

Figure 4.6. Shear Failure Envelope for the Unsaturated Soil Condition

Table 4.3. Unconsolidated-Undrained Test Results for the Unsaturated Soil Condition

Depth, ft (m)	w (%)	γ_{dry}, pcf (kN/m^3)	Cohesion, c, psi (kPa)	Friction Angle, ϕ, °
1.0 – 3.0 (0.3 – 0.9)	21.2	98.6 (15.8)	7.10 (49)	7.5
3.0 – 5.0 (0.9 – 1.5)	16.9	106.6 (17.1)	11.25 (77.6)	14.5
5.0 – 10.0 (1.5 – 3.0)	15.7	119.17 (19.1)	17.45 (120.3)	7.5
> 10.0 (> 3.0)	12.9	110.96 (17.8)	8.98 (61.9)	28.6

Figure 4.5 depicts the stress-strain curves of the clay in Soil Layer 3, with confining pressures ranging from 10 – 40 psi (69 - 276 kPa). Once the confining pressures are achieved, the deviator stress, σ_1, is applied and increased at a constant rate of strain until failure of the soil specimen in shear. These curves are used to plot the Mohr's circles allowing the cohesion and friction angle to be determined from the shear failure envelope as shown in Figure 4.6. The cohesion intercept is 11.25 psi (77.6 kPa) and the friction angle is 14.5°. The Mohr's circles for Soil Layers 2, 4, and 5 were also drawn, the shear failure envelope plotted, and the cohesion and friction angles were determined from the respective graphs with their values shown in Table 4.3.

4.2.2.3.2. Saturated Condition

Three (3) unconsolidated-undrained triaxial tests were also conducted on each of the clay soils from Soil Layers 2 through 5 after soaking them to a saturated condition. Saturation greater than 90% was achieved as per the following equation:

$$\text{Saturated unit weight} = \gamma_{sat} = \frac{G_s \gamma_\omega (1+\omega)}{1+G_s \omega} \quad (4.1)$$

Following saturation, samples were immediately subjected to shearing "at a rate of approximately 1% / minute for a plastic material" (ASTM D2850-03a). Figures 4.7 and 4.8 present these test results. These are regarded as undrained total strength parameters as tests were conducted in the unconsolidated and undrained condition.

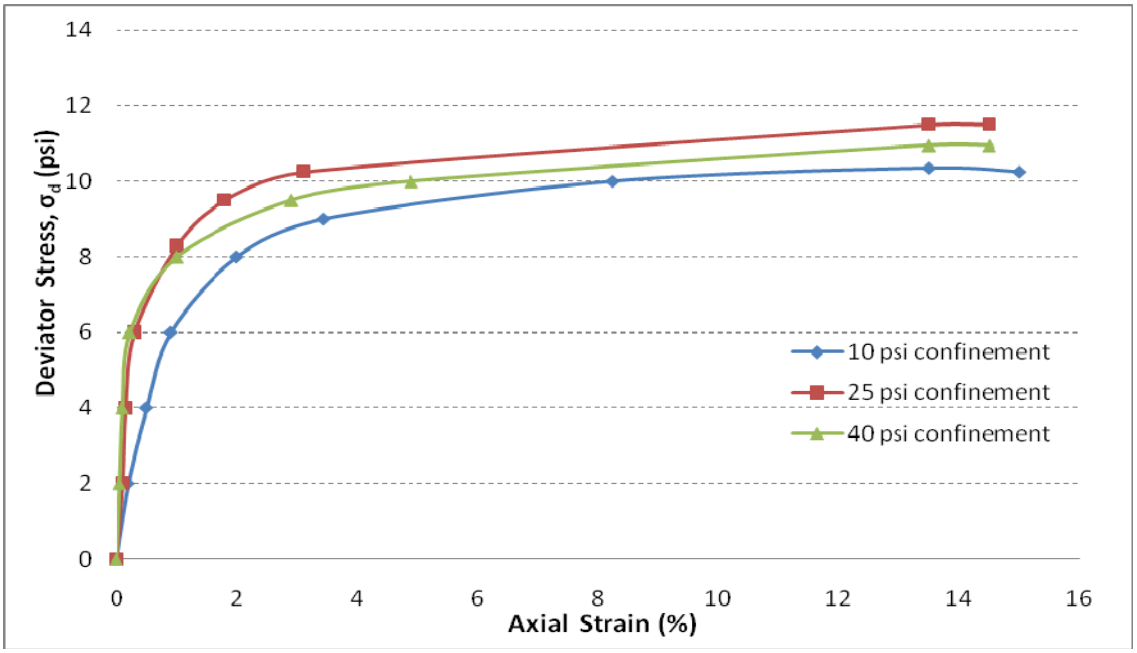

Figure 4.7. UU Test Results for Saturated Soil Layer 3

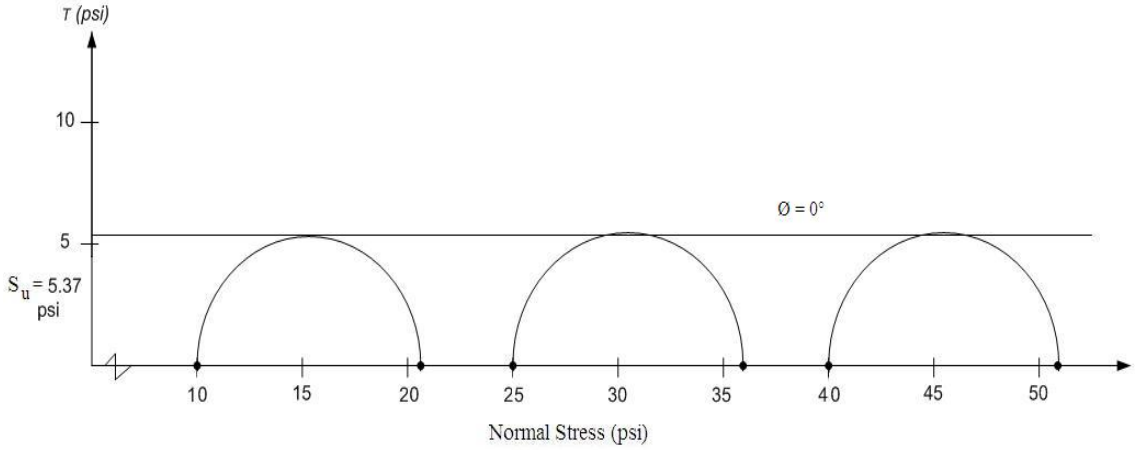

Figure 4.8. Shear Failure Envelope for the Saturated Soil Condition

Table 4.4. Unconsolidated-Undrained Test Results for the Saturated Condition

Depth ft (m)	w (%)	γ_{dry}, pcf (kN/m^3)	Undrained Shear Strength, s_u, psi (kPa)
1.0 – 3.0 (0.3 – 0.9)	32.3	98.6 (15.8)	5.97 (41.2)
3.0 – 5.0 (0.9 – 1.5)	26.3	106.6 (17.1)	5.37 (37.0)
5.0 – 10.0 (1.5 – 3.0)	19.2	119.2 (19.1)	3.75 (25.9)
> 10.0 (> 3.0)	17.1	110.9 (17.8)	3.06 (21.1)

Figure 4.7 depicts the stress-strain curves of the clay in Soil Layer 3 with the same confining pressures used in the unsaturated soil condition. Once the confining pressures are achieved, the deviator stress, σ_1, is applied and increased at a constant rate of strain until failure of the soil specimen in shear. These curves are used to plot the Mohr's circles allowing the cohesion and friction angle to be determined from the shear failure envelope as shown in Figure 4.6. As expected, these tests provided undrained shear strengths, s_u/cohesion, with undrained friction angle values close to 0 degrees since samples were saturated and unconsolidated. The undrained shear strength (cohesion) intercept is 5.37 psi (37.0 kPa). The Mohr's circles for Soil Layers 2, 4, and 5 were also drawn, the shear failure envelope plotted, and the undrained shear strengths (cohesions) determined from the respective graphs with their values shown in Table 4.4. The undrained shear strength values became lower as the soil PI decreased. In other words, the undrained shear strength will be lower for lean clays.

4.2.2.4 One-Dimensional (1-D) Swell Pressure Test

The 1-D swell pressure test was performed on the clay soils in Soil Layers 2 and 3 according to the procedures described in Section 3.3.2.4. The results of the swell pressures are shown in Table 4.5 below.

Table 4.5. Swell Pressure Test Results

Soil Sample	w (%)	γ_{dry}, pcf (kN/m^3)	Swell Pressure, ksf (kPa)
Soil Layer 2 1.0 – 3.0 ft (0.3 – 0.9 m)	21.2	98.6 (15.8)	1.28 (61.3)
Soil Layer 3 3.0 – 5.0 ft (0.9 – 1.5 m)	18.0	106.6 (17.1)	0.49 (23.5)

Note: w – Moisture Content and γ_{dry} – Dry Density

From Table 4.5, the swell pressures of Layer 2 are higher than those of Layer 3. This agrees with the Plasticity Index of these clays; the higher the PI, the higher the swell pressure due to the soil swelling in the presence of additional moisture. The pressure developed in the expansive clay (CH) found in Layer 2 is due to the low permeability and high plasticity of the soil. Overall, the swell pressure values measured for Soil Layers 2 and 3 are considerably high enough to potentially pose uplift problems in the field.

4.2.2.5 Three-Dimensional (3-D) Free Swell Test

The 3-D free swell test measures the capability of the clay to expand in three (3) directions when soaked under water. The three (3) values measured were vertical, radial, and volumetric strains as described in Section 3.3.2.5. Figures 4.9 through 4.14 depict the swell strains of the clays from Layers 2 and 3 when conditioned to the dry of OMC, at OMC, and wet of OMC moisture contents. The field density values are also plotted in each graph. Figures 4.9 and 4.12 show the curves measured in the vertical direction for Soil Layers 2 and 3. Figures 4.10 and 4.13 show the curves measured in the radial direction for Soil Layers 2 and 3. Figures 4.11 and 4.14 show the curves measured in the volumetric direction for Soil Layers 2 and 3. Table 4.6 presents the numeric values of swell strains at different compaction and natural moisture contents and for all three swell components.

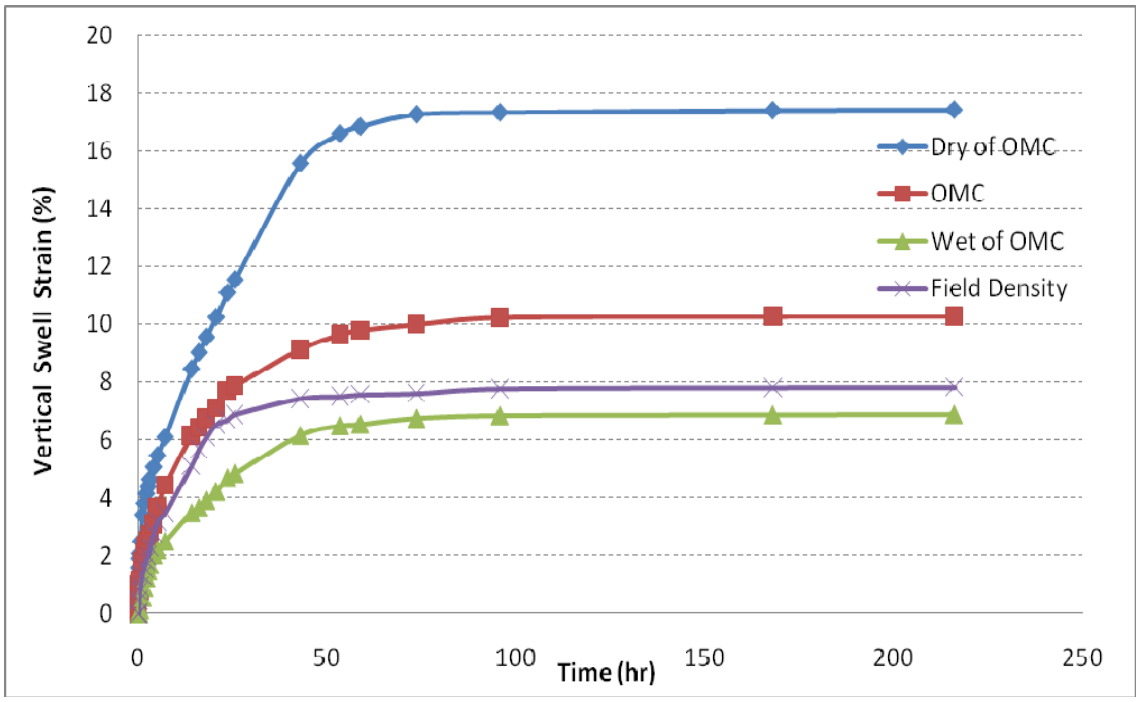

Figure 4.9. Vertical Swell Strain Results for Soil Layer 2 at Three Different Moisture Contents with One Field Density

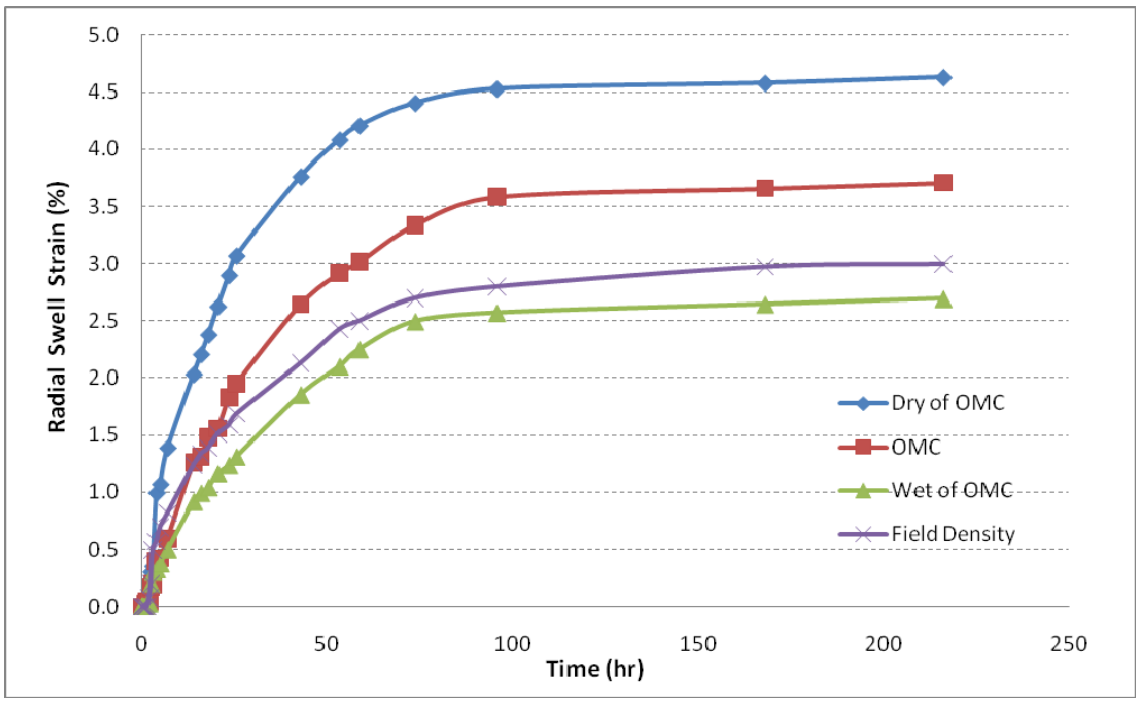

Figure 4.10. Radial Swell Strain Results for Soil Layer 2 at Three Different Moisture Contents with One Field Density

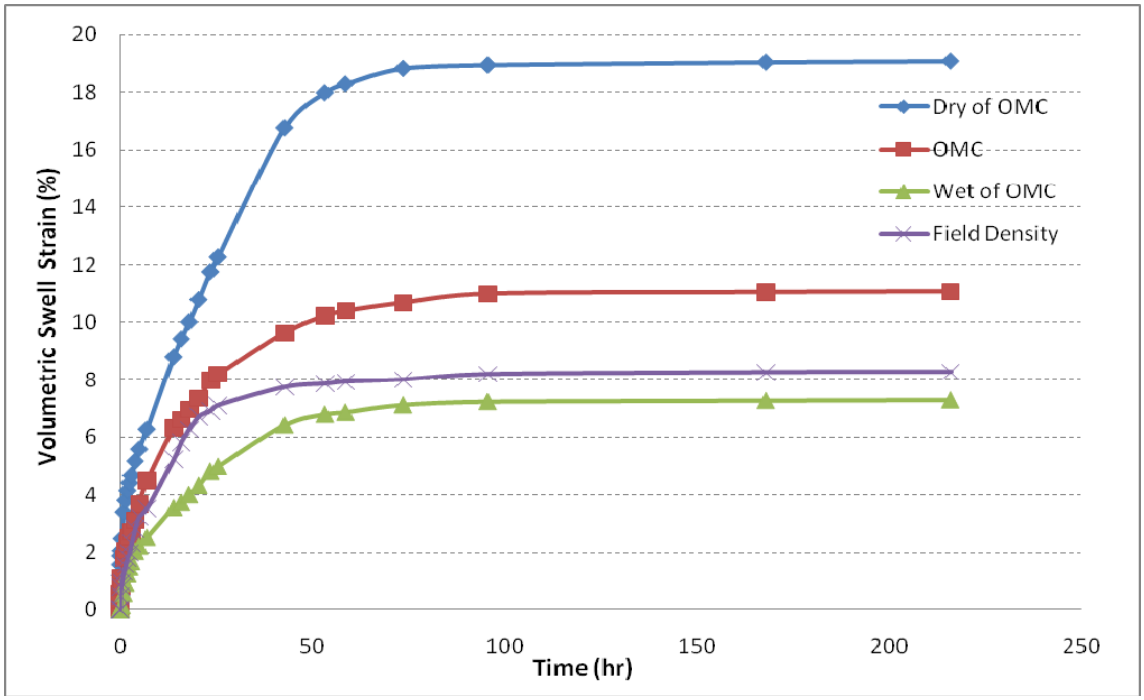

Figure 4.11. Volumetric Swell Strain Results for Soil Layer 2 at Three Different Moisture Contents with One Field Density

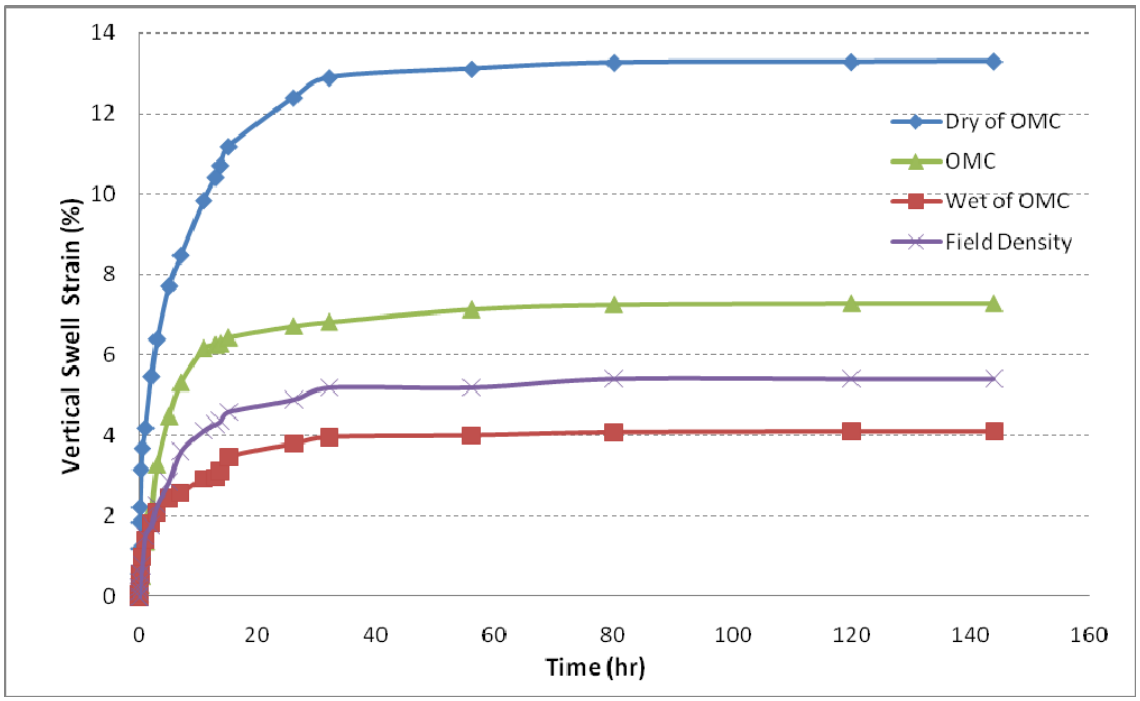

Figure 4.12. Vertical Swell Strain Results for Soil Layer 3 at Three Different Moisture Contents with One Field Density

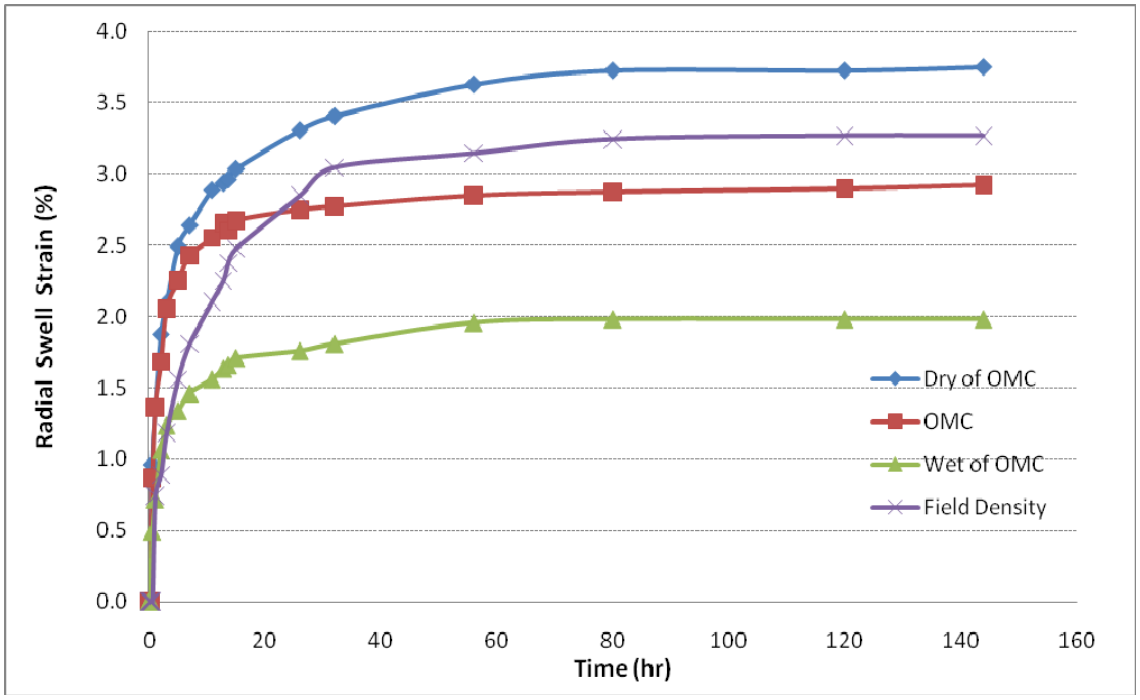

Figure 4.13. Radial Swell Strain Results for Soil Layer 3 at Three Different Moisture Contents with One Field Density

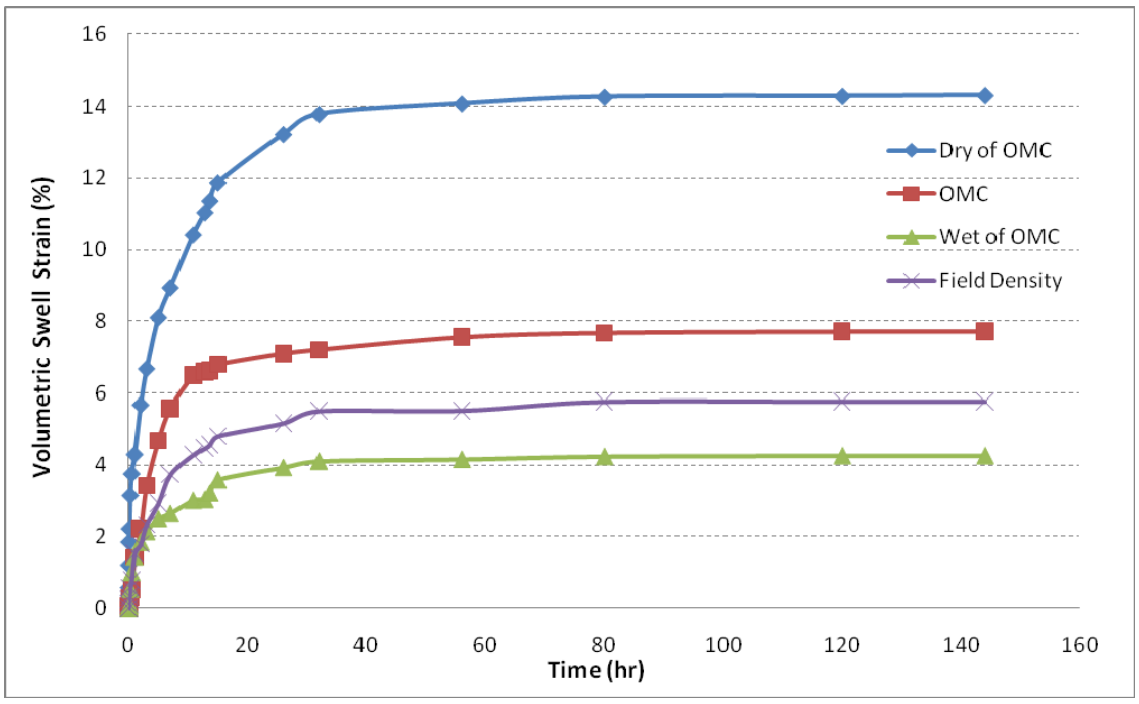

Figure 4.14. Volumetric Swell Strain Results for Soil Layer 3 at Three Different Moisture Contents with One Field Density

Table 4.6. Three-Dimensional (3-D) Volumetric Swell Strain Test Results

Description	Swell Strain (%)	
Moisture Condition	Soil Layer 2 1.0 – 3.0 ft (0.9 - 1.5 m)	Soil Layer 3 3.0 – 5.0 ft (1.5 - 3.0 m)
95 % Dry of OMC		
Vertical	17.44	13.30
Radial	4.63	3.73
Volumetric	19.09	14.32
OMC		
Vertical	10.29	7.28
Radial	3.71	2.87
Volumetric	11.07	7.71
95 % Wet of OMC		
Vertical	6.90	4.10
Radial	2.69	1.98
Volumetric	7.28	4.26
Field Density		
Vertical	7.83	7.28
Radial	3.00	3.24
Volumetric	8.28	5.77

Based on these results and those shown in Table 4.1, it can be concluded that Soil Layers 2 and 3 both have high swelling potential. The soil encountered between the 1.0 and 3.0 ft (0.9 - 1.5 m) depths of Layer 2 has a volumetric swell strain (for the OMC condition) value greater than 10% and this value indicates a high degree of expansion potential as per the problematic volumetric swell characterizations mentioned by Chen (1988). In addition, the soils encountered in Soil Layer 3 exhibited a PI value of 28, a linear shrinkage strain of 8.4%, and a volumetric swell strain of 7.7%. Again, these values indicate that this soil layer is a problematic expansive soil layer as per the soil characterizations mentioned by Chen (1988).

4.2.2.6 Three-Dimensional (3-D) Shrinkage Test

The 3-D shrinkage test measures the capability of the clay to diminish in the radial and vertical directions when subjected to drying. This test was performed according to the procedures listed in Section 3.3.2.6. Table 4.7 presents the numeric values of the shrinkage strains at three (3) different moisture contents.

Table 4.7. Volumetric Shrinkage Strain Test Results

Description	Shrinkage Strain (%)	
Moisture Condition	Soil Layer 2 1.0 – 3.0 ft (0.9 - 1.5 m)	Soil Layer 3 3.0 – 5.0 ft (1.5 - 3.0 m)
95 % Dry of OMC		
Vertical	1.93	1.34
Radial	1.70	1.19
Volumetric	5.24	3.68
OMC		
Vertical	3.01	1.87
Radial	1.97	1.73
Volumetric	6.79	5.22
95 % Wet of OMC		
Vertical	4.37	2.91
Radial	2.19	2.58
Volumetric	8.51	7.85

These test results indicate that the present soils undergo large volumetric shrinkage strains when subjected to drying. Such strains are expected to induce problematic soil conditions in the field during drought type situations. The swell potential is maximized when the soil loses its' moisture to an almost completely dry state when subjected to extended drought periods common to Texas.

4.3 Summary

The results achieved from these tests agree with published data as presented earlier. More careful scrutiny of the hypothetical failure mechanisms will be performed due to the differences in the clay soils.

CHAPTER 5

DESIGN AND CONSTRUCTION OF DRILLED SHAFTS

5.1 Introduction

Three test sets were designed and constructed on the selected site in 2009. Each test set contained four (4) test shafts of various diameters and depths. Two (2) different reaction shafts sizes were designed to accommodate the anticipated loads required on the individual test shafts to create deflections or displacements under inclined loading. The following sections describe the design and construction process. Additional information is included in the Appendices.

5.2 Design

5.2.1 Overall Design of the Field Test Setup

As a part of the main objective of this research to study the loading of drilled shafts in the inclined direction, a preliminary design was developed to mimic the cable barrier system used in the field that had failed as shown in Figure 1.1. This is one of the few inclined load field tests performed in the country based upon a thorough Literature Review. The design plan layout, as shown in Figure 5.1, was designed to have three (3) test sets completely separated from each other to eliminate any influence from any test performed at an adjacent set.

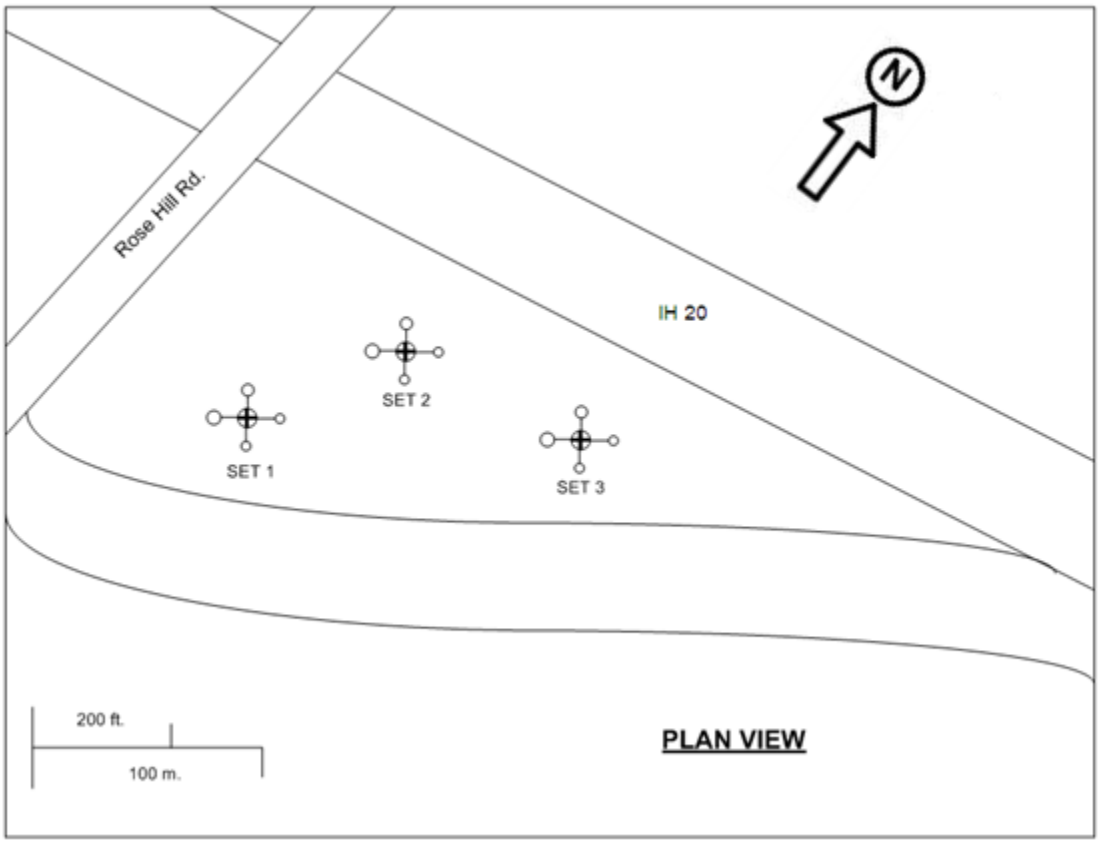

Figure 5.1. Plan View of Design Test Setups

One full test set system was comprised of one (1) reaction shaft and four (4) test shafts. A horizontal distance of 20 ft (6.1 m) was used between the reaction and test shafts per set. The angle of force acting toward each test shaft was set at 16.1 degrees (an approximate 6:1 slope) to copy the angle of the currently installed cable barrier system.

5.1.2 Design of the Reaction and Test Shafts

Originally, the dimensions of the drilled shafts that failed in the field were 2 ft (0.6 m) in diameter and 6 ft (1.8 m) deep (Heady, 2007). One of the hypothesized failure mechanisms was that of increased tensile forces due to cold weather providing additional load to the drill shaft foundations on each end of the cable barrier system run. Due to the inclination of the cable from the last vertical support to the drill shaft foundation, lateral and vertical loading had to be considered as discussed in Chapter 2. In lateral load testing, the distance between the test shaft

and the reaction shaft is a very important parameter. Stress created in the soil around the reaction shaft during the test can influence the results of the test shafts. A distance of 20 ft (6.1 m) between each test shaft and its' corresponding reaction shaft was selected based on ASTM Test Method D3966-07, Standard Test Method for Piles under Lateral Loads.

5.2.2.1 Reaction Shaft Design

One of the important steps for this testing was to design each reaction shaft such that the loading sequence followed in the procedure would not influence the test results of the test shafts.

The reaction shafts were used as foundations to subject inclined loads to the test shafts. A steel Dywidag bar was used between each reaction and test shaft which simulated the tension mobilized in the three-cable barrier system. Each test set was designed to provide the identical 16.1 degree slope from each reaction shaft to each of its' component test shafts. The reaction shaft had to be designed rigid enough to resist significant movements during load testing that would in no manner affect the test shaft reactions. The lateral pile load analysis software, LPILE, was used in the design to compute loads expected in the reaction shafts. The three (3) reaction shafts were designed to be 3 ft (0.9 m) and 4 ft (1.2 m) in diameter and 35 ft (10.7 m) deep.

5.2.2.2 Test Shaft Design

In order to determine the most effective size(s) of drilled shafts to be required in future project plans for expansive soil environments, three (3) different test shaft diameters of 1 ft (0.3 m), 2 ft (0.6 m), and 3 ft (0.9 m) and three (3) different depths of 6 ft (1.8 m), 10 ft (3.0 m) and 14 ft (4.3 m) were designed. These dimensions were based upon the size of the failed foundations (see Figure A.1) and those found in other manufacturers' specifications.

5.2.2.3. Design Results

Computed deflection results of all test shafts using the forces calculated from predicted thermal- and swell-induced forces in winter and summer conditions are shown in Table 5.1.

Based on the analyzed lateral displacements on all shafts, the percent differences in surface lateral movements were determined and are included in Table 5.2.

Table 5.1. Predicted Lateral Deflection of Drilled Shafts at the Ground Surface

Test Shaft Number Diameter x Depth	Deflection at Ground Surface Winter Time in. (mm)	Deflection at Ground Surface Summer Time in. (mm)
1 1 ft x 6 ft (0.3 m x 1.8 m)	N.A.	1.26 (32)
2 1 ft x 10 ft (0.3 m x 3.0 m)	1.03 (26)	0.30 (7.6)
3 1 ft x 14 ft (0.3 m x 4.3 m)	0.91 (23)	0.32 (8.1)
4 2 ft x 6 ft (0.6 m x 1.8 m)	N.A.	0.79 (20)
5 2 ft x 10 ft (0.6 m x 3.0 m)	0.51 (13)	0.15 (3.8)
6 2 ft x 14 ft (0.6 m x 4.3 m)	0.28 (7.1)	0.09 (2.3)
7 3 ft x 6 ft (0.9 m x 1.8 m)	N.A.	0.75 (19)
8 3 ft x 14 ft (0.9 m x 4.3 m)	0.22 (5.6)	0.06 (1.5)
Reaction Shafts Diameter x Depth	Deflection at Ground Surface Winter Time in. (mm)	Deflection at Ground Surface Summer Time in. (mm)
3 ft x 35 ft (0.9 m x 10.7 m)	3.9 (100)	1.6 (40)
4 ft x 35 ft (1.2 m x 10.7 m)	2.0 (50)	0.8 (20)

Note: N.A. means the deflection of the pile head was high due to the computed deflection being larger than the allowable deflection limit.

From Table 5.1, the first reaction shaft, 3 ft (0.9 m) diameter and 35 ft (10.7 m) deep, can be used with the test shafts of 6 ft (1.8 m) depths. This becomes possible due to the high

computed lateral deflections of the short test shafts when compared with small lateral deflection experienced by the reaction shaft. From this data, it was predicted that all of the test shafts would not be influenced by the movements of the reaction shafts during lateral loading.

Table 5.2. Predicted Percent Difference in Lateral Movements of the Reaction and Test Shafts

Test Shaft Number Diameter x Depth	Percent Difference of Lateral Movement (%) in Winter		Percent Difference of Lateral Movement (%) in Summer	
	Reaction Shaft 1	Reaction Shaft 2	Reaction Shaft 1	Reaction Shaft 2
1 1 ft x 6 ft (0.3 m x 1.8 m)	N.A.	N.A.	2.8	1.6
2 1 ft x 10 ft (0.3 m x 3.0 m)	9.3	5.1	11.7	6.5
3 1 ft x 14 ft (0.3 m x 4.3 m)	10.5	5.7	11.1	6.2
4 2 ft x 6 ft (0.6 m x 1.8 m)	N.A.	N.A.	4.5	2.5
5 2 ft x 10 ft (0.6 m x 3.0 m)	18.8	10.2	24.3	13.5
6 2 ft x 14 ft (0.6 m x 4.3 m)	33.6	18.3	39.1	21.7
7 3 ft x 6 ft (0.9 m x 1.8 m)	N.A.	N.A.	4.7	2.6
8 3 ft x 14 ft (0.9 m x 4.3 m)	44.0	24.0	56.3	31.3

Note: N.A. means the deflection of the pile head could not be analyzed due to the computed deflection being larger than the allowable deflection limit.

For the larger reaction shaft, 4 ft (1.2 m) diameter and 35 ft (10.7 m) deep, it was computed that the load tests could be conducted on test shafts of 10 ft (3.0 m) and 14 ft (4.3 m) depth. This was determined from the computed percent differences in the lateral deflections which varied from a low of 5% to 24%, with the highest value computed for the winter test condition. For Test Shaft 8 (3 ft or 0.9 m x 14 ft or 4.3 m), the percent difference is slightly high

for summer test conditions. Hence, load tests need to be interpreted by considering the influence of the reaction test set movements on the test results.

From the analyzed predictions above, test shafts in the winter condition have higher lateral deflections and bending moments than for the summer condition. Cable tensions in the summer conditions are lower than the winter conditions and the uplift force in the summer season (dry season) are also low resulting in less deflection values than calculated for the winter conditions.

The field load test system included a means of applying the inclined load in order to be able to measure the deflections and compute the lateral loads of the drilled shafts. The inclined load used in the calculations was based on an increase in cable tension due to low ambient temperatures, not due to impact loading. The overall system is presented in Figures 5.2 and 5.3 which show the schematics of plan and elevation views of the three test sets and how each one is different from the other two. The steel rebar reinforcement plans for the reaction and test shafts that were used are shown in Appendix A.

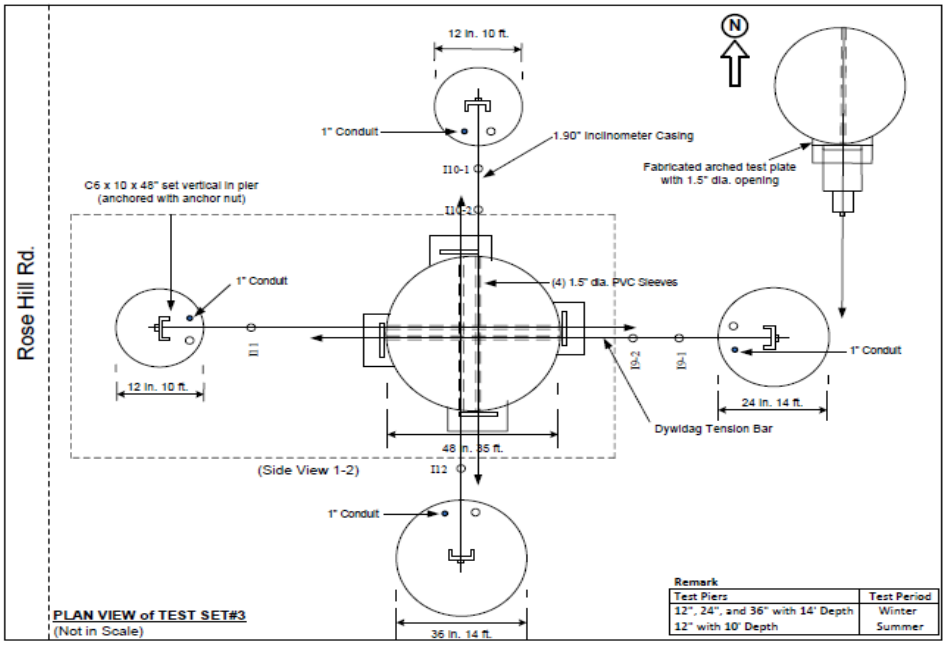

Figure 5.2. Typical Plan View of Test Setup

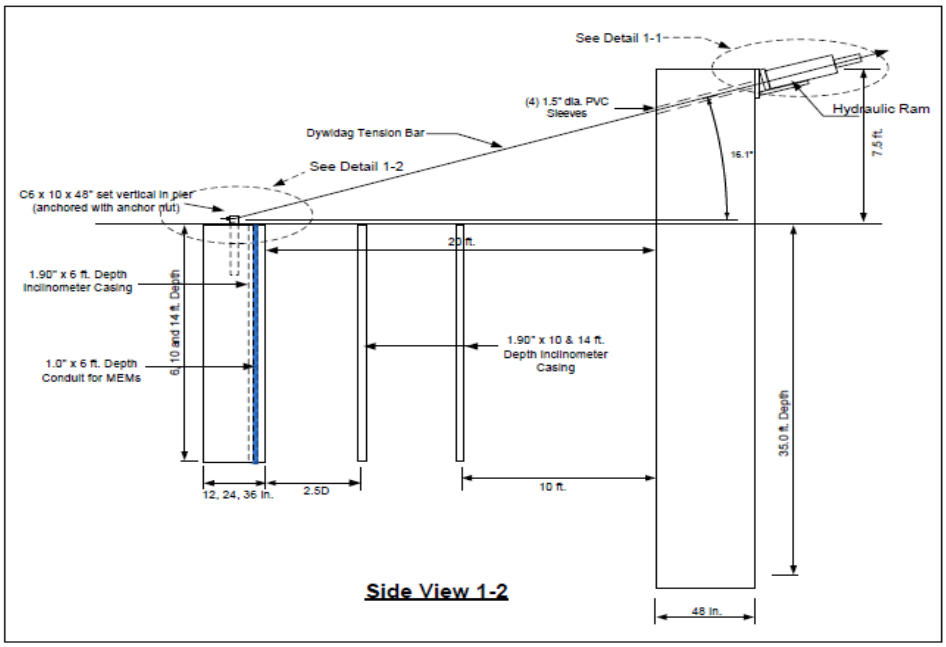

Figure 5.3. Typical Elevation View of Test Setup

5.3 Construction

5.3.1 Final Layout of the Field Test Setup

The drilled shaft installation plan (configuration of shaft location) was modified in the field to accommodate the speed of construction with the available equipment. The final test setups that were constructed are shown in Figure 5.4. The required spacing between the reaction and test shafts were retained per the design requirements. The close proximity of the three (3) test setups to each other were not expected to influence the loading nor the final results.

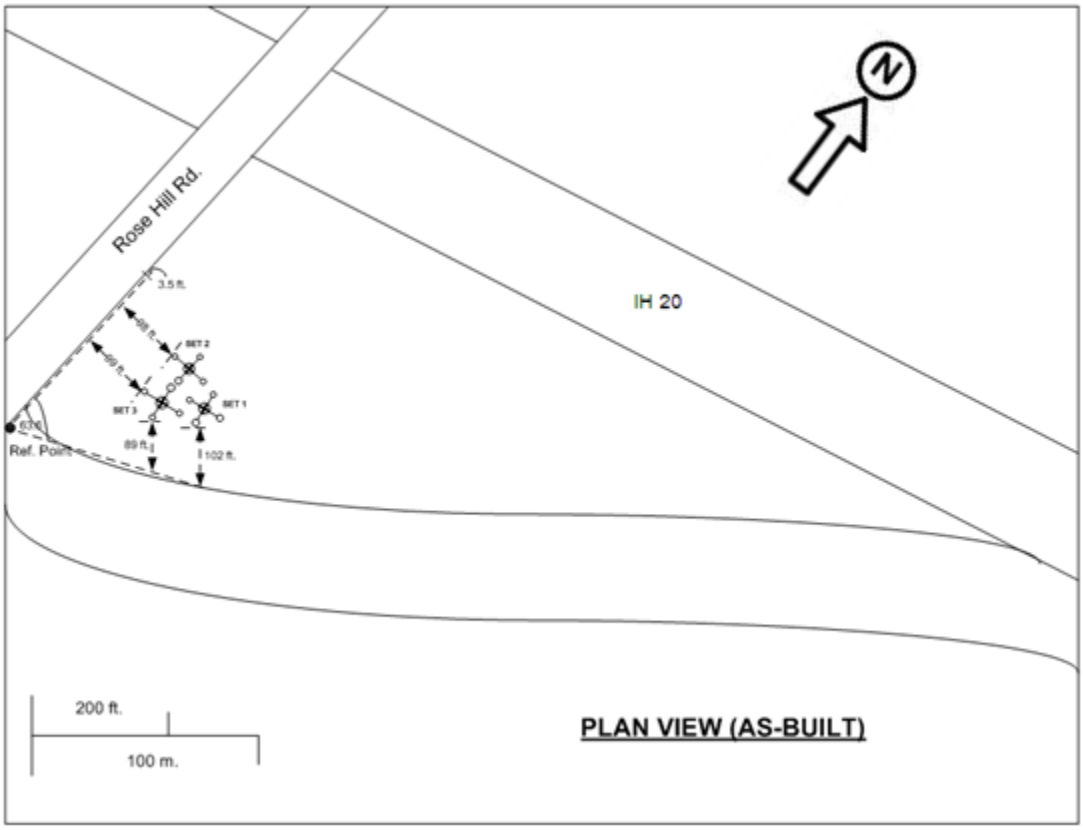

Figure 5.4. Plan View of As-Built Test Setups

5.3.2 Construction Process

5.3.2.1 Steel Reinforcement Cage Construction

Construction commenced at the test site on June 8, 2009. The first task was to tie the steel rebar into the circular cages used in typical drill shaft construction. Two separate crews began tying the steel; one crew built and tied the three (3) reaction shafts (Figure 5.5) while a second crew built and tied the twelve (12) test shafts (Figure 5.6). Different size vertical rebar was used as well as spiral rebar to hold the cages together. This was accomplished on June 8 and 9, 2009.

(a) (b)

Figure 5.5. Construction of the First Reaction Shaft Reinforcement Cage Showing (a) Main Bars and Spiral Rebar and (b) Spacing and Tying Spiral Rebar

Figure 5.6. Construction of a Test Shaft Reinforcement Cage

5.3.2.2 Inclinometer and MEMS-SAA Casing Construction and Placement

Inclinometer casing, 2.75 in. (70 mm) diameter, was measured, cut, and tied onto the steel reinforcement cages prior to installation for use by Durham Geo Slope Indicator's Digitilt Readout measurement System. Additionally, 1.25 in. (32 mm) PVC pipe was measured, cut, and tied to the steel reinforcement cages for use by the MEMS-SAA sensor system for in-place deformation data collection during loading application. These can be seen in Figure 5.7.

(a) (b)

(c)

Figure 5.7. Construction of Casings with (a) Inclinometer Casings (Blue), (b) MEMS-SAA Casing (White), and (c) Casings Attached to Steel Reinforcement Bars

5.3.2.3 Reaction and Test Drill Shaft Construction

The drilling to create the drill shaft holes was started on June 9, 2009. The first drilled hole encountered slight sloughing or caving of the in-situ soil at about the 18 - 20 ft (5.0 - 6.1 m) depth (Figure 5.8). No casing was used due to a lack of borehole data to determine the groundwater elevations. Extra care was taken by slowing the drilling operation and as a result, soil caving did not occur in the drilling of the other two reaction shafts.

Figure 5.8. Drilling of Reaction Shaft Holes

5.3.2.4 Final Assembly of the Test Shaft Parts

While drilling operations were on-going, the steel reinforcement cages were prepared by connecting both the inclinometer (blue casing) and the MEMS-SAA instrumentation (white casing) and the steel channels (Figure 5.9). The steel channels were used to attach the Dywidag bars to each reaction and test shaft to perform the load testing.

Figure 5.9. Channel Steel Tied to Steel Reinforcement Cage

5.3.2.5 Installation of the Reaction and Test Shafts

Each steel reinforcement cage was carefully lifted into a vertical position (Figure 5.10), moved into position over each drilled hole, and then carefully lowered into the hole until they were approximately 3 in. (76 mm) above the bottom of the hole. A gravel concrete mix was then poured into each hole until the drilled hole was completely filled to the groundline (Figure 5.11).

Concrete material was supplied by Texas Industries Inc. (TXI) and the mix design details are given in Appendix B. It was a highly flowable, nonsegregating concrete mix that was easily spread into place to fill the formwork without using mechanical vibration. TXI's mix design number for the concrete was P40PSIN. This mix design computed a water/cement ratio of 0.46 with a slump of 6 in. (150 mm) or more (see Figures B.1 and B.2).

(a) (b)

Figure 5.10. Setting the Steel Reinforcement Cages with (a) A Crane and (b) Aligning into the Drilled Hole

(a)

(b)

(c)

Figure 5.11. Pouring Concrete: (a) Into the Drilled Hole, (b) Keeping Cage From Hole Walls, and (c) Typical Final Shaft

5.3.2.6 Reaction Shaft Above the Ground Construction

For the three (3) reaction shafts, the steel reinforcement cages were extended above the groundline to their designed height prior to the application of a cardboard sonotube and concrete. Cardboard sonotube was used to extend the concrete reaction shafts 7 ft (2.1 m) and 7.5 ft (2.3 m) above the groundline (Figure 5.12) to provide the proper angles and lengths of the Dywidag bars in direct proportion to those used by the median cable barrier system manufacturers.

(a) (b)

Figure 5.12. Reaction Shaft Construction: (a) Setting Sonotube Casing for Reaction Shaft, and (b) 7 and 7.5 ft (2.1 and 2.3 m) Tall Sonotube Casing

5.3.2.7 Dywidag System Construction

PVC pipes measuring 2 in. (50 mm) in diameter were cut and placed through the sonotube walls at the 16.1° angle (Figure 5.13) to allow the future tensioning of the Dywidag system by connecting it to the test shafts. The angle of placement (16.1 degrees for an approximate 6:1 slope) of the PVC pipes matches the angles of the cables connected to the drilled shafts in the field. The same gravel mix supplied by TXI that was used for the drilled shafts was also used to fill in around the steel reinforcement cage up to the top of each piece of sonotube to create the reaction shafts (Figure 5.14).

(a) (b)

Figure 5.13. Dywidag Construction: (a) Installing the PVC Pipe, and
(b) Check of Angle for Dywidag Bars

(a) (b)

Figure 5.14. Sonotube Installations: (a) Pouring Concrete in Sonotubes, and
(b) Final View of Test Setup Area

5.3.2.8 Initial Inclinometer Readings in the Reaction and Test Shafts

Initial inclinometer data was collected on June 15, 2009, six (6) days after installation of all the reaction and test shafts (Figure 5.15).

(a) (b)

Figure 5.15. Taking Initial Inclinometer Readings: (a) Inclinometer in Casing, and (b) Recording Data

5.3.2.9 Additional Inclinometer Installations

Nineteen (19) additional inclinometers were installed between the reaction and test shafts on August 14, 2009. The holes were drilled with a 3.5 in. (90 mm) auger powered by a small generator and turned with a hydraulic-driven chuck as shown in Figure 5.16.

(a) (b)

Figure 5.16. Test Shaft Inclinometer Installation: (a) Auger, and (b) Drilling Operation

Thirteen (13) days were allowed to elapse before any inclinometer readings were taken to allow the grout time to solidify. Initial inclinometer readings were taken on August 27, 2009. Additionally, the sonotube casing for the easternmost reaction shaft was removed exposing the concrete and effectually stopping the cement hydration process and the strength gain. The sonotube on the other two reaction shafts was removed on September 5, 2009. Likewise as with the removal of the sonotube on the first reaction shaft, the cement hydration and strength gain were stopped at this time.

5.4 Field Quality Control Checks

5.4.1 Concrete Strength Tests

In construction, it is necessary to have quality control checks in order to validate that the structures in the field perform as predicted in the Design phase. For this research project, checks on the concrete were performed by randomly collecting samples from different concrete trucks that provided the concrete for the reaction and test shafts. A total of five (5) cylinder specimens were made. Three (3) samples were collected and specimens made from each reaction shaft and the other two (2) samples were randomly collected and specimens made from the test shafts. The dimensions of the cylindrical specimens was 6 in. (150 mm) diameter and 12 in. (300 mm) long as specified in ASTM Test Method C31/C31M – 09, Standard Practice for Making and Curing Concrete Test Specimens in the Field.

After making the cylinders, all specimens were left in the field for approximately two (2) days to allow them to field cure and minimize damage during transportation back to the laboratory. All five (5) specimens were cured in lime water for an additional 26 days. After completion of the standard 28 days, the specimens were taken out of the water. All specimens were capped on the top and bottom with sulfur compound prior to breaking. This provided a 100 percent contact between the base and loading plates and the surfaces of the concrete cylinders as required by ASTM Test Method C617 - 09a, Standard Practice for Capping Cylindrical Concrete Specimens and as shown in Figure 5.17.

Figure 5.17. Concrete Cylinder Specimens with Capping Compound

Compression strength tests conducted per ASTM Test Method C39/C39M - 09, Standard Test Method for Compressive Strength of Cylindrical Concrete Specimens. The testing machine primarily performs compressive strength testing and has a capacity of about 400 kips (1,814 kN) for both compression and tension (Figure 5.18). The target compressive strength of the concrete based on the mix design was 4000 psi (27,579 kPa). In providing the load to the specimens, they were individually placed between the base and the loading plates and the loading was applied and manually controlled at a rate of 300 lb/sec (1.36 kN/sec) until the specimens failed as shown in Figure 5.19.

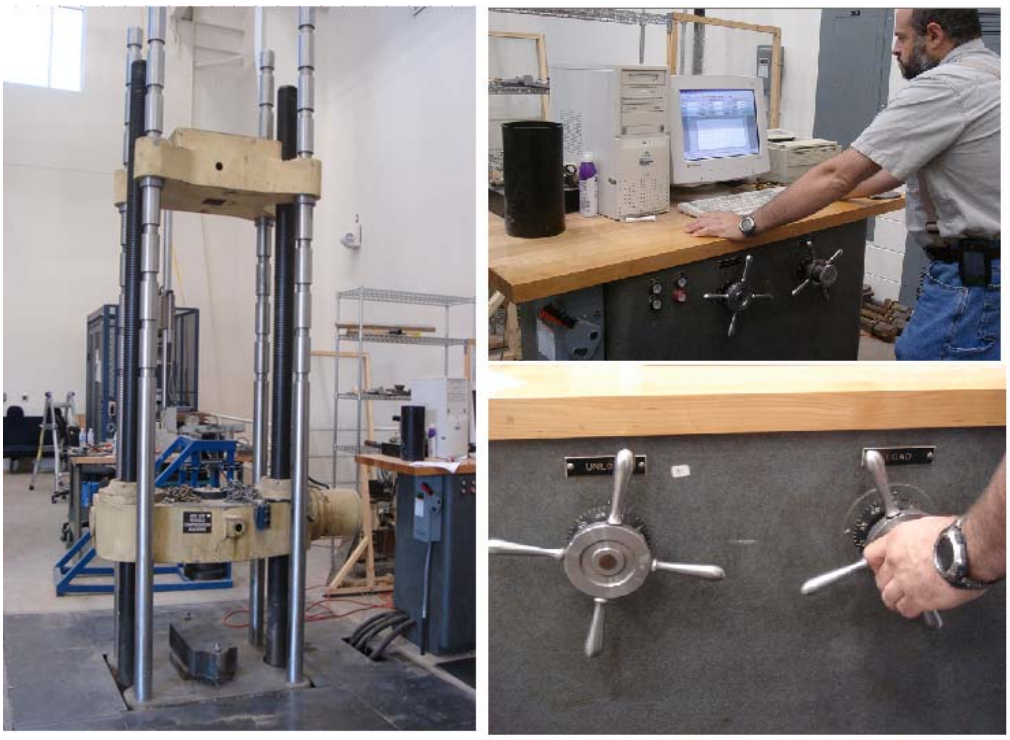

Figure 5.18. The 400 kip Tinius Olsen Tensile and Compression Machine used for Testing

(a) (b)

Figure 5.19. Compressive Strength: (a) Test Setup, and (b) Failed Concrete Specimen

The results and interpretations are automatically collected by the testing machine with all of the results summarized as shown in Table 5.3.

Table 5.3. Compressive Strength Test Results

Specimen No.	Peak Strength, psi (kPa) at 28 days
1	4075 (28,096)
2	4037 (27,834)
3	3972 (27,386)
4	4116 (28,379)
5	4033 (27,807)

From the results, the average compressive strength of all five (5) specimens is equal to 4046.6 psi (27,900 kPa) with a Standard Deviation (SD) equal to 53.54 psi (369 kPa). Although one specimen broke at a compressive strength lower than 4000 psi (27,579 kPa), it was more than 90% of the design concrete strength of 3600 psi (24,821 kPa) and was deemed acceptable.

5.5 Steel Reinforcement Bar Sizes Used Per Shaft

5.5.1 Reaction Shafts

Eighteen (18) No. 7 bars for the 36 in. (0.9 m) and thirty-two (32) No. 7 bars for the 48 in. (1.2 m) were used per reaction shaft at the spacing shown on the plan sheet in Figure C.6. The No. 3 spiral hoop rebar was placed on 5 in. (127 mm) centers along the lengths of the steel rebar.

5.5.2 Test Shafts

Four (4) No. 6 bars were used for the 12 in. (0.3 m) test shaft, eight (8) No. 6 bars were used for the 24 in. (0.6 m) test shaft, and eighteen (18) No. 6 bars were used for the 36 in. (0.9 m) test shaft at the spacing shown on the plan sheet in Figure C.7. No. 4 circular rebar was placed on 18 in. (457 mm) centers along the lengths of the steel rebar.

5.6 Summary

The design of the three (3) test sets consisted of three (3) reaction shafts with four (4) test shafts associated with each reaction shaft. This number of test sets allowed for using variable test shaft sizes varied for diameter and depth. This also provided repeatability to compare test data. The construction of the test sets was laid out according to the design but was placed closer than designed due to construction efficiency. This was not expected to affect the results between test shafts. Construction of the shafts and installation of the casings for sensors was accomplished successfully. The concrete used for the shaft construction was properly batched per the design as reported per the strength breaks.

CHAPTER 6

FIELD TESTING, RESULTS, AND ANALYSIS

6.1 Introduction

The field test data, results, and analysis of the three (3) test shafts tested in the summer condition and the three (3) test shafts tested in the winter condition are included in this chapter. Identical diameters and depths of tested shafts were used for the summer and winter conditions to allow a direct comparison of the results due to soil moisture and cable temperature changes.

6.2 Field Testing and Data Acquisition

6.2.1 Summer Condition

6.2.1.1 Field Testing

Field testing and acquisition of applied loads, inclinometer, MEMS-SAA, and elevation data was performed on September 30, 2009. The Dywidag bars and the hydraulic piston system for applying the tension load on the Dywidag bar were brought to the site. One (1) test shaft for each reaction shaft per test set was tested. The three (3) test shafts selected for the summer condition were 1 ft x 6 ft (0.3 m x 1.8 m), 1 ft x 10 ft (0.3 m x 3 m), and 2 ft x 10 ft (0.6 m x 3 m) sizes. One (1) test shaft per test set was selected and subjected to inclined loading through the Dywidag bar connecting the reaction and the test shaft. Incremental loads were applied using a hydraulic piston placed against the back of the reaction shaft. For the test shafts, lateral movements were measured by both inclinometer and MEMS-SAA (Micro-Electro-Mechanical System – ShapeAccelArray) sensors. In addition, the final vertical movement of the reaction shafts was measured at the center of the test shaft both before and after the start of each test by using standard survey equipment.

The inclinometer that was used was Durham Geo Slope Indicator's Datamate II Digitilt Readout measurement system.

The MEMS-SAA (Micro-Electro-Mechanical System - ShapeAccelArray) device was selected for comparison to the standard inclinometer data collection system. The MEMS-SAA is an array of sensors and microprocessors that measures deformation in the horizontal and vertical directions when the casing moves. The casing used in this project was a 1.25 in. (32 mm) white PVC pipe. The main characteristics of the MEMS-SAA system pertinent to this project are that each one (1) foot (12 inch) segment has three accelerometers, segments are connected by flexible joints, in-array microprocessors collect and send digital data, measurements are based on tilt-like inclinometer measurements, and the system measures deformation at hundreds of locations (Source: http://www.measurandgeotechnical.com/. 2010).

Figure 6.1 shows the MEMS-SAA cable being carefully rolled out. Since it contains sensors at every 1 ft (0.3 m) increment, care was taken to insure that the cable did not become kinked nor twisted. It stayed in the casing inside the test shaft during the entire test period.

Figure 6.1. MEMS-SAA Probe System

The Dywidag bar (Figure 6.2a) was 1-1/4 in. (32 mm) in diameter and long enough to span the 20 ft (6.1 m) horizontal distance between the reaction and test shaft plus through the test shaft steel channel and past the reaction shaft to include the hydraulic piston stand, piston, and threaded nuts (Figure 6.2b) on each end to allow the bar to be tightened (Figure 6.2c).

(a)

(b)

(c)

Figure 6.2. Dywidag System Parts: (a) Dywidag Bars, (b) Dywidag Bar Retaining Nut, and (c) Complete Test Setup

The hydraulic piston shelf (Figure 6.3a) was built from 1/2 in. (12.5 mm) plate steel. Two (2) individual shelves were constructed; one (1) for the 36 in. (0.9 m) reaction shaft and one (1) for the 48 in. (1.2 m) reaction shaft. The vertical portion was bent to the curvature of each reaction shaft to allow it to pull snugly against the shaft once tension was applied to the Dywidag bar. The shelf supported the piston's weight during operation to relieve any friction due to gravity and allow full horizontal tension on the bar. Figure 6.3b shows the hydraulic piston setup.

(a)

(b)

Figure 6.3. Dywidag Tensioning System: (a) Hydraulic Piston Shelf, and (b) Hydraulic Pump Setup

Figure 6.4a shows a reaction shaft with the Dywidag bar pushed through at the 16.1° angle. Additional white PVC pipe can be seen extending out of the reaction shaft which would be used for the other three (3) test shafts for that test set. Figure 6.4b shows the Dywidag bar placed through the steel channel placed into the concrete for the test shaft. The threaded nut retains the bar onto the steel channel in the test shaft. The MEMS-SAA and inclinometer casings can be seen extending above the concrete.

(a)

(b)

Figure 6.4. Dywidag Bar System: (a) Dywidag Bar in Place for Testing, and (b) Retaining Nut Attached to Test Shaft Steel Channel

Placement of the hydraulic piston shelf and the hydraulic piston are shown in Figure 6.5a. Due to the piston's weight, a minimum of two (2) people had to work to put this into place. Figure 6.5b shows final placement. The black hoses extending from the piston are for the hydraulic system to apply tension to the Dywidag bar.

(a)

(b)

Figure 6.5. Hydraulic Piston Setup for Tensioning: (a) Installing the Hydraulic Piston (b) Hydraulic Piston and Retaining Nut

Figure 6.6a shows the full hydraulic piston setup. The pump and gauge are setting on the ground. The calibration charts for the gauge are shown in Figure 6.6b and were used to determine the amount of tension applied versus the pump pressure shown on the gauge.

(a) (b)

Figure 6.6. Hydraulic Tensioning System: (a) Tensioning System Setup, and (b) Hydraulic Pump Calibration Records

6.2.1.2 Data Acquisition

Pressure was applied to the pump through the controller as shown in Figure 6.7a. Once tension was created in the Dywidag bar, readings were taken from the dial gauge at the test shaft which showed movement per amount of tension applied (Figure 6.7b).

(a)

(b)

Figure 6.7. Test Shaft Loading: (a) Applying Tensioning Loads, and
(b) Test Shaft Deflection due to Loading

After each incremental tension was applied, inclinometer, MEMS-SAA, and elevation readings were taken. Inclinometer readings were taken at the test shaft and the mid-point inclinometer casings as shown in both figures. This was performed within a span of five (5) minutes.

(a)

(b)

Figure 6.8. Collecting Inclinometer Readings: (a) Test Shaft. and at the (b) Mid-Point

A view of all three (3) data collection systems, inclinometer, MEMS-SAA, and elevations are shown in Figure 6.9. The suite of three (3) data collection systems was used to insure that proper accuracy was accomplished.

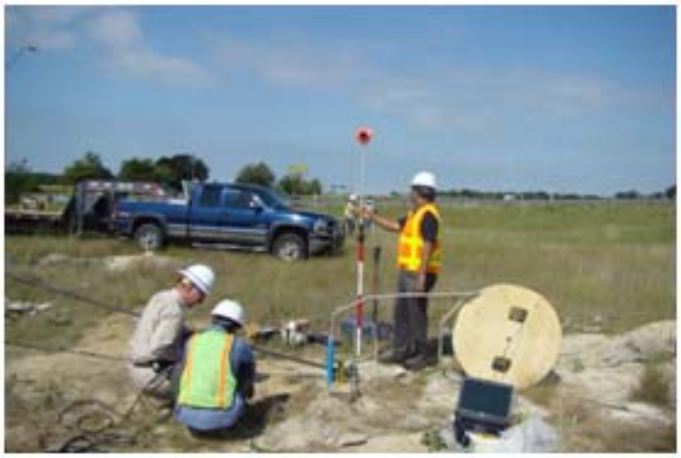

Figure 6.9. Collection of Inclinometer, MEMS-SAA Probe,
and Elevation Survey Readings

6.2.2 Winter Condition

6.2.2.1 Field Testing

Field testing and acquisition of applied loads, inclinometer, MEMS-SAA, and strain gauge data on the last nine (9) test shafts was performed on February 9, 10, 15, 16, and 17, 2010. Cold weather had settled into the area with the highs in the low 40s and lows in the upper 20s as shown in Figure 6.10. The three (3) test shafts selected from the nine (9) total tested for this winter condition were again 1 ft x 6 ft (0.3 m x 1.8 m), 1 ft x 10 ft (0.3 m x 3 m), and 2 ft x 10 ft (0.6 m x 3 m) sizes. These sizes were purposefully designed and tested for direct comparison between the summer and winter conditions to directly determine seasonal change affects on the drilled shafts and soil directly in contact with the concrete.

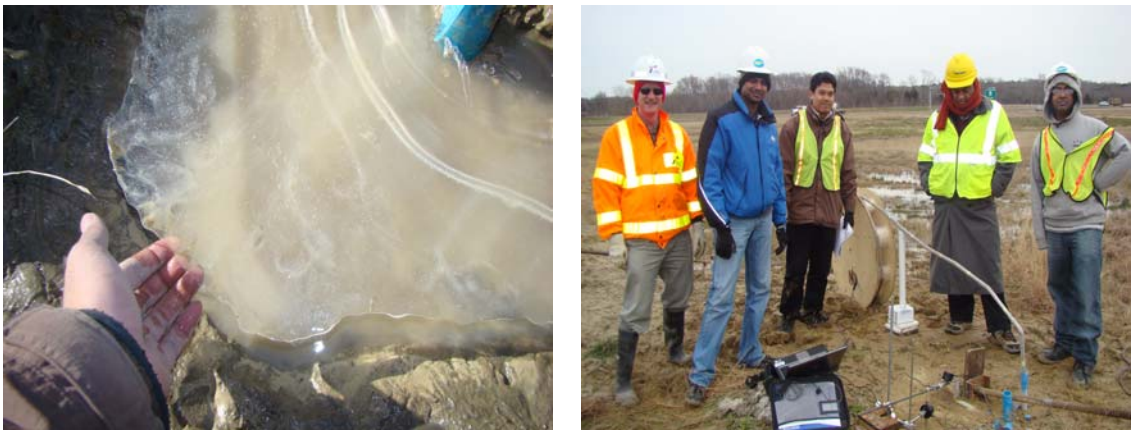

(a) (b)

Figure 6.10. Cold Weather Conditions: (a) Ice, and (b) Cold Weather Garments

The soil was totally saturated from numerous semi-weekly rain events that swept through the area between October 2009 and February 2010 as shown in Figure 6.11. The area did receive a record snowfall of 12 in. (300 mm) in a 24-hour period on February 11, 2010 adding a little more than 1 in. (25 mm) of additional moisture into the soil.

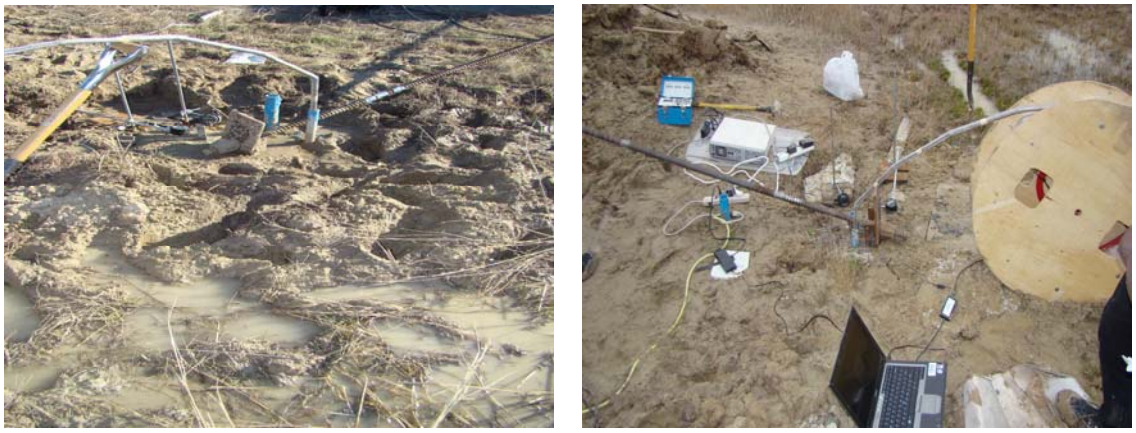

(a) (b)

Figure 6.11. Totally Saturated Field Condition: (a) Totally Saturated Soil, and (b) Mud

Between the summer and winter testing, the researchers determined that strain data from the Dywidag bar would be beneficial to compare against the pressure measured on the hydraulic pump gauge. Strain gages were placed at two (2) locations on the Dywidag bars

between each reaction and test shaft; one (1) approximately 18 in. (0.5 m) and one (1) approximately 12 in. (300 mm) away from the test and reaction shafts, respectively. A typical gauge placement and the receiver are shown in Figure 6.12.

(a) (b)

Figure 6.12. Strain Gauge Instrumentation: (a) Gauge Attached, and (b) Data Receiver

Figure 6.13 shows some of the area between the reaction and test shafts that had received additional soil overburden due to the rains eroding the soil spoil piles from the drilling into the lower areas. The extra soil was dug out manually in order to locate a few missing inclinometer casings that had been buried.

Figure 6.13. Spoil Overburden Soil Removed Between Shafts

6.2.2.2 Data Acquisition

The third tested shaft experienced failure in the concrete during the applied loading as shown in Figure 6.14. After the applied load could not be sustained and the final inclinometer and MEMS-SAA data was collected, additional tension was applied to the Dywidag bar to see how the test shaft would react. As anticipated, the test shaft concrete and the steel channel started tipping out of the ground. Continued tension might have contributed to flexural failure of the concrete shaft within top few feet of the shaft. Failure of this type can allow the barrier system cables to become slack and negate their purpose.

Figure 6.14. Test Shaft Concrete Broken Horizontally

The ninth and final test shaft was tested in the early night hours. The researchers were prepared and used flashlights to enable them to apply the loads and take the inclinometer readings as shown in Figure 6.15. The strain gauge and MEMS-SAA data was stored in the separate collection systems as had been accomplished for the previous eleven tests and did not need illumination.

(a) (b)

Figure 6.15. Night Testing: Using Flashlights for (a) Instrumentation, and (b) Crack Identification

All twelve (12) test shafts were field tested successfully with three (3) in the summer condition and the nine (9) in the winter condition. Data from the inclinometer readings, MEMS-SAA, elevation survey, and strain gauges was collected and brought back to the laboratory for downloading and analysis. This information is included in Section 6.4 of this chapter.

6.3 Field Test Observations

6.3.1 Observations

Several different failure mechanisms were observed during testing. As shown in Figure 6.16a, the concrete at the ground surface actually cracked. Figures 6.16b and 6.16c show separation of the concrete for the test shaft from the adjoining soil. This indicates movement of the test shaft toward the reaction shaft.

(a)

(b)

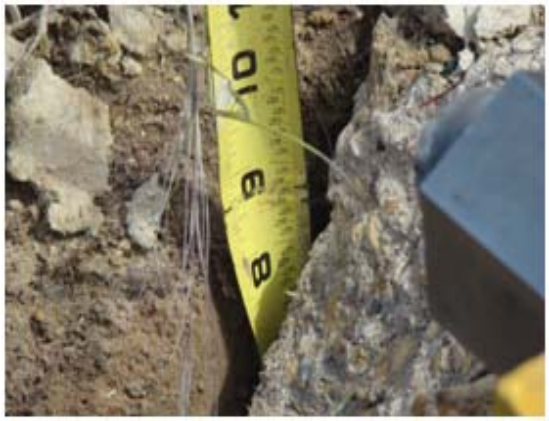

(c)

Figure 6.16. Test Shaft Failure: (a) Cracked Concrete, (b) Soil-Test Shaft Separation (Distance), and (c) Soil-Test Shaft Separation (Depth)

Figure 6.17a shows yielding and imminent failure of the steel channel in a test shaft. This was of great concern to the testers' safety and was corrected with the addition of a steel plate to reinforce the steel channel (Figure 6.17b) allowing the shaft to fail rather than the channel.

(a)

(b)

Figure 6.17. Field Adjustment to Eliminate Yielding Steel Channels: (a) Steel Channel Yielding, and (b) Extra Plate Added

6.4 Data and Analysis

6.4.1 Load Data

The load data was recorded using two (2) different methods; hydraulic applied load gauge and strain gage based load calculation. The hydraulic applied load gauge was calibrated prior to use in the summer condition. An additional digital load gauge was considered for use to check the hydraulic gauge but was not available in time for the summer testing. During the months between the summer and winter conditions, the strain gage method was selected and made ready for use prior to the winter condition testing. Data for both is shown below.

6.4.1.1 Hydraulic Applied Load Gage

The actual loads applied to the Dywidag bars versus the time of application for each load are shown in Figures 6.18a through 6.18c. The graphs for the winter testing are shown because the actual force is the force applied by the hydraulic applied load minus the strain gauge value. The extended horizontal portions of the graphs are the loads at which the inclinometer readings were taken.

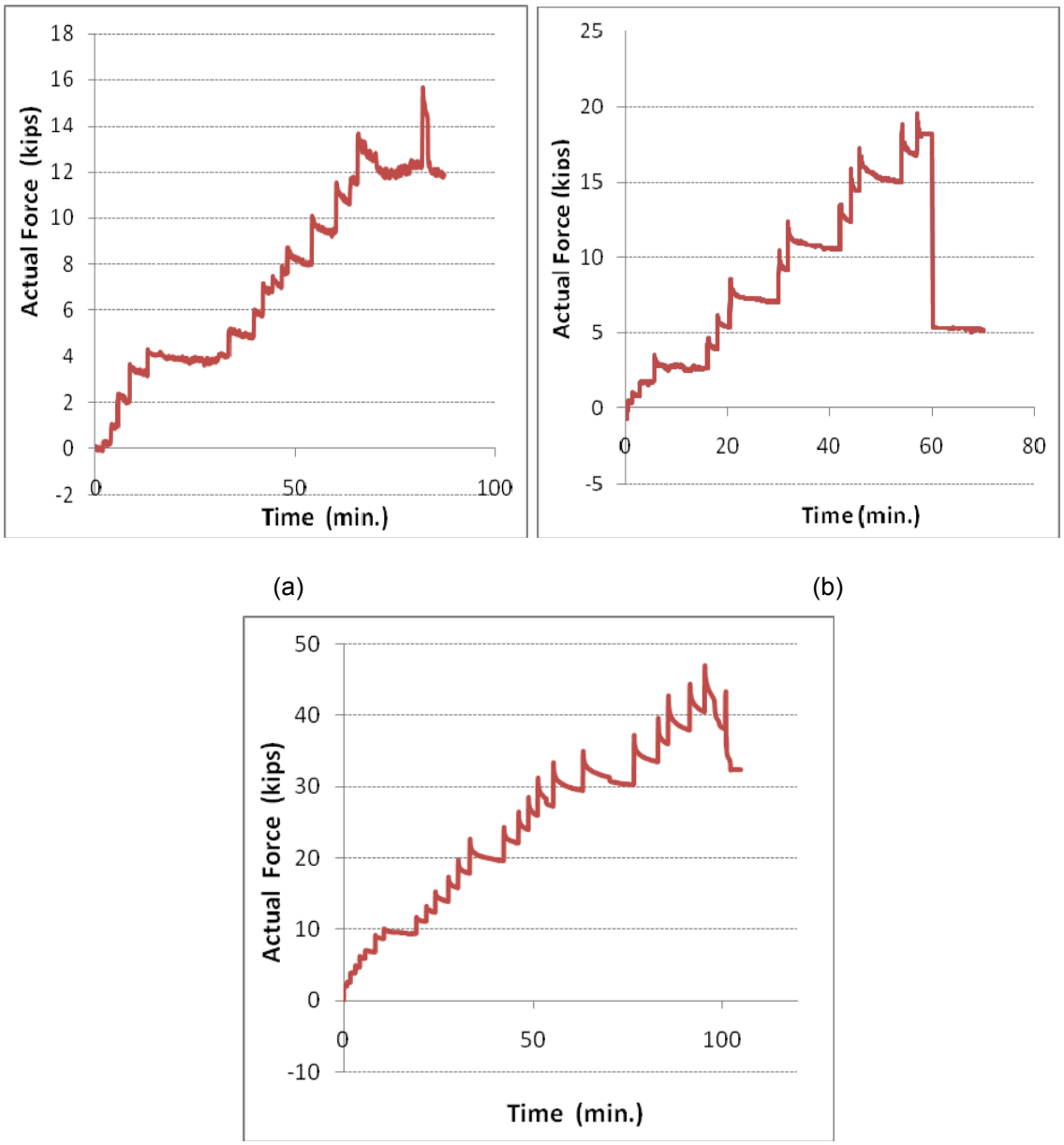

Figure 6.18. Actual Force per Time:
(a) 1 ft diameter x 6 ft depth (b) 1 ft diameter x 10 ft depth (c) 2 ft diameter x 10 ft depth
(Winter Condition)

The last three (3) graphs mirror the trends for each test shaft when compared to the actual load versus time graphs for the winter condition as shown in Figures 6.18a through 6.18c above. This validates the calibration of the hydraulic piston application system.

6.4.2 Lateral Displacement Data

6.4.2.1 Inclinometer and MEMS-SAA Displacement Plots

Both inclinometer readings and MEMS-SAA readings were collected during testing on each test shaft. The inclinometer displacement data was collected at certain incremental loads while the MEMS-SAA data was continuously read and stored through a laptop computer used onsite. The plots created from the field collected data for both the inclinometer and MEMS-SAA systems are shown in Figures 6.19 through 6.24 for each of the three (3) test shaft sizes. The plots are for the inclinometer and MEMS-SAA casings originally installed in the test shaft steel reinforcement cages and for the inclinometer casings located between the reaction and test shafts. For the 1 ft (0.3 m) test shafts, additional inclinometer readings were taken at the two (2) diameter of the test shaft and mid-point locations from the test shaft to the reaction shaft. For the 2 ft (0.6 m) test shafts, additional inclinometer readings were taken at the mid-point location from the test shaft to the reaction shaft. The first three (3) figures are plots from the data collected in the summer condition and the last three (3) figures are plots from the data collected in the winter condition. Table 6.1 summarizes the maximum lateral movement in the influence zone between the reaction and test shafts due to the load applied.

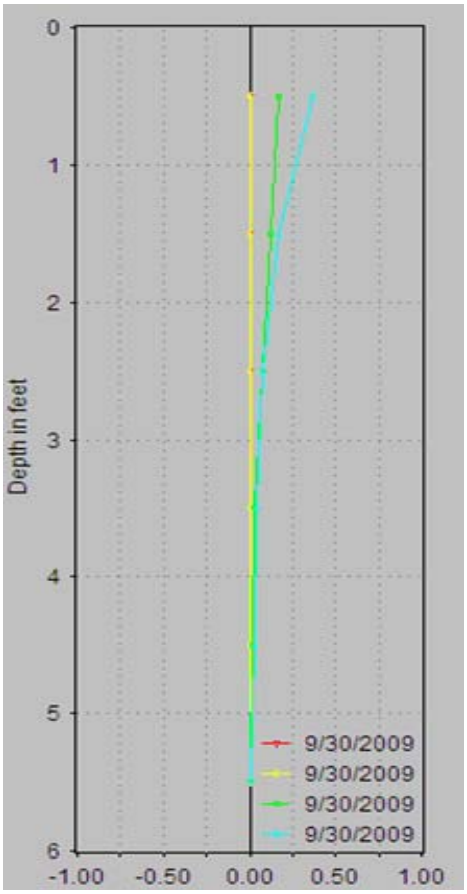

(a)

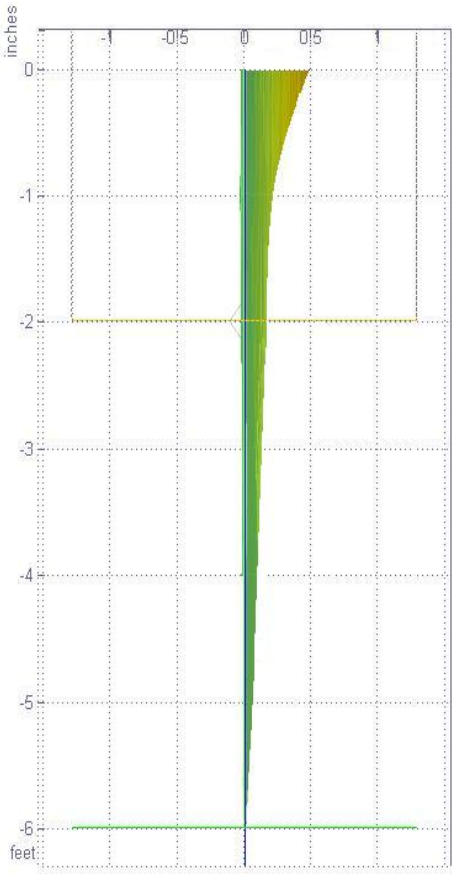

(b)

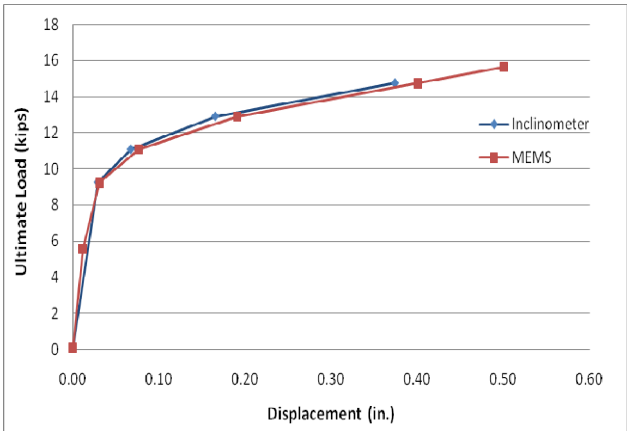

(c)

Figure 6.19. Test Shaft (1 ft diameter x 6 ft depth) Displacemant Data:
(a) Inclinometer, (b) MEMS-SAA, and (c) Ultimate Load versus Displacement Comparison
(Summer Condition)

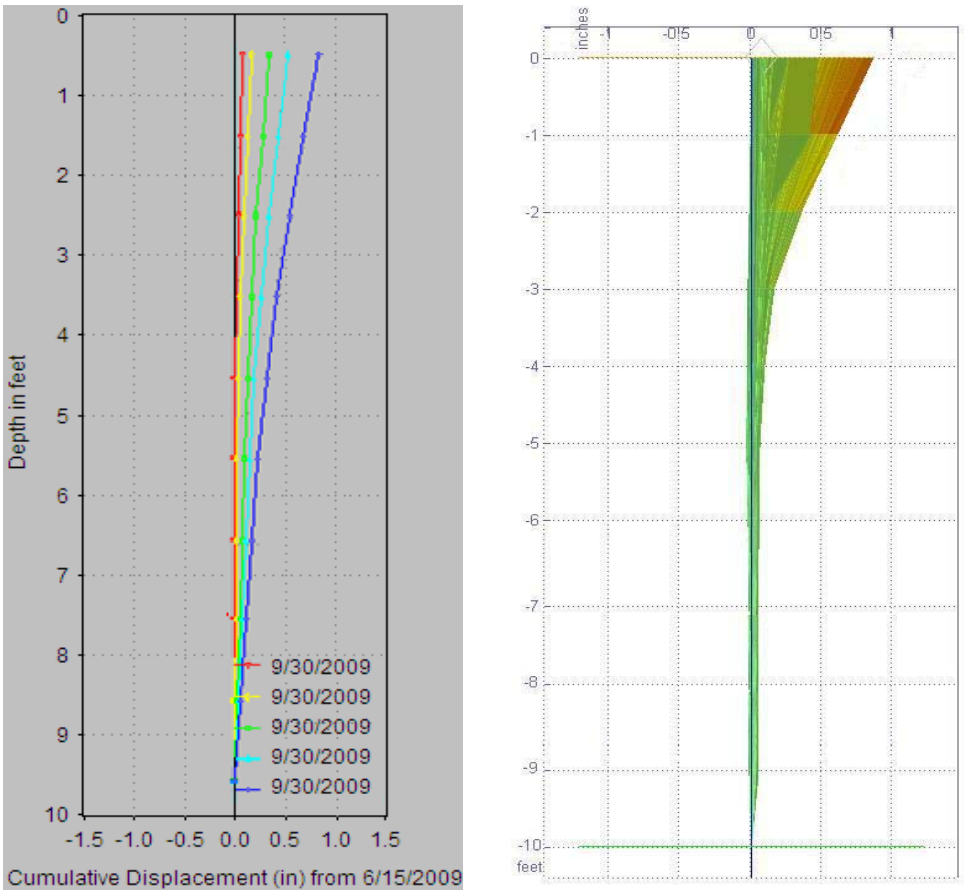

(a) (b)

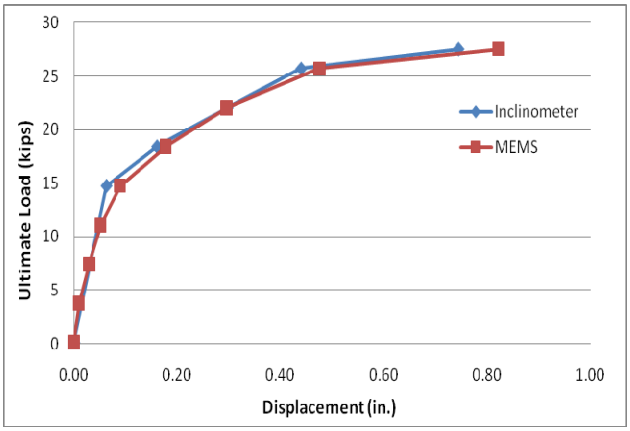

(c)

Figure 6.20. Test Shaft (1 ft diameter x 10 ft depth) Displacemant Data:
(a) Inclinometer, (b) MEMS-SAA, and (c) Ultimate Load versus Displacement Comparison
(Summer Condition)

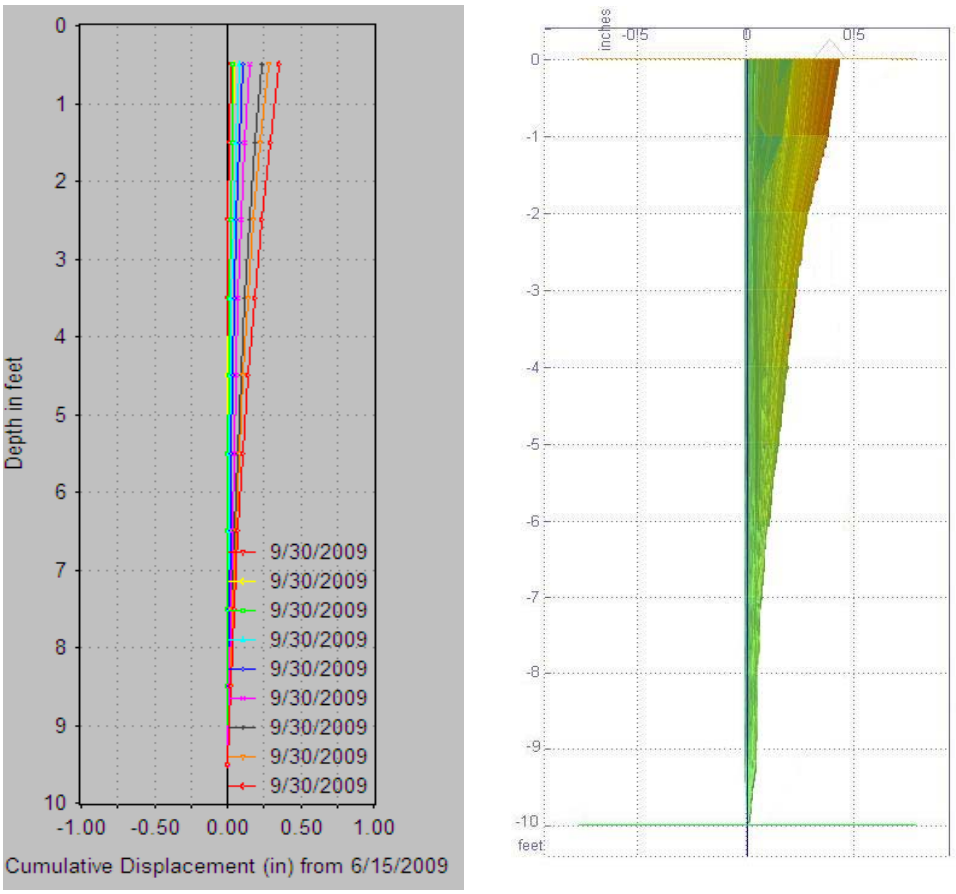

(a) (b)

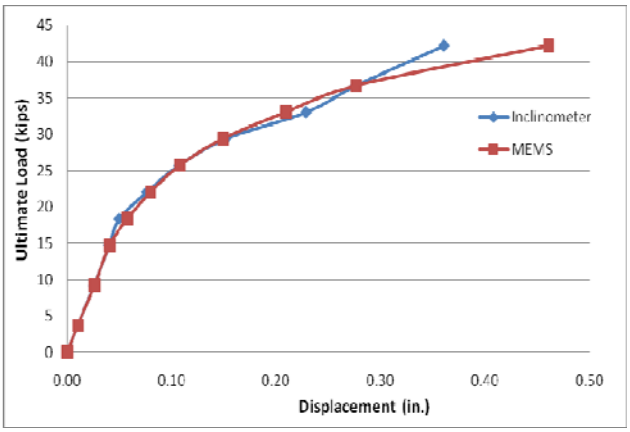

(c)

Figure 6.21. Test Shaft (2 ft diameter x 10 ft depth) Displacemant Data:
(a) Inclinometer, (b) MEMS-SAA, and (c) Ultimate Load versus Displacement Comparison
(Summer Condition)

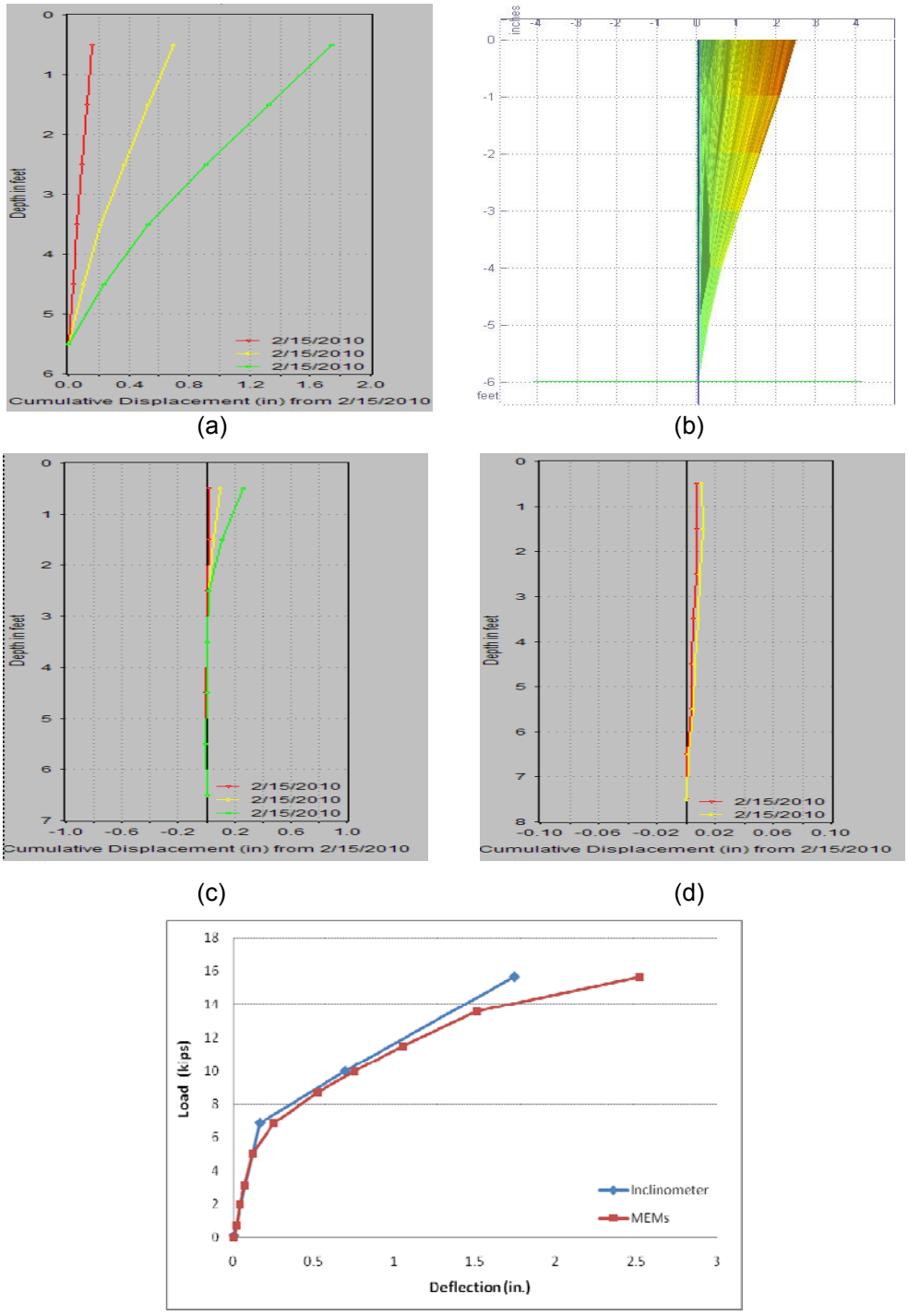

Figure 6.22. Test Shaft (1 ft diameter x 6 ft depth) Displacemant Data: (a) Inclinometer, (b) MEMS-SAA, (c) Inclinometer at 2D of Test Shaft (d) Inclinometer at the Middle of Test Shaft and Reaction Shaft and (e) Ultimate Load versus Displacement Comparison (Winter Condition)

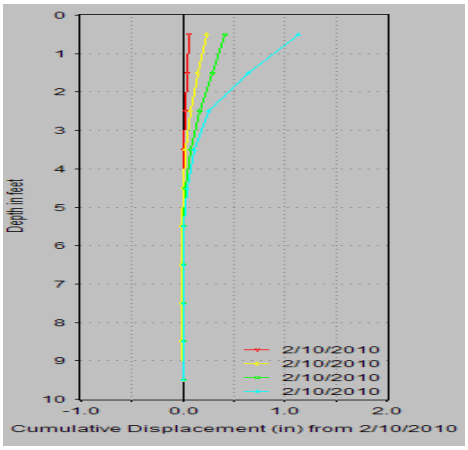

(a)

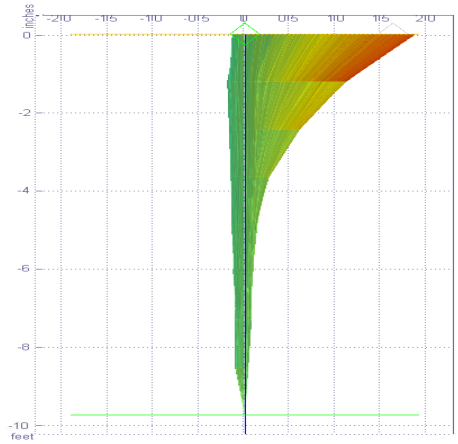

(b)

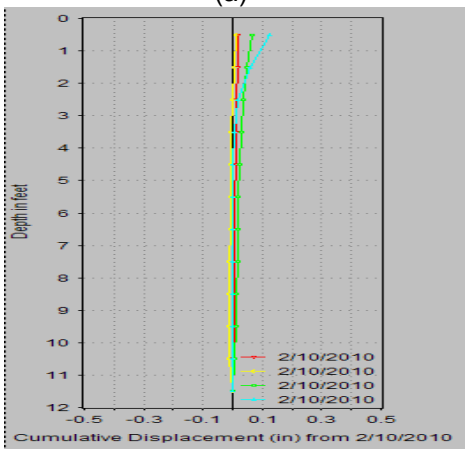

(c)

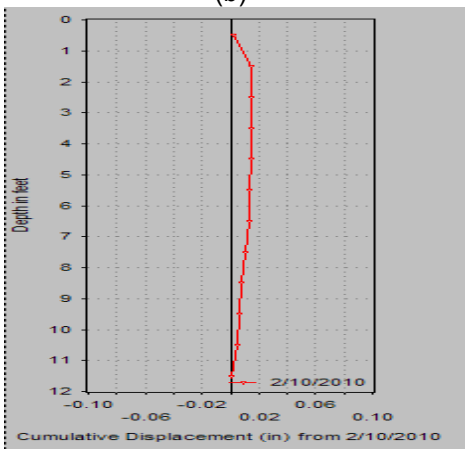

(d)

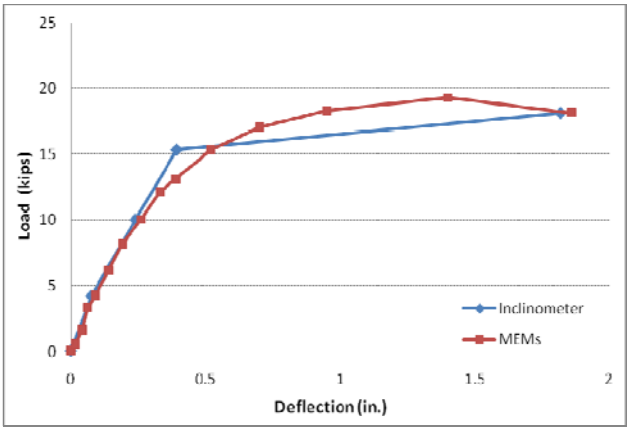

(e)

Figure 6.23. Test Shaft (1 ft diameter x 10 ft depth) Displacemant Data: (a) Inclinometer, (b) MEMS-SAA, (c) Inclinometer at 2D of Test Shaft (d) Inclinometer at the Middle of Test Shaft and Reaction Shaft and (e) Ultimate Load versus Displacement Comparison (Winter Condition)

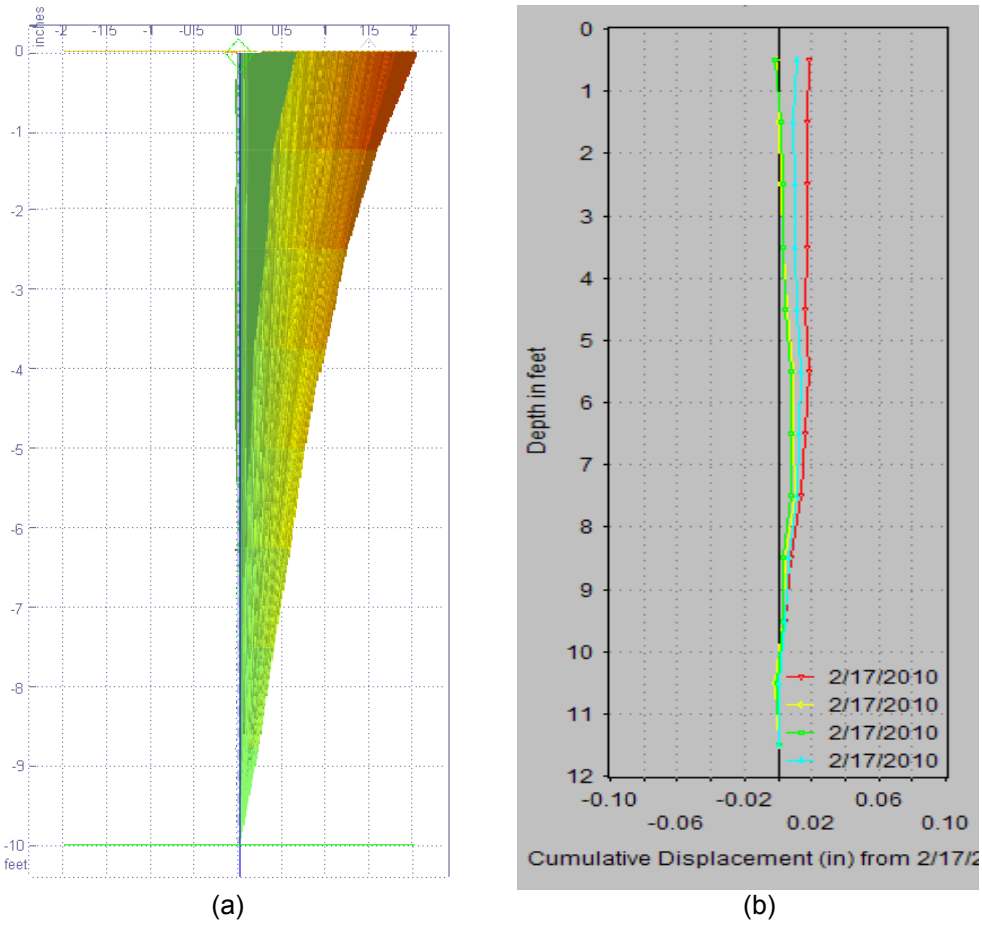

Figure 6.24. Test Shaft (2 ft diameter x 10 ft depth) Displacemant Data:
(a) MEMS-SAA, (b) Inclinometer at 2D of Test Shaft, and
(c) Ultimate Load versus Displacement Comparison
(Winter Condition)

It can be seen from these figures that the MEMS-SAA data tracked very closely to the inclinometer data. It is repeated in the additional six (6) test shafts that were tested in the winter condition.

Table 6.1. Maximum Lateral Movement in the Influence Zone
Due to the Load Applied to the Shafts

Test Set	Dimension Diameter x Depth ft x ft (m x m)	Lateral Movement at 2 Diameters from Test Shaft in. (mm)	Lateral Movement at Midpoint between Reaction and Test Shaft in. (mm)
1	1 x 6 (0.3 x 1.8)	0.27 (6.9)	0.016 (0.40)
2	1 x 10 (0.3 x 3)	0.12 (3.0)	0.017 (0.43)
2	2 x 10 (0.6 x 3)	N.A.	0.018 (0.46)

This provides very valuable information to allow future research and investigations to use the MEMS-SAA system. For the rest of this analysis, displacement results will be reviewed using the MEMS-SAA data, where applicable, in lieu of the inclinometer data.

6.4.2.2 MEMS-SAA Comparison Plots (Summer versus Winter)

From the continuous data collected by the MEMS-SAA system, the data collected during the summer condition (dry season) and the winter condition (wet season) for the three (3) test shaft sizes are plotted in Figures 6.25a through 6.25c.

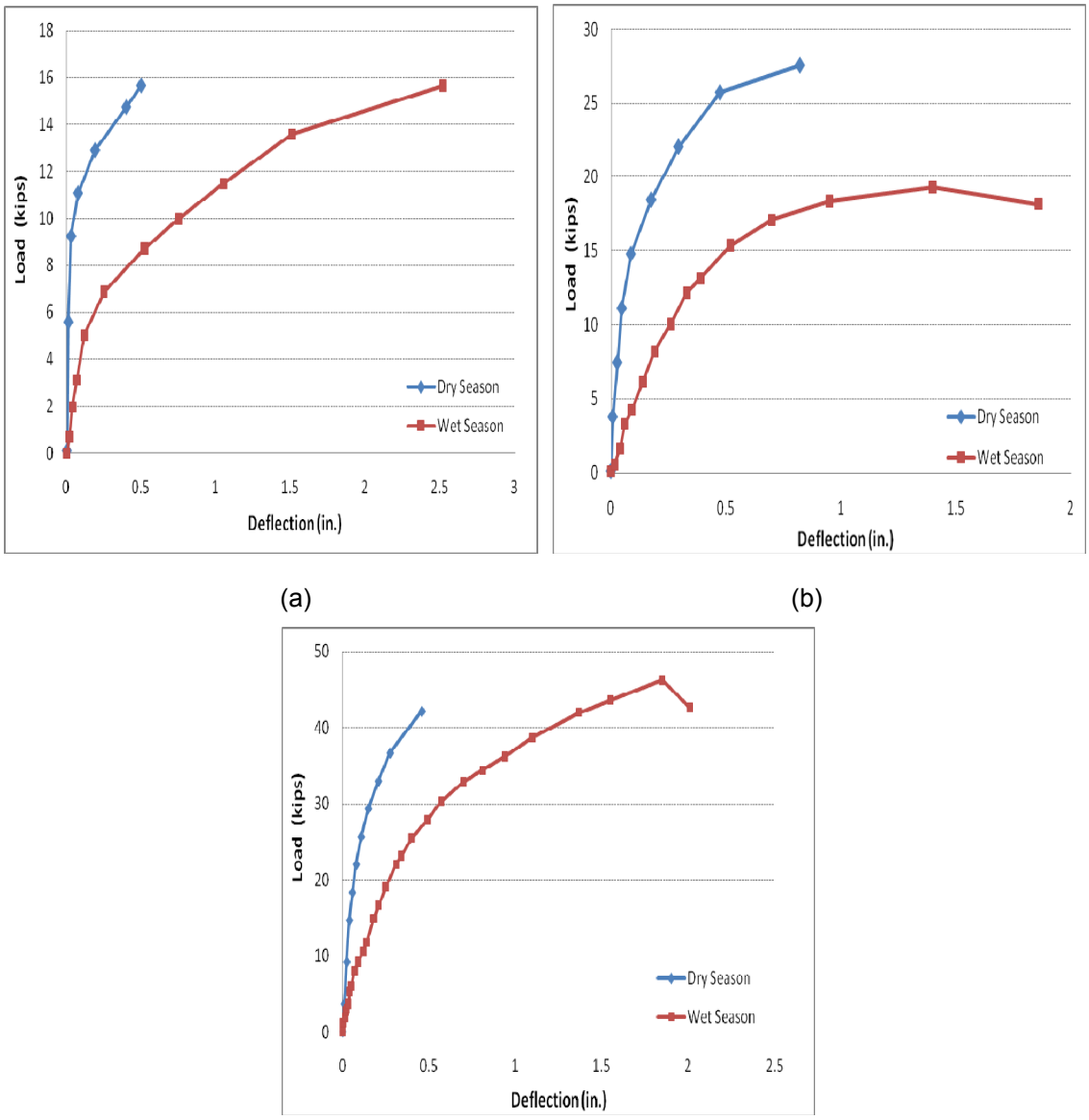

Figure 6.25. MEMS-SAA Plots for Summer Condition (Dry Season)
and Winter Condition (Wet Season):
(a) 1 ft diameter x 6 ft depth, (b) 1 ft diameter x 10 ft depth, and (c) 2 ft diameter x 10 ft depth

In all three (3) figures, the data clearly shows that there was significantly more deflection or displacement of the test shafts during the winter condition (wet season). This was also clearly observed and noted during field testing and can be seen in Figures 6.26a and 6.26b.

(a)

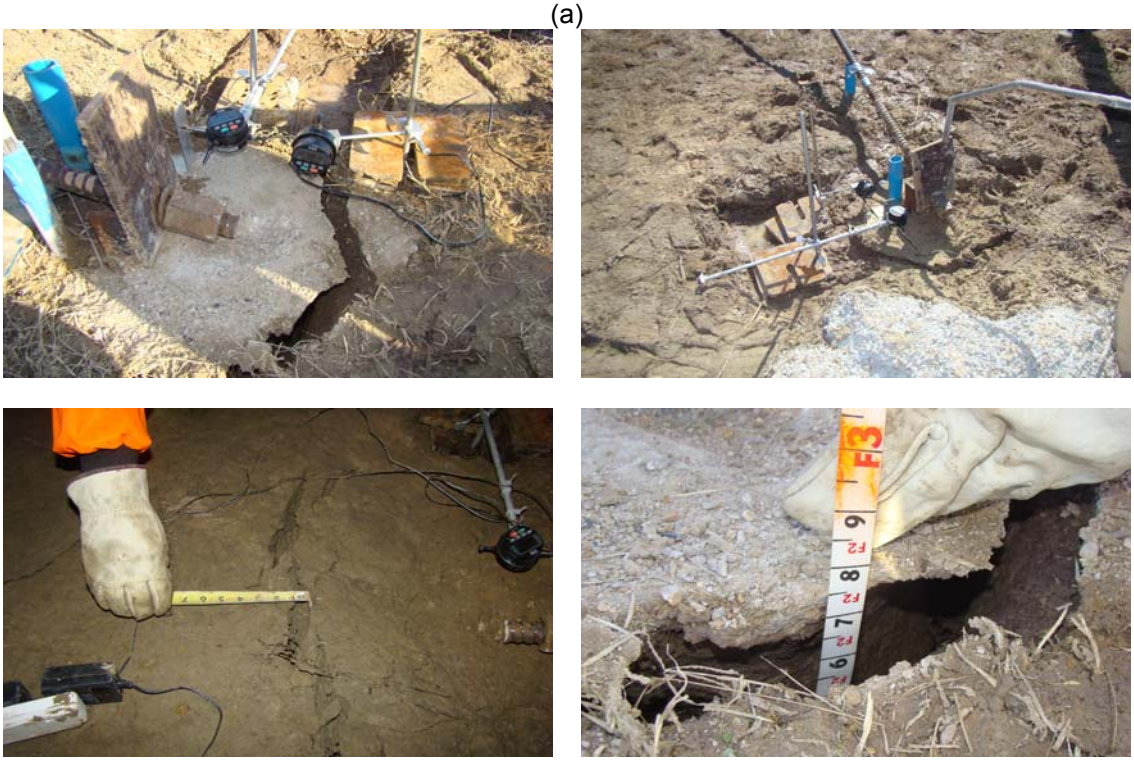

(b)

Figure 6.26. Test Shaft Displacement: (a) Summer Condition and (b) Winter Condition

6.4.2.3 Load and Deflection Data (Summer and Winter Conditions)

The load versus deflection at the groundline plots are shown in Figures 6.27 through 6.29 below. This shows the amount of deflection at the shaft head in the free-head condition as there was no collar nor pad placed around the top of the test shaft heads. This setup is typical for cable median barrier system placed on TxDOT highways. Recent observations in other parts of the state have notated some applications with a fixed-head which would lessen the amount of lateral deflection.

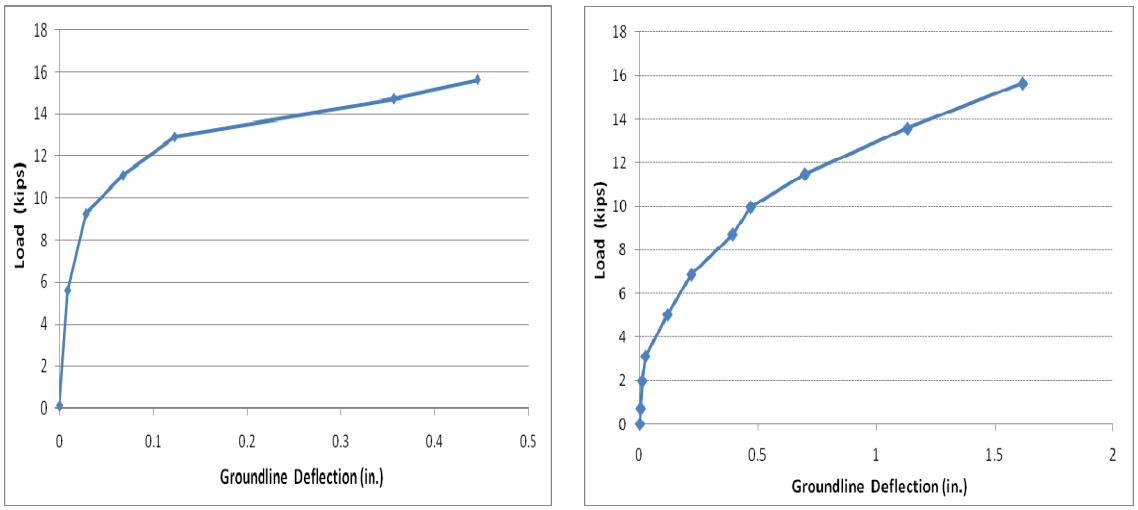

(a) (b)

Figure 6.27. Load versus Groundline Deflection
1 ft diameter x 6 ft depth
(a) Summer Condition (b) Winter Condition

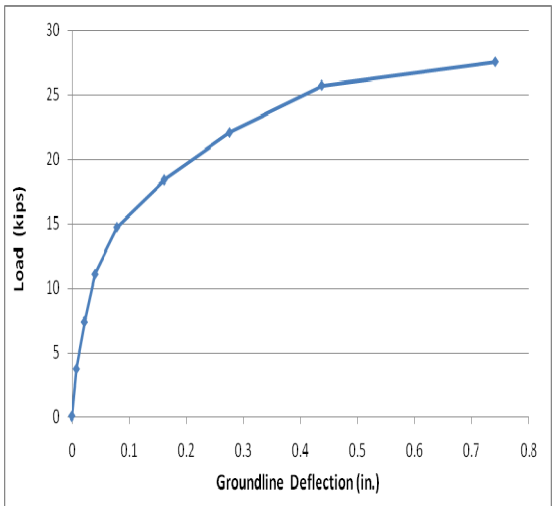

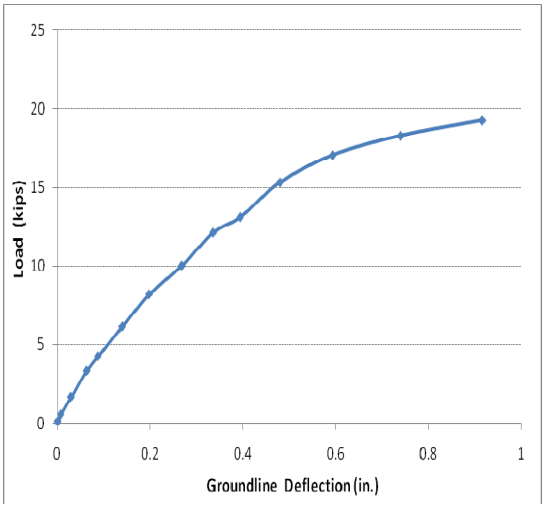

(a) (b)

Figure 6.28. Load versus Groundline Deflection
1 ft diameter x 10 ft depth
(a) Summer Condition (b) Winter Condition

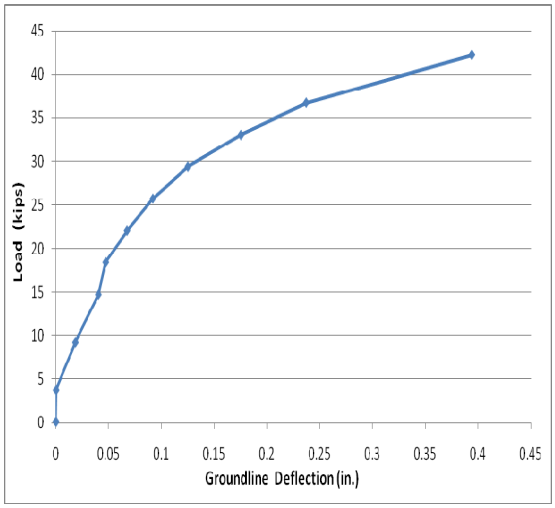

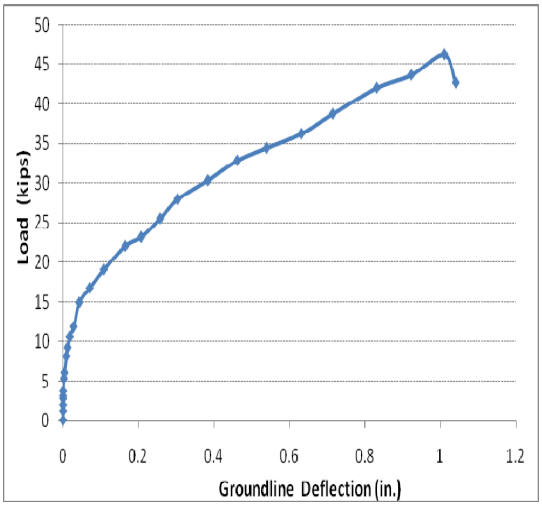

(a) (b)

Figure 6.29. Load versus Groundline Deflection
2 ft diameter and 10 ft depth
(a) Summer Condition (b) Winter Condition

The final lateral displacement readings from the field testing for all six (6) shafts, summer and winter conditions, are shown in Tables 6.2 and 6.3.

Table 6.2. Maximum Design Capacity versus Lateral Displacement (Summer Condition)

Test Set	Dimension Diameter x Depth ft x ft (m x m)	Maximum Capacity kips (kN)	Maximum Lateral Displacement at the Groundline in. (mm)
1	1 x 6 (0.3 x 1.8)	15.66 (69.66)	0.45 (11.4)
2	1 x 10 (0.3 x 3)	27.55 (122.55)	0.74 (18.8)
2	2 x 10[1] (0.6 x 3)	42.19 (187.67)	0.39 (9.9)

Note 1: The loading on this test shaft was stopped prior to full failure when the channel started to yield and bend and thereby affecting the workers' safety.

Table 6.3. Maximum Design Capacity versus Lateral Displacement (Winter Condition)

Test Set	Dimension Diameter x Depth ft x ft (m x m)	Maximum Capacity kips (kN)	Maximum Lateral Displacement at the Groundline in. (mm)
1	1 x 6 (0.3 x 1.8)	15.65 (69.61)	1.81 (46.0)
2	1 x 10 (0.3 x 3)	19.28 (85.76)	0.92 (23.4)
2	2 x 10 (0.6 x 3)	46.21 (205.55)	1.04 (26.4)

The maximum capacity values were computed for the summer condition by recording the values read directly from the gauge and applying the calibration curve conversion. The maximum capacity values were computed for the winter condition by recording the values read directly from the gauge and subtracting the strain gauge values collected during loading on the Dywidag bar.

6.4.3 Analysis

Three (3) test shafts were tested in the summer condition (September 2009) and the additional nine (9) test shafts were tested in the winter condition (February 2010). In the summer condition the three (3) shafts tested were 1 ft x 6 ft, 1 ft x 10 ft, and 2 ft x 10 ft. The

same identical size shafts were tested in the winter condition from the nine (9) remaining test shafts. Broms method was used to calculate the ultimate lateral bearing capacity on all six (6) test shafts and the results are shown in Table 6.4. Within the Broms method, s_u values from the laboratory remolded samples were used in the calculations and are listed in Table 6.4 for comparison.

Table 6.4. Comparison of Ultimate Lateral Load using Broms Method

Test Set	Diameter x Depth ft x ft (m x m)	Full Scale Test Summer Condition lbs (kN)	Full Scale Test Winter Condition lbs (kN)	Q_{ult} lbs (kN)	
				Broms' Method	
				Broms[1]	FHWA[2]
1	1 x 6 (0.3 x 1.8)	15,659 (69.65)	15650 (69.61)	6,343	6,978
2	1 x 10 (0.3 x 3.0)	27,554 (122.57)	19280 (85.76)	14,915	15,512
2	2 x 10 (0.6 x 3.0)	42,194 (187.69)	46210 (205.55)	19,091	17,898

Note 1: Calculated from Helwany, 2007 textbook, Figure 8.23a.
Note 2: Calculated using FHWA-HI-97-013, 1998, Figure 2.25.

The difference in the ultimate lateral load values between the summer and winter conditions is attributed to the change of stiffness; brittle failure in the summer condition and flexible failure in the winter condition. This is the most important factor limiting the lateral movement of the drilled shafts.

The values listed using the Broms method and the FHWA (FHWA-HI-97-013, 1998) method are close. Based on these values, these methods are deemed as very conservative when designing foundations for inclined loading.

6.5 Summary

The field tests that were conducted were very representative of the conditions that existed when the two (2) shafts failed in the winter of 2006-2007. The field test results compared closely with the design predictions confirming a similar climatic environment.

The MEMS-SAA data collection system tracked very close to the standard inclinometer values and was deemed better due to its' ability to continuously track movement.

The drilled shaft movements were found to be considerably greater when tested in the winter condition. This proved the hypothesis that a saturated soil and an increase in cable tension due to colder temperatures could provide enough inclined force to pull short foundations out of the ground thereby mitigating the necessary tension to keep the cables intact for cross-over impacts.

CHAPTER 7

SUMMARY AND CONCLUSIONS

7.1 Introduction

The objective of the original research project focused on the failure mechanisms of the foundation drill shafts for a cable barrier system installed by TxDOT. The failure occurred in 2007 when the area south of Terrell in Kaufmann County, Texas had received an abundance of rain and experienced unusually cold weather for an extended period. It was hypothesized that soil expansion causing uplift and tensile forces in the cables created by the colder weather caused the failures. The researchers developed a plan to confirm or reject this hypothesis. This thesis research effort mainly focused on site selection, site soil characterization, load test facility design and construction, and discussion of the load test results. The following describes some of the major findings and summary results from this thesis research effort.

7.2 Summary and Conclusions

A test site was located on IH20 at Rose Hill Road, being near the site of the two previous failures, in an area that would readily accommodate the construction equipment, provide unrestricted access, and provide safety from the travelling public.

Preconstruction field investigation and laboratory testing yielded soil that was classified as silty sand, high-plasticity clay, and lean clay. The two clay soils were of significant interest to the researchers for this study. From these test results, it was deemed that the selected site was very satisfactory for the continuation of the installation of the design test sets in the field. Additionally, weather conditions during the past nine months from June 2009 to February 2010 allowed the researchers to perform load tests under summer- and winter-like conditions that contributed to the two actual cable barrier systems failures three years earlier.

The testing plan and design of the reaction and test drill shafts of varying sizes was performed by the UTA research team in which the author was a contributing partner. Design of the test setups was performed to ensure proper distance between the reaction and test shafts and the test results obtained were analyzed later to address these effects. Construction of the shafts was completed in June 2009. Three test sets were designed with four test shafts associated per reaction shaft. Two reaction and eight different test shaft sizes were designed. Duplicate test shaft sizes of 1 ft x 6 ft (0.3 m x 1.8 m), 1 ft x 10 ft (0.3 m x 3 m), and 2 ft x 10 ft (0.6 m x 3 m) were constructed to allow for comparison testing of identically sized drilled shafts for both the summer and winter conditions. Testing of all drilled shafts was successfully completed.

In September 2009, field testing for the summer condition (dry and hot) occurred. This consisted of testing one test shaft from each of the three reaction shafts. As the hypothesis focused on soil expansion and cold weather, these three tests were only used for comparison purposes here. In February 2010, the additional nine shafts were subjected to load tests under ideal field winter conditions (totally saturated soil and cold temperatures). The area also unexpectedly received a record 24-hour snowfall of 12 in. (300 mm) adding to the continuance of the soil being totally saturated. Ice lenses were seen on the water that was ponded on the ground surface indicating freezing temperatures during the night. The 1 ft (0.3 m) and 2 ft (0.6 m) test shafts experienced large lateral and vertical displacements due to the load testing during this winter condition. Cracking of the concrete, both horizontally and vertically, was observed on several of the test shafts. The 3 ft (0.9 m) shafts did not experience displacement nor material failure. The following summarizes a few major conclusions from this research.

7.3 Conclusions

1. Site selection and soil characterization showed that the upper strata contained soils that can be characterized as expansive in nature. The volumetric swell strains of Soil Layers 2 and 3 are 11.1% and 7.7% and the linear/volumetric shrinkage strains are 12.1/6.8% and 8.4/5.22%, respectively. These results indicate that the present soils are close to the surface are indeed expansive.
2. The load test design includes a design of the reaction and the test shaft configuration and spacings between them. Preliminary LPILE analyses conducted on these reaction and test shafts using the hypothetical lateral loads estimated from tensile loads in the cables showed that a spacing of 20 ft between each reaction and test shaft for the given testing condition resulted in lesser influence of the reaction shaft movements on the test results.
3. The load tests in the inclined configuration were successful and the field load testing went smoothly as per the design. Ultimate inclined loads were successfully obtained for the majority of the tests conducted. Though the channel section to which the Dywidag bar was connected had yielded in one test, this was quickly was corrected with additional splicing, resulting in the completion of the test. Subsequent tests on all of the other test shafts were conducted by providing the same additional splicing at each of the steel channel pieces. Overall, the inclined load tests were conducted successfully in these north Texas soil conditions.
4. Tests under inclined loads showed different failure modes at different seasonal periods. These include large lateral and vertical movements for smaller diameter shafts to breaking of the shafts near the ground surface zones due to high tensile stresses being developed from the loadings.

5. Tests conducted on the shafts of identical dimensions in the summer and winter conditions showed that the load-displacement response in the hot and dry season condition (summer) was close to the brittle failure condition whereas in the wet and cold season condition (winter), the response was close to the flexible failure condition.
6. Ultimate loads on the smaller test shafts appear not to be influenced by the weather conditions; however, the 2 ft diameter shafts yielded higher ultimate loads in the summer condition tests than in the winter condition tests.
7. Broms method, which is normally used for free-head drilled shafts in one layer soil conditions, with assumptions, was used to predict the ultimate lateral loads in the design phase of this research project. After completion of the field tests under inclined loading, the predicted design results were not close to the predicted inclined ultimate loads but neither are largely different from the field measured results.

7.4 Additional Research

Further analyses of the test results are well beyond the scope of this thesis research and a few research directions have been identified and are given here:

A. Analysis of the field data using LPILE, AllPile, or other more recent software analysis programs with various soil models including soil continuum models that will entail more variables associated with this research.
B. Inclusion of uplift conditions will provide more insights into the variations in inclined loads.
C. Investigation of the concrete failure in the drilled test shafts. This horizontal failure exacerbates the tipping issue and can make the cables become slack which is a less than desirable action.

APPENDIX A

MANUFACTURER DESIGN PLAN SHEET

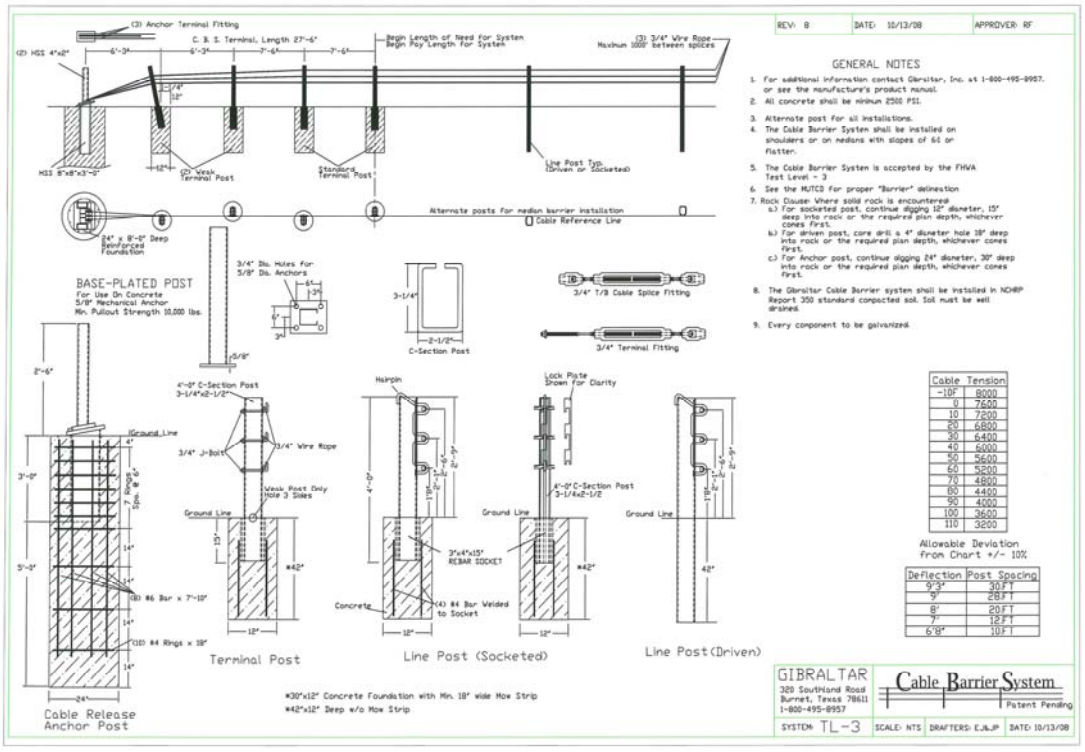

Figure A.1. Manufacturer Typical Design Plan Sheet

APPENDIX B

CONCRETE MIX DESIGNS

TEXAS DEPARTMENT OF TRANSPORTATION

HYDRAULIC CEMENT CONCRETE MIX DESIGN & CONTROL
Material Properties

SAMPLE ID:		SAMPLED DATE:	
TEST NUMBER:		LETTING DATE:	
SAMPLE STATUS:		CONTROLLING CSJ:	
COUNTY:		SPEC YEAR:	2004
SAMPLED BY:		SPEC ITEM:	
SAMPLE LOCATION:		SPECIAL PROVISION:	
MATERIAL CODE:		CLASS:	CLASS C
MATERIAL NAME:			
PRODUCER:			
AREA ENGINEER:		PROJECT MANAGER:	

COURSE\LIFT:		STATION:		DIST. FROM CL:	

AGGREGATE PROPERTIES (FROM LABORATORY TESTING)

	Percentage (%)	Aggregate Type/Source	Specific Gravity (SSD)	Rodded Unit Weight (U_{DRY})	Fineness Modulus (FM)	Free (Surface) Moisture (%)	Absorption (%)
Test Method			Tex-403-A	Tex-404-A	Tex-402-A	Tex-409-A	Tex-403-A
Coarse Aggregate 1:	100	TXI Beckett Road Pea Gravel	2.65	121.20		0.3	0.1
Coarse Aggregate 2:							
Coarse Aggregate 3:							
Coarse Aggregate 4:							
Total Coarse Aggr.:	100	<= Must equal 100					
Fine Aggregate 1:	100	TXI Ferris	2.65		2.72	6.0	0.1
Fine Aggregate 2:							
Total Fine Aggr.:	100	<= Must equal 100					

CEMENTITIOUS MATERIALS

	Percentage by Weight, (%)	Pozzolan Type/Source	Specific Gravity	% NA_2O equivalent in cement*
Hydraulic cement	80	TXI Midlothian Ty I/II	3.15	
Fly Ash	20	Boral Headwaters	2.50	
Ground Granulated Blast Furnace Slag				
Silica Fume				
UFFA				
Metakaolin				
Other Pozzolan				
Total Cementitious Matl:	100	<= Must equal 100		

* Only required if Mix Design Options 6 or 7 are used.

CHEMICAL ADMIXTURES

	Type/Source	Type	Dosage (fl oz./100 lbs. cement)	% Solids
Air entraining admixutre				
Set Retarder				
Accelerator				
Water reducer	W.R. Grace Mira 85	A	16.90	
High-range water reducer				
Water reducing retarder				
High-range water reducing retarder				
Lithium nitrate admixture				
Corrosion inhibitor				

OTHER MATERIALS

	Type/Source	Specific Gravity	Dosage (lbs/CY)
Fibers			

Figure B.1. Concrete Design Material Properties

TEXAS DEPARTMENT OF TRANSPORTATION

HYDRAULIC CEMENT CONCRETE MIX DESIGN & CONTROL
Mix Proportions based on ACI 211.1-91®

SAMPLE ID:		SAMPLED DATE:	
TEST NUMBER:		LETTING DATE:	
SAMPLE STATUS:		CONTROLLING CSJ:	
COUNTY:		SPEC YEAR:	2004
SAMPLED BY:		SPEC ITEM:	
SAMPLE LOCATION:		SPECIAL PROVISION:	
MATERIAL CODE:		CLASS:	CLASS C
MATERIAL NAME:			
PRODUCER:			
AREA ENGINEER:		PROJECT MANAGER:	#VALUE!

COURSE\LIFT:		STATION:		DIST. FROM CL:	

Nom. Max. Agg. Size, (inches):	0.5	Air Entrained?:	No.	Slump, (inches):	6	Exposure:	NA
Mix Design Option?:		See Item 421.4.A.6		Mix design target strength, (psi):			4800
Basic Water Demand, lb/CY:	383	Water Adjustment Factor:	0.66	Controlling w/c or w/cm:			0.45
ASTM C 1260 % Expansion		*Approved Lab Used?:*		*lb. sika/1 per cu. yd.*			

	Mix Component	lb/CY	%/CY	fl oz.	Specific Gravity	Density, lbs/ft3	Approx. Sacks	Absolute Vol. (ft^3)	Weight (lbs/CY)	Weight† (lbs/CY)
Paste	Water	253			1.00	62.4		4.05	253	156
	Total Cementitious	562								
	Portland Cement		80		3.15	196.6	4.79	2.29	450	
	Flyash		20		2.5	156.0	1.19	0.72	112	
	GGBF Slag									
	Silica Fume									
	UFFA									
	Metakaolin									
	Other Pozzolan									
	Air entraining admixture:									
	Set retarder									
	Accelerator									
	Water Reducer			94.98				0.10		
	High-Range Water Reducer									
	Water Reducing Retarder									
	Hi-Range H20 Reducing Retarder									
	Lithium Nitrate Admixture									
	Corrosion Inhibitor									
	Paste Volume=Total (water + cm)							**7.16**		
Air	Approximate Entrapped Air*:		0.0					0.00		
	Specified Value**:		Need Exposure							
	Air + Paste Volume:							**7.16**		
Other	Fibers:									
	.									

			Sp. Gr. SSD	Unit Weight, lbs/ft^3:	Bulk Vol. = b/b_0 x 27, ft^3		Absolute Vol. (ft^3)	Weight (lbs/CY)	Weight† (lbs/CY)
Aggregate	Total Aggregate Volume, ft^3:						19.84		
	Coarse Aggregate Factor (CAF):	0.55							
	Coarse Aggregate 1:	100	2.65	121.2	14.85		10.89	1800	1805
	Coarse Aggregate 2:								
	Coarse Aggregate 3:								
	Coarse Aggregate 4:								
	Mix vol. subtotal:						18.05		
	Weighted Average FM:	2.7							
	Fine Aggregate 1	100	2.65				8.95	1480	1569
	Fine Aggregate 2								

	CY	Absolute Vol. (ft^3)	Weight (lbs/CY)	lbs/ft3
Total Weight:			4095	
Size of Truck, CY:				
Est. Total Weight / Truck :			0	
Total Absolute Volume:				
Theoretical Weight of Concrete Computed on an Air-Free Basis (see Tex-417-A):				
Design Yield (Unit Weight):				151.7

* Only applicable for non-air-entrained concrete

** Only applicable for air-entrained concrete

† Weight adjusted based on aggregate moisture, aggregate absorption, and admixture water content

Figure B.2. Concrete Design Mix Proportions

Table B.1. Concrete Quantities
Test Set 1

Concrete (Class C)			
12 in. (0.3 m) Diameter Test Shaft			
Item	Diameter, in. (m)	Length, ft (m)	Volume, ft^3 (m^3)
Concrete	12 (0.3)	6.5 (2.0)	5.11 (0.14)
24 in. (0.6 m) Diameter Test Shaft			
Concrete	24 (0.6)	6.5 (2.0)	20.42 (0.58)
36 in. (0.9 m) Diameter Test Shaft			
Concrete	36 (0.9)	6.5 (2.0)	45.95 (1.30)
36 in. (0.9 m) Diameter Reaction Shaft			
Concrete	36 (0.9)	42.0 (12.8)	296.88 (8.41)

Table B.2. Concrete Quantities
Test Set 2

Concrete (Class C)			
12 in. (0.3 m) Diameter Test Shaft			
Item	Diameter, in. (m)	Length, ft (m)	Volume, ft^3 (m^3)
Concrete	12 (0.3 m)	10.5 (3.2)	8.25 (0.23)
24 in. (0.6 m) Diameter Test Shaft			
Concrete	24 (0.6)	10.5 (3.2)	32.99 (0.93)
24 in. (0.6 m) Diameter Test Shaft			
Concrete	24 (0.6)	10.5 (3.2)	32.99 (0.93)
48 in. (1.2 m) Diameter Reaction Shaft			
Concrete	48 (1.2)	42.5 (13.0)	534.07 (15.12)

Table B.3. Concrete Quantities
Test Set 3

Concrete (Class C)			
12 in. (0.3 m) Diameter Test Shaft			
Item	Diameter, in. (m)	Length, ft (m)	Volume, ft^3 (m^3)
Concrete	12 (0.3 m)	14.5 (4.4)	11.39 (0.32)
24 in. (0.6 m) Diameter Test Shaft			
Concrete	24 (0.6)	14.5 (4.4)	45.55 (1.29)
36 in. (0.9 m) Diameter Test Shaft			
Concrete	36 (0.9)	14.5 (4.4)	102.49 (2.90)
48 in. (1.2 m) Diameter Reaction Shaft			
Concrete	48 (1.2)	42.5 (13.0)	534.07 (15.12)

Table B.4. Total Concrete Quantities for all Three Test Sets

Concrete (4000 psi) All Test Sets	
Item	Total Volume, ft^3 (m^3)
Concrete	1433.27 (40.59)
Item	Total Volume, yd^3 (m^3)
Concrete	53.08 (40.58)

APPENDIX C

STEEL REINFORCEMENT DETAILS

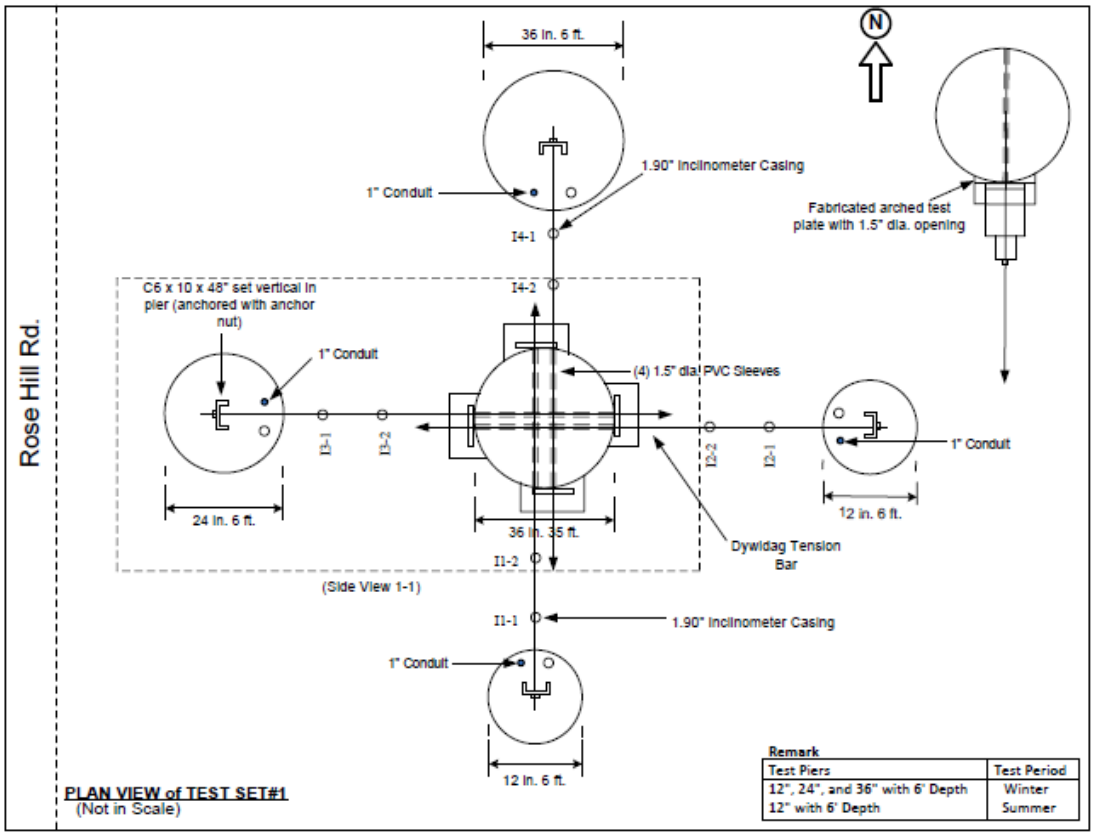

Figure C.1. Plan View of Test Set 1

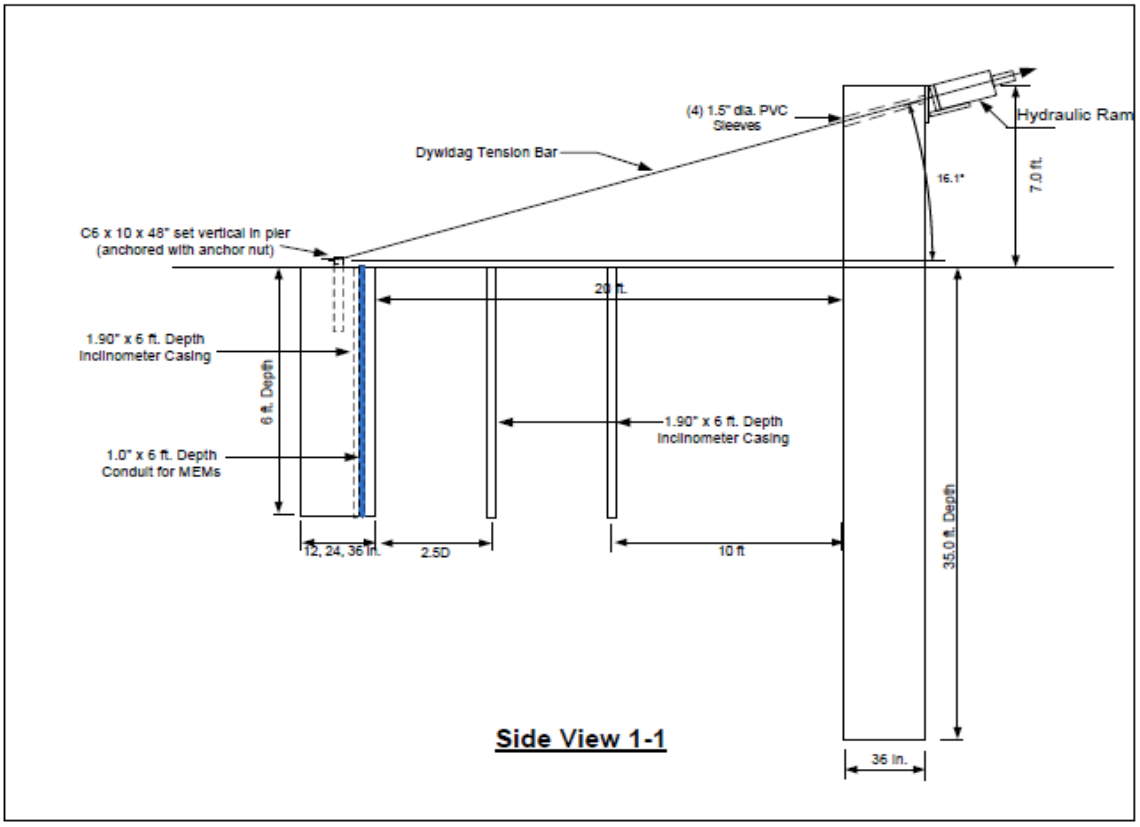

Figure C.2. Elevation View of Test Set 1

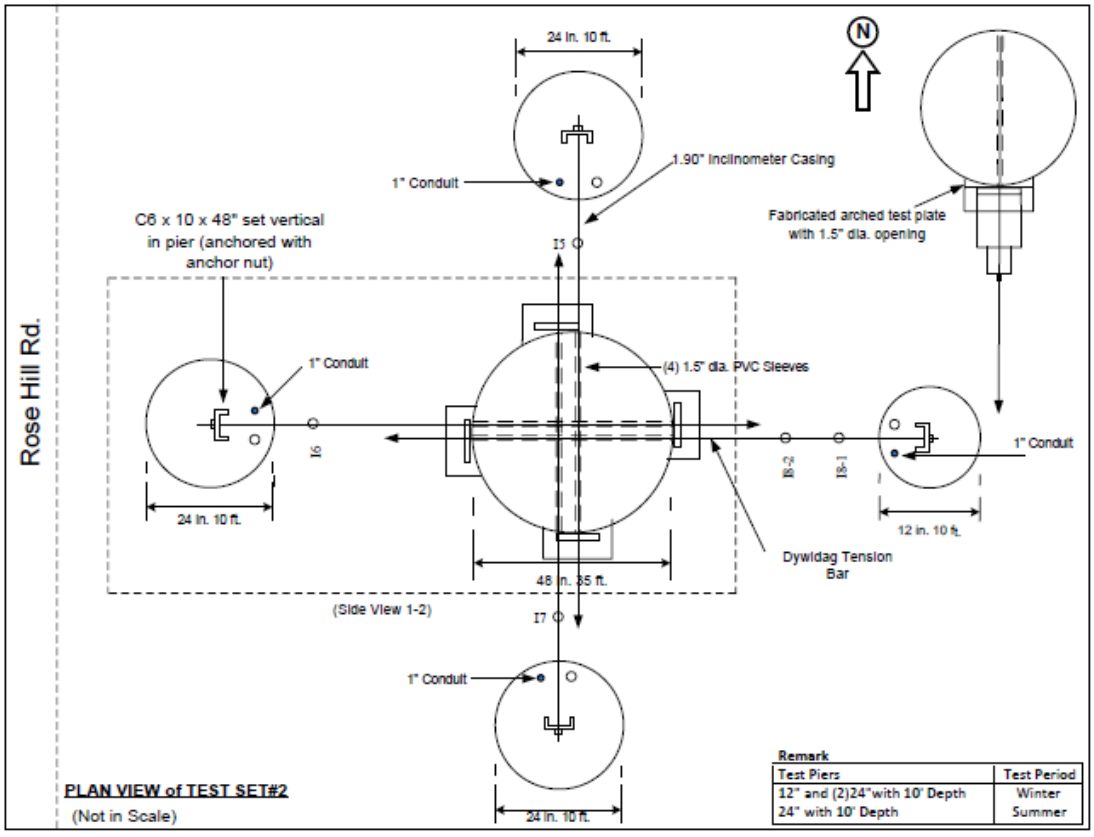

Figure C.3. Plan View of Test Set 2

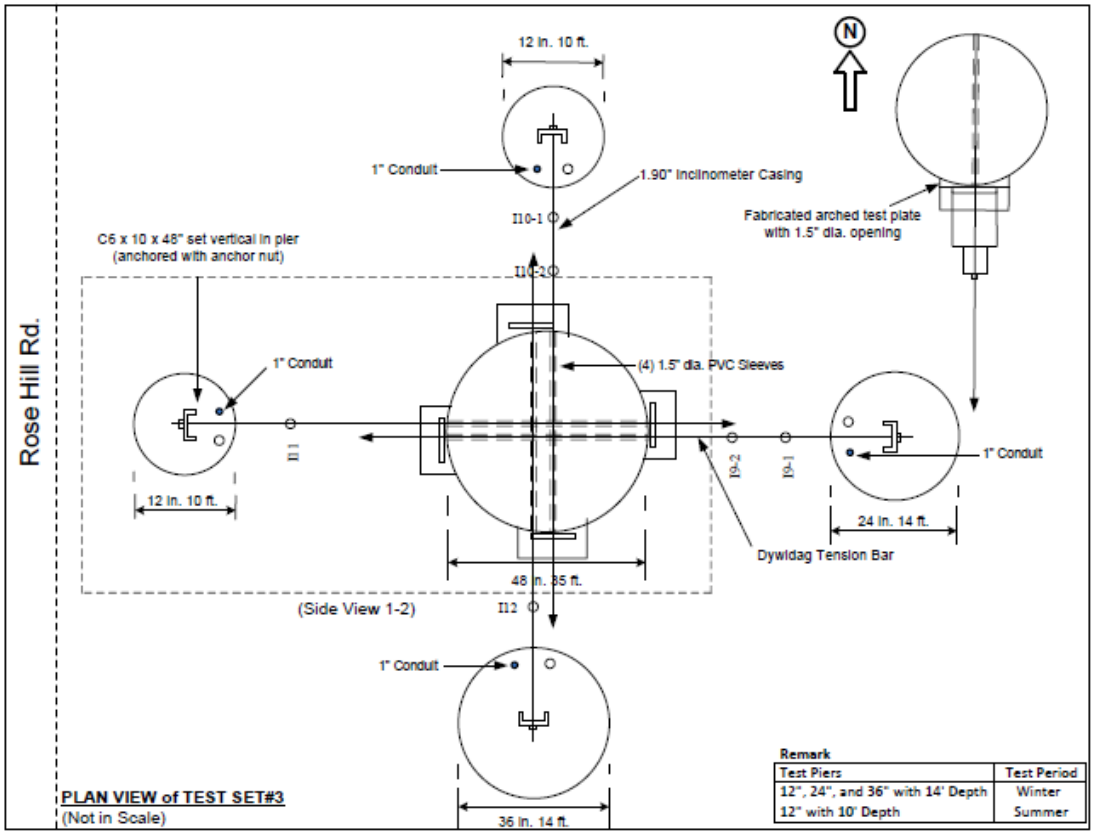

Figure C.4. Plan View of Test Set 3

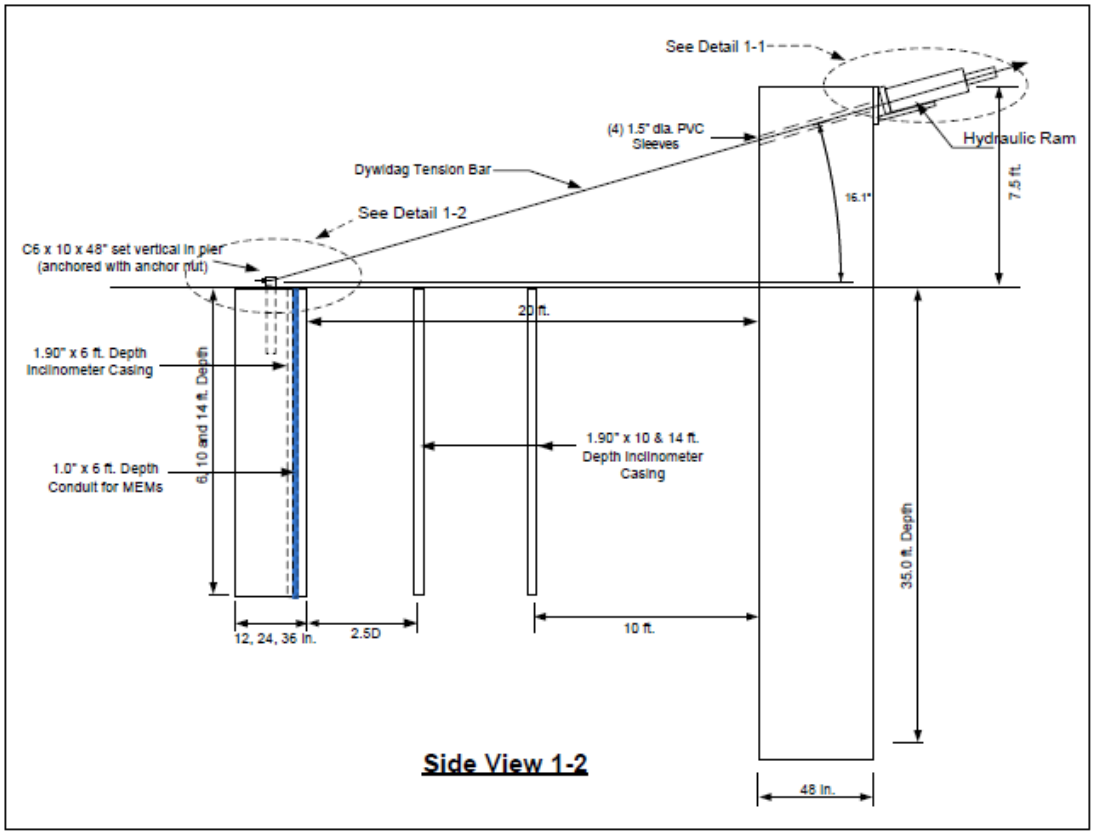

Figure C.5. Elevation View of Test Sets 2 and 3

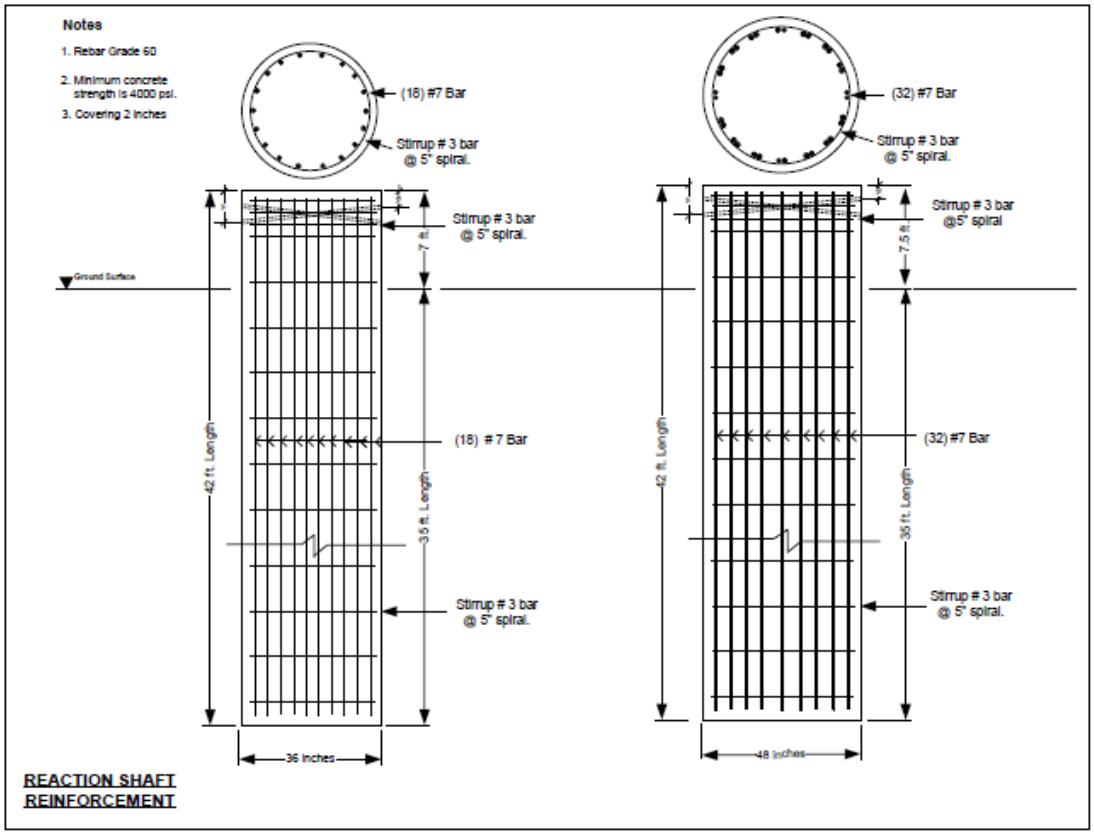

Figure C.6. Steel Reinforcement Plan Sheet for the Reaction Shafts

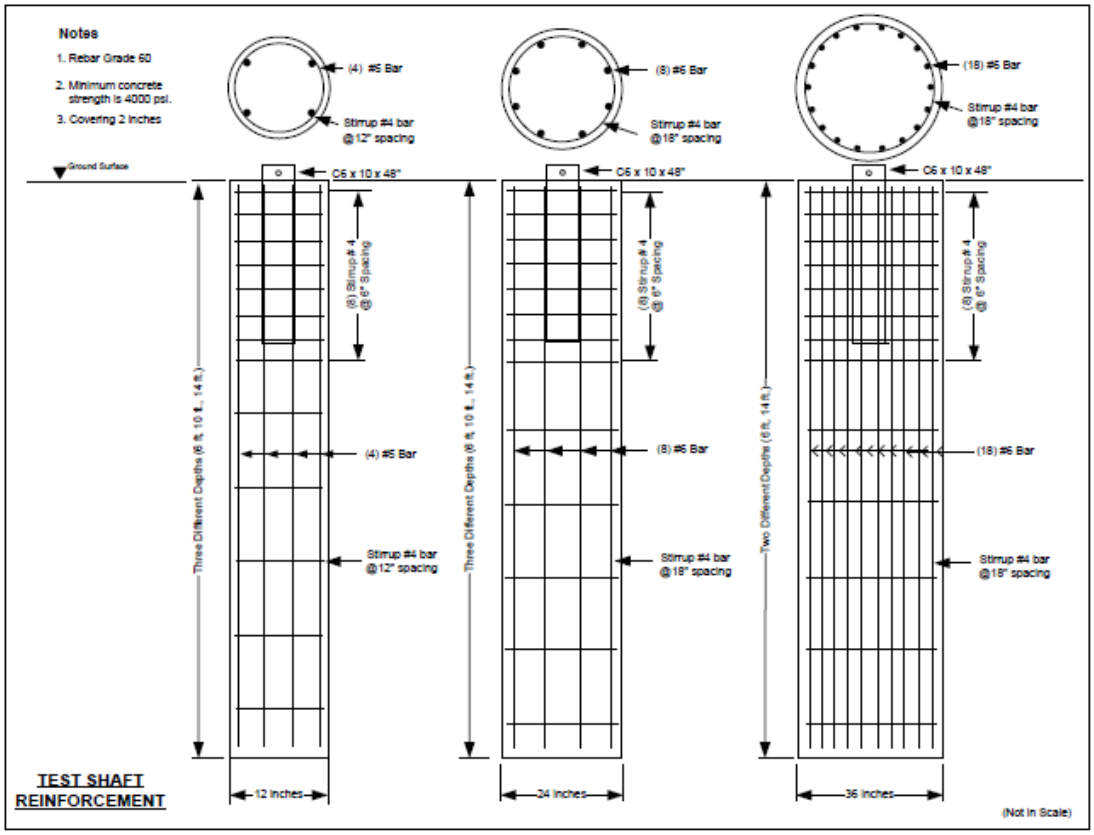

Figure C.7. Steel Reinforcement Plan Sheet for the Test Shafts

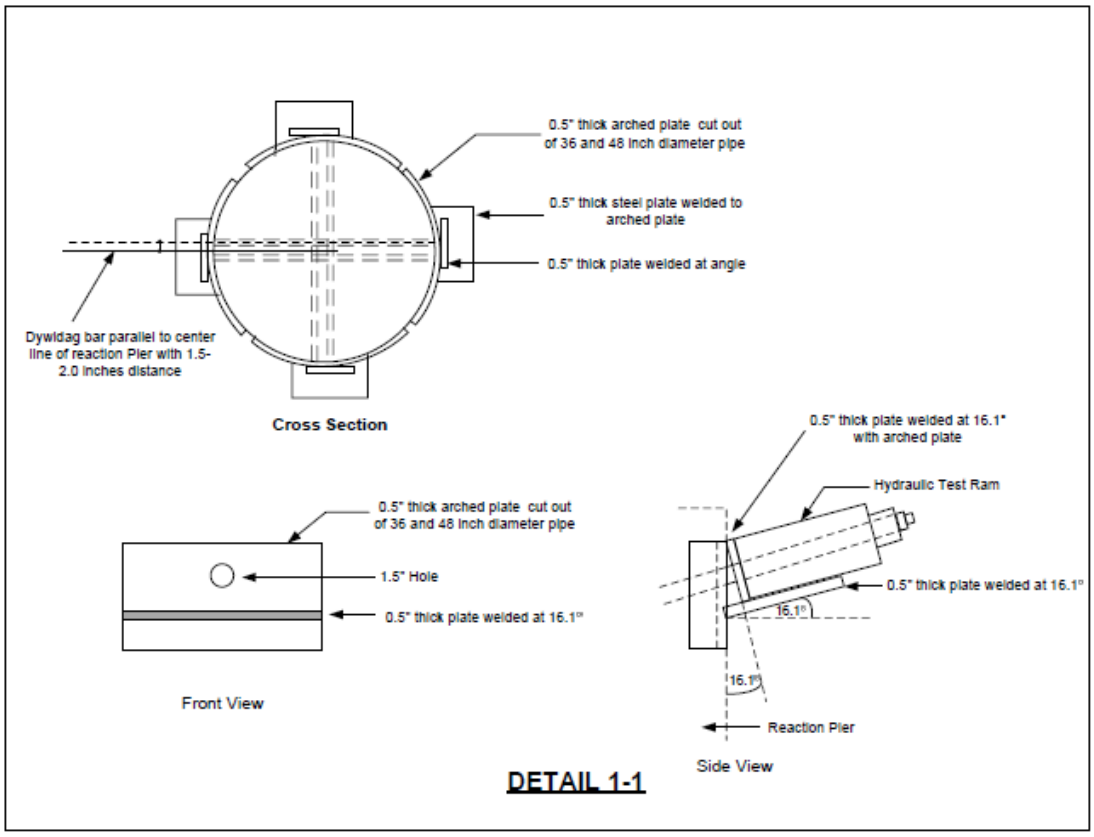

Figure C.8. Typical Sections of Dywidag Bar Setup

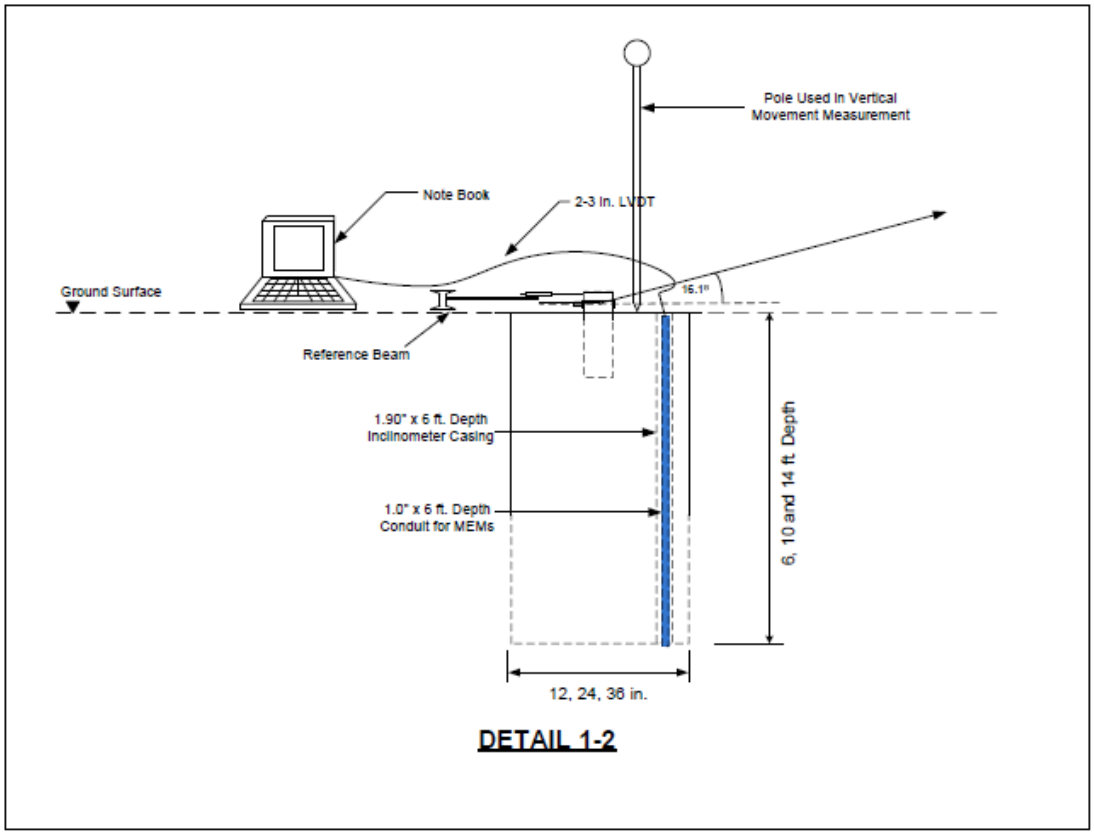

Figure C.9. Typical Section for LVDT and Data Acquisition

Table C.1. Original Design of Main Rebars in the Drilled Shafts

Original Design		
Concrete:		
Diameter	24.00	in.
Area	452.39	in^2
f_c'	2.50	ksi
Bearing Capacity of the concrete:		
f_c' x Area	1130.97	kip
No. 6 Rebar:		
Diameter	0.75	in.
Area	0.44	in^2
Pieces of rebar	8	pcs
f_y	60	ksi
Capacity of Rebar:		
f_y x Area x Pieces of rebar	211.20	kip
Analysis:		
Capacity of the section	1342.17	kip
% Reinforcement in the original cross-section area	0.78	%

Table C.2. Design Trial 1 of Main Rebars in the Drilled Shafts

Design Trial 1			
Concrete:			
Diameter	**12.00**	inches	
Area	113.10	in^2	
f_c'	2.50	ksi	
Bearing Capacity of the concrete:			
f_c' x Area	282.74	kip	
Rebars in the section need to tolerate the force:			
= capacity of section – bearing capacity of the concrete	1059.43	kip	
Trial 1:			
a. Use No. 6 Rebar in the cross-sectional area	0.44	in^2	
b. Minimum yield strength of Grade 60	60,000	psi	
c. Strength of 1 – No. 6 Rebar	26.40	kip	
d. Number of No. 6 Rebar pieces	40.12992	pcs	Not OK
Trial 2:			
a. Use No. 10 Rebar in the cross-section area	1.27	in^2	
b. Minimum yield strength of Grade 60	60,000	psi	
c. Strength of 1 – No. 10 Rebar	76.20	kip	
d. Number of No. 10 Rebar pieces	13.90328	pcs	OK

Table C.3. Design Trial 2 of Main Rebars in the Drilled Shafts

Design Trial 2			
Concrete:			
Diameter	**36.00**	inches	
Area	1017.88	in^2	
f_c'	2.50	ksi	
Bearing Capacity of the concrete:			
f_c' x Area	2544.69	kip	
Rebars in the section need to tolerate the force:			
= capacity of section - bearing capacity of the concrete	1202.52	kip	
Trial 1:			
a. Keep same percent of reinforcement in the cross-sectional area	0.78	%	
b. Area of a No. 6 Rebar	0.44	in^2	
c. Total Area of Reinforcement	7.92	in^2	
d. Number of No. 6 Rebar	18	pcs	OK

Table C.4. Steel Reinforcement Quantities for Test Set 1

Rebar (Grade 60) Test Set 1			
1 ft (0.3 m) Diameter Test Shaft			
Item	Number of Pieces	Length, ft (m)	Total Length, ft (m)
Main (No. 10 Rebar)	14	6.17 (1.88)	86.38 (26.33)
Stirrup (No. 4 Rebar)	10	6.28 (1.91)	62.83 (19.15)
2 ft (0.6 m) Diameter Test Shaft			
Main (No. 6 Rebar)	8	6.17 (1.88)	49.36 (15.04)
Stirrup (No. 4 Rebar)	10	7.85 (2.39)	78.54 (23.94)
3 ft (0.9 m) Diameter Test Shaft			
Main (No. 6 Rebar)	18	6.17 (1.88)	111.06 (33.85)
Stirrup (No. 4 Rebar)	10	9.42 (2.87)	94.25 (28.73)
3 ft (0.9 m) Diameter Reaction Shaft			
Main (No. 7 Rebar)	18	41.67 (12.70)	750.06 (228.62)
Stirrup (No. 3 Rebar)	45	9.42 (2.87)	424.12 (129.27)

Table C.5. Steel Reinforcement Quantities for Test Set 2

Rebar (Grade 60)			
1 ft (0.3 m) Diameter Test Shaft			
Item	Number of Pieces	Length, ft (m)	Total Length, ft (m)
Main (No. 10 Rebar)	14	10.17 (3.10)	142.38 (43.40)
Stirrup (No. 4 Rebar)	13	6.28 (1.91)	81.68 (24.90)
2 ft (0.6 m) Diameter Test Shaft			
Main (No. 6 Rebar)	8	10.17 (3.10)	81.36 (24.80)
Stirrup (No. 4 Rebar)	13	6.28 (1.91)	81.68 (24.90)
3 ft (0.9 m) Diameter Test Shaft			
Main (No. 6 Rebar)	18	10.17 (3.10)	81.36 (24.80)
Stirrup (No. 4 Rebar)	13	7.85 (2.39)	102.10 (31.12)
4 ft (1.2 m) Diameter Reaction Shaft			
Main (No. 7 Rebar)	32	41.67 (12.70)	1333.44 (406.43)
Stirrup (No. 3 Rebar)	45	12.57 (3.83)	565.49 (172.36)

Table C.6. Steel Reinforcement Quantities for Test Set 3

Rebar (Grade 60)			
1 ft (0.3 m) Diameter Test Shaft			
Item	Number of Pieces	Length, ft (m)	Total Length, ft (m)
Main (No. 10 Rebar)	14	14.17 (4.32)	198.38 (60.47)
Stirrup (No. 4 Rebar)	15	6.28 (1.91)	94.25 (28.73)
2 ft (0.6 m) Diameter Test Shaft			
Main (No. 6 Rebar)	8	14.17 (4.32)	113.36 (34.55)
Stirrup (No. 4 Rebar)	15	7.85 (2.39)	117.81 (35.91)
3 ft (0.9 m) Diameter Test Shaft			
Main (No. 6 Rebar)	18	14.17 (4.32)	255.06 (77.74)
Stirrup (No. 4 Rebar)	15	9.42 (2.87)	141.37 (43.09)
4 ft (1.2 m) Diameter Reaction Shaft			
Main (No. 7 Rebar)	32	41.67 (12.70)	1333.44 (406.43)
Stirrup (No. 3 Rebar)	45	12.57 (3.83)	565.49 (172.36)

Table C.7. Total Steel Reinforcement Quantities for all Three Test Sets

Rebar (Grade 60) All Test Sets			
Item	Number of Pieces	Length, ft (m)	Total Length, ft (m)
No. 3 Rebar (Reaction Shafts)	135	34.56 (10.53)	1555.10 (473.99)
No. 4 Rebar (Test Shafts)	114	67.51 (20.58)	854.51 (260.45)
No. 6 Rebar	78	61.02 (18.60)	691.56 (210.79)
No. 7 Rebar	82	125.01 (38.10)	3416.94 (1041.48)
No. 10 Rebar	42	30.51 (9.30)	427.14 (130.19)

APPENDIX D

FIELD TEST DATA FOR TEST SHAFT DEFLECTIONS

Table D.1. Field Deflection Data for Test Shaft 1 (1 ft x 6 ft (0.3 m x 1.8 m))

Time (min)	Load (psi)	Load (kips)	Actual Load (kips)	Horizontal Deflection (mm)	Horizontal Deflection (in.)	Vertical Deflection (mm)	Vertical Deflection (in.)
0	0	0.104	0.103962875	0	0	0	0
0	100	1.934	1.933665875	0.078	0.00307086	0	0
0.17	200	3.764	3.760695875	0.256	0.01007872	0.004	0.00015748
2.30	300	5.594	5.5879115	0.598	0.02354326	0.016	0.00062992
6.05	400	7.424	7.418022875	2.984	0.11748008	0.69	0.0271653
10.19	500	9.254	9.243493625	5.533	0.21783421	0.69	0.0271653
24.24	600	11.084	11.07178588	9.946	0.39157402	2.742	0.10795254
31.23	700	12.914	12.90219425	16.888	0.66488056	4.344	0.17102328
49.48	800	14.744	14.72747938	22.708	0.89401396	4.944	0.19464528
56.52	850	15.659	15.63947225	33.7	1.326769	5.516	0.21716492
1.04.05	900	16.574	16.55139088	46.072	1.81385464	7.374	0.29031438

Table D.2. Field Deflection Data for Test Shaft 2 (1 ft x 10 ft (0.3 m x 3 m))

Time (min)	Load (psi)	Load (kips)	Actual Load (kips)	Horizontal Deflection (mm)	Horizontal Deflection (in.)	Vertical Deflection (mm)	Vertical Deflection (in.)
0	0	0.104	0.103665875	0	0	0	0
0	100	1.934	1.932997625	0.16	0.0062992	0.16	0.0062992
1.08	200	3.764	3.7629605	0.722	0.02842514	0.16	0.0062992
2.43	300	5.594	5.591883875	1.584	0.06236208	0.16	0.0062992
5.26	400	7.424	7.421809625	2.602	0.10244074	0.314	0.01236218
15.53	500	9.254	9.250398875	4.14	0.1629918	0.764	0.03007868
17.49	600	11.084	11.07921088	5.508	0.21684996	0.81	0.0318897
20.14	700	12.914	12.9082085	7.9	0.311023	0.932	0.03669284
29.43	800	14.744	14.7370205	10.324	0.40645588	2.052	0.08078724
31.36	900	16.574	16.56624088	13.208	0.51999896	2.16	0.0850392
41.44	950	17.489	17.48012713	15.18	0.5976366	2.602	0.10244074
43.49	1000	18.404	18.39431038	17.07	0.6720459	2.602	0.10244074
45.30	1050	19.319	19.308902	18.8	0.740156	3.464	0.13637768
53.51	1100	20.234	20.22289963	23.272	0.91621864	3.928	0.15464536
56.44	1050	19.319	9.250398875	13.756	0.54157372	3.532	0.13905484

Table D.3. Field Deflection Data for Test Shaft 3 (2 ft x 10 ft (0.6 m x 3 m))

Time (min)	Load (psi)	Load (kips)	Actual Load (kips)	Horizontal Deflection (mm)	Horizontal Deflection (in.)	Vertical Deflection (mm)	Vertical Deflection (in.)
0	0	0.104	0.104	0	0	0	0
0.18	100	1.934	1.932552125	0	0	0	0
1.07	200	3.764	3.76214375	0	0	0	0
2.06	300	5.594	5.591141375	0	0	0	0
2.06	400	7.424	7.421067125	0	0	0	0
3.18	500	9.254	9.249545	0.002	0.00007874	0	0
4.27	600	11.084	11.0788025	0.044	0.00173228	0	0
5.54	700	12.914	12.90739175	0.086	0.00338582	0.002	0.00007874
8.34	800	14.744	14.736575	0.22	0.0086614	0.02	0.0007874
10.50	900	16.574	16.5655355	0.304	0.01196848	0.034	0.00133858
13.23	1000	18.404	18.39460738	0.444	0.01748028	0.09	0.0035433
22.01	1100	20.234	20.22338225	0.706	0.02779522	0.1	0.003937
24.23	1200	22.064	22.05204575	1.084	0.04267708	0.116	0.00456692
27.51	1300	23.894	23.8798925	1.788	0.07039356	0.132	0.00519684
30.24	1400	25.724	25.70792488	2.738	0.10779506	0.138	0.00543306
33.33	1500	27.554	27.53666263	4.182	0.16464534	0.004	0.00015748
42.33	1600	29.384	29.36621713	5.25	0.2066925	0.082	0.00322834
46.22	1700	31.214	31.194101	6.532	0.25716484	0.082	0.00322834
48.55	1800	33.044	33.02205913	7.7	0.303149	0.032	0.00125984
51.27	1900	34.874	34.84960888	9.733	0.38318821	0.088	0.00346456
55.35	2000	36.704	36.67871788	11.716	0.46125892	0.096	0.00377952
1.03.20	2100	38.534	38.5086065	13.688	0.53889656	0.098	0.00385826
1.16.45	2200	40.364	40.335785	16.028	0.63102236	0.18	0.0070866
1.23.10	2300	42.194	42.1635575	18.14	0.7141718	0.212	0.00834644
1.25.57	2400	44.024	43.99144138	21.102	0.83078574	0.372	0.01464564
1.31.57	2500	45.854	45.82021625	23.422	0.92212414	0.414	0.01629918
1.35.25	2600	47.684	47.65515388	25.644	1.00960428	0.478	0.01881886
1.41.15	2650	46.599	45.82144138	26.422	1.04023414	2.106	0.08291322

APPENDIX E

FIELD CONSTRUCTION AND TESTING PHOTOGRAPHS





Figure E.1. Reaction Shaft Steel Reinforcement Cage Construction

Figure E.2. Test Shaft Steel Reinforcement Cage Construction

Figure E.3. Reaction and Test Shaft Installation

Figure E.4. Dywidag Bar Installation at Test Shaft

Figure E.5. Typical Test Shaft Testing Preparation

Figure E.6. Applying Load to the Test Shafts

Figure E.7. Measuring Lateral and Vertical Displacement
(Summer and Winter Conditions)

Figure E.8. Summer Condition Test Shaft Movements

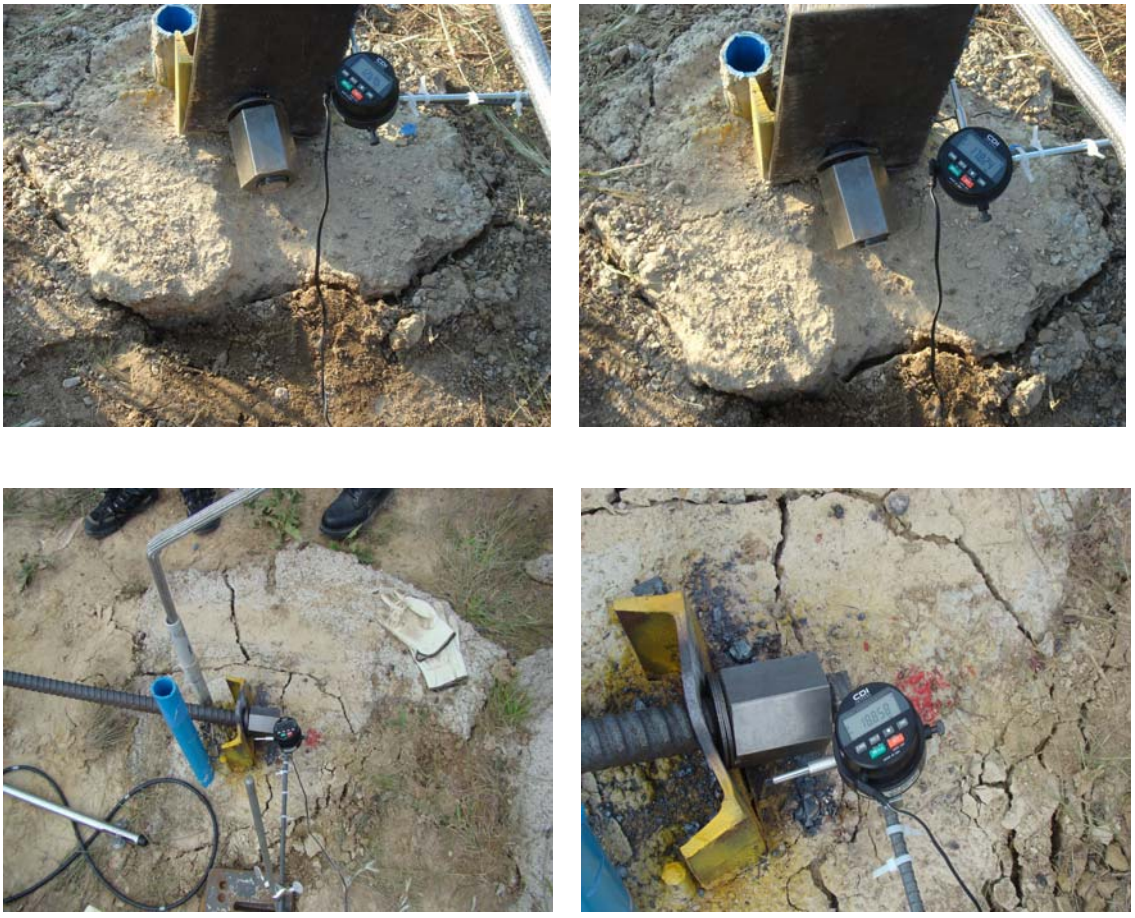

Figure E.9. Summer Condition Test Shaft Concrete Failures

Figure E.10. Winter Condition Test Shaft Movements

Figure E.11. Winter Condition Test Shaft Concrete Failures

Figure E.12. Additional Winter Condition Test Shaft Movements

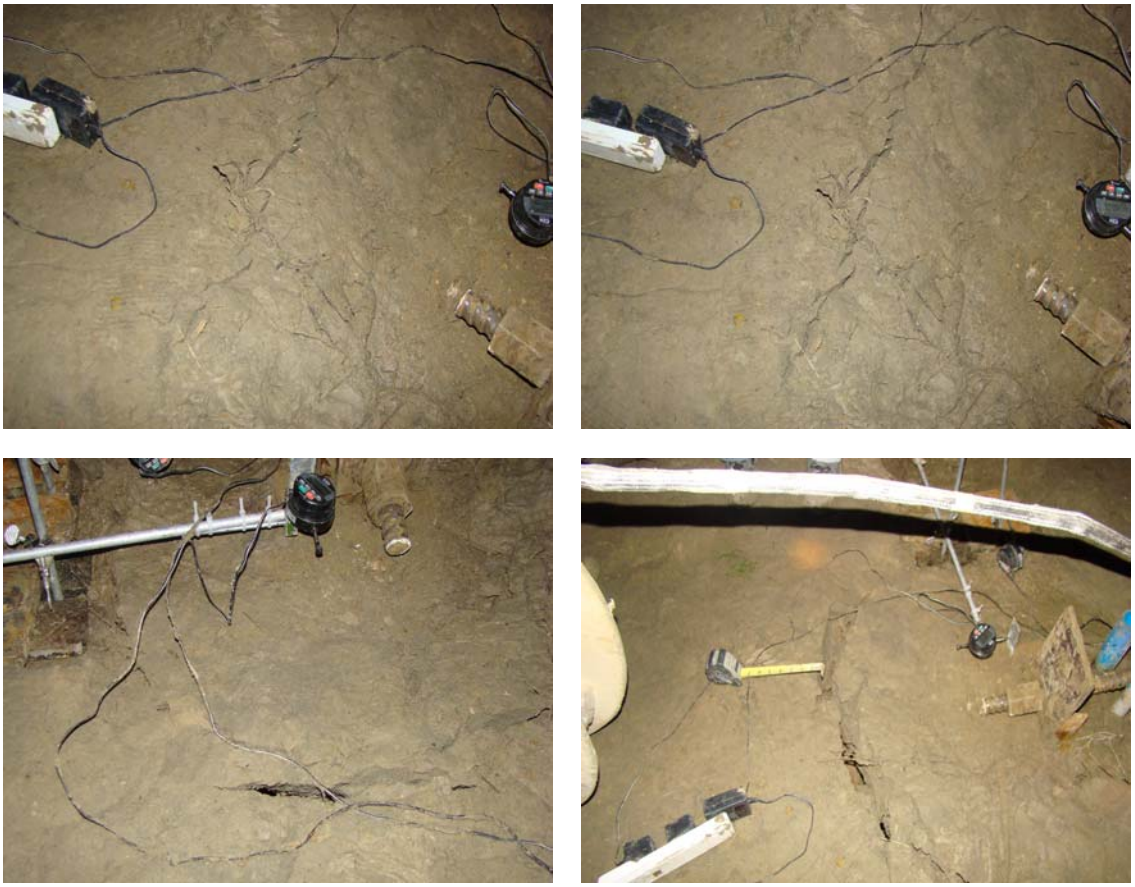

Figure E.13. Winter Condition Test Shaft Failures at Night

REFERENCES

1. Abendroth, R. E., Greimann, L. F., and Ebner, P. B. (1989). Abutment pile design for jointless bridges. *Journal of Structural Engineering,* ASCE, Volume 115(11), pp. 2914-2929.

2. Alberson, D. C. (2006). Update on guidelines for the selection of cable barrier systems. *NCHRP Project,* Volume 20-7(210).

3. Albin, R.B., Bullard D.L., Jr., and Menges, W.L. (2001). Washington State cable median barrier. *Transportation Research Record*, Volume 1743, pp. 71-79.

4. Al-Khafaf and Hanks, R. J. (1974). "Evaluation of the Filter Paper Method for Estimating Soil Water Potential." *Soil Science*, Volume 117, pp. 194–99.

5. Al–Saoudi, N.K.S. and Salim, H.M. (1998). "The behaviour of groups of reinforced concrete model piles in expansive soil". *Proceedings of the 2nd International Conference on Unsaturated Soils,* Beijing, Volume 1, August, pp. 321–326.

6. Anderson, Peter L., (2005). "Increased Use of MSE Abutments," International Bridge Conference, 2005.

7. Applied Soil Mechanics with ABAQUS Applications by Sam Helwany, 2007, John Wiley and Sons, Inc., Hoboken, New Jersey.

8. Ashour, M., Norris, G., and Pilling, P. (1998). Lateral Loading of a Pile in Layered Soil Using the Strain Wedge Method, *Journal of Geotechnical and Geoenvironmental Engineering*, ASCE, Volume 124, No. 4, pp. 303-315.

9. Ashour et al., (2002). Strain Wedge Model Capability of Analyzing Behavior of Laterally Loaded Isolated Piles, Drilled Shafts, and Pile Groups, *Journal of Bridge Engineering,* Volume 7, No. 4, July 2002, pp. 245-254.

10. ASTM Standard C31/31M-09. "Standard Practice for Making and Curing Concrete Test Specimens in the Field." *Annual Book of ASTM Standards,* 4(8), ASTM International, West Conshohocken, Pa.

11. ASTM Standard C39/39M-09. "Standard Test Method for Compressive Strength of Cylindrical Concrete Specimens." *Annual Book of ASTM Standards,* 4(8), ASTM International, West Conshohocken, Pa.

12. ASTM Standard C617-09a. "Standard Practice for Capping Cylindrical Concrete Specimens." *Annual Book of ASTM Standards,* 4(8), ASTM International, West Conshohocken, Pa.

13. ASTM Standard D698-07. “Standard Test Method for Laboratory Compaction Characteristics of Soil Using Standard Effort (12,400 ft-lbf/ft^3(600 kN/m^3)).” *Annual Book of ASTM Standards,* Soil and Rock, ASTM International, West Conshohocken, Pa.

14. ASTM Standard D2487-10. “Standard Classification of Soils for Engineering Purposes (Unified Soil Classification System).” *Annual Book of ASTM Standards,* Soil and Rock, ASTM International, West Conshohocken, Pa.

15. ASTM Standard D2850-03a. “Standard Test Method for Unconsolidated-Undrained Triaxial Compression Test on Cohesive Soils.” *Annual Book of ASTM Standards,* ASTM International, West Conshohocken, Pa.

16. ASTM Standard D3080-04. “Standard Test Method for Direct Shear Test of Soils Under Consolidated Drained Conditions.” *Annual Book of ASTM Standards,* ASTM International, West Conshohocken, Pa.

17. ASTM Standard D3966-07. “Standard Test Method for Piles under Lateral Loads”, *Annual Book of ASTM Standards,* Soil and Rock, ASTM International, West Conshohocken, Pa.

18. ASTM Standard D4318-10. “Standard Test Methods for Liquid Limit, Plastic Limit, and Plasticity Index of Soils.” *Annual Book of ASTM Standards,* Soil and Rock, ASTM International, West Conshohocken, Pa.

19. ASTM Standard D4546-08. “Standard Test Methods for One-Dimensional Swell or Settlement Potential of Cohesive Soils,” *Annual Book of ASTM Standards*, ASTM International, West Conshohocken, Pa.

20. ASTM Standard D5298-03. “Standard Test Method for Measurement of Soil Potential (Suction) Using Filter Paper,” *Annual Book of ASTM Standards,* ASTM International, West Conshohocken, Pa.

21. Aung, K. K., Rahardjo, H., Leong, E. C., and Toll, D. G. (2001). “Relationship between porosimetry measurement and soil-water characteristic curve for an unsaturated residual soil.” *Geotechnical and Geological Engineering*, Volume 19, pp. 401–416.

22. Bhushan, K., Haley, S.C., and Fong, P. T. (1979). Lateral Load Tests on Drilled Piles in Stiff Clays. *Journal of Geotechnical Engineering Division,* ASCE, Volume 105 (GT 8), pp. 969–985.

23. Brinch Hansen, J. (1961). The ultimate resistance of rigid piles against transversal forces. *Geoteknisk Institutute Bulletin,* Volume 12. Copenhagen, Denmark.

24. Broms, B.B. (1964a). Lateral resistance of piles in cohesive soils. *Journal of Soil Mechanics and Foundation Division,* Volume 90(SM2), pp. 27–63.

25. Broms, B.B. (1964b). Lateral resistance of piles in cohesionless soils. *Journal of Soil Mechanics and Foundation Division,* Volume 90(SM3), pp. 123–157.

26. Broms, B.B. (1965). Design of Laterally Loaded Piles. *Journal of Soil Mechanics and Foundation Division,* Volume 91(SM3), pp. 77–79.

27. Cameron, D.A. and Walsh, P.F. (1981). ”Timber piles for residential foundations in expansive soil”. *1st National Local Government Engineering Conference, Adelaide*, August, pp. 165–169.

28. Casagrande, A. (1932b). Discussion of “A New Theory of Frost Heaving” in A.C. Benkelman and F.R. Ohlmstead (Eds), *Proceedings of the Highway Research Board,* Volume 11, pp. 168–172.

29. Chapel, T. A. and Nelson, J.D. (1998). ”Field investigation of helical and concrete piles in expansive soil”. *Proceedings of the 2nd International Conference on Unsaturated Soils, Beijing, August, Technical Committee of the 2nd International Conference on Unsaturated Soils Editions*, Volume 1, pp. 206–211.

30. Chen, F. H (1988). *Foundations on Expansive Soils, 2nd Edition*. New York: Elsevier Science Publications.

31. Cooner, S. In-Service Evaluation of Cable Median Barrier Performance. https://tti.tamu.edu/documents/0-5609-P1.pdf, August, 2008, p.1-4.

32. Craig, R. R. (1999). *Mechanics of Materials 2nd edition*. New York, USA: John Wiley and Sons, Inc., New York, NY.

33. Davisson, M. T., and Robinson, K. E. (1965). Bending and buckling of partially embedded piles. *Proc, 6th Int. Conf. on Soil Mechanics and Foundation Engineering,* Volume 2, pp. 243–246.

34. Day, R.W. (2006). *Foundation Engineering Handbook*. New York, NY: McGraw-Hill.

35. Duffy, D. and Charania, E. (1984). ”Study of pile uplift characteristics in swelling clays using a newly developed test”. *Proceedings of the 5th International Expansive Soils Conference*, Adelaide, May, Volume 1, pp. 75–79.

36. Duncan, J.M., Evans, L. T., Jr., and Ooi, P. S. K. (1994). Lateral load analysis of single piles and drilled shafts. *Journal of Geotechnical Engineering,* ASCE, Volume 120(6), pp. 1018–1033.

37. Dunnavant, T.W. and O’Neill, M.W. (1985), “Performance, analysis and interpretation of a lateral load test of a 72-inch-diameter bored pile in overconsolidated clay”, *Report UHCE 85-4,* 57 pp.. Department of Civil Engineering, University of Houston, Texas.

38. Dunnavant, T. W. and O’Neill, M.W. (1989). Experiment p-y Model for Submerged, Stiff Clay. *Journal of Geotechnical Engineering,* ASCE, Volume 115(1), pp. 95–114.

39. Easterling,A. Personal Communication. TxDOT Fort Worth District, District Maintenance Office, 2010.

40. Federal Highway Administration Publication No. FHWA-HI-97-013, “Design and Construction of Driven Pile Foundations”, November 1998.

41. Federal Highway Administration Publication No. FHWA-IP-84-11, “Handbook on Design And Construction of Drilled Shafts Under Lateral Load”, 1984.

42. Federal Highway Administration Publication No. FHWA-SA-96-071, “Mechanically Stabilized Earth Walls and Reinforced Soil Slopes – Design and Construction Guidelines”. August 1997.

43. Fredlund, D.G. and Rahardjo (1993). *Soil Mechanics for Unsaturated Soils*, John Wiley and Sons, Inc., New York, NY.

44. Fredlund, D.G., Xing, A., and Huang, S. (1994). “Predicting the permeability function for unsaturated soils using the soil-water characteristic curve.” *Canadian Geotechnical Journal*, Volume 31, No. 4, August 1994, pp. 533–546.

45. Greimann, L. F. et al. (1987). *Pile design and tests for integral abutment bridges, Final Report.* Ames, Iowa: Iowa DOT Project HR-273, Iowa State University, Engineering Research Institute, Ames, IA, 88060.

46. Greis, J.E. and Muchard, M.K., Final Report of Lateral STAT*NAMIC* Load Testing DFW Connector – Site 1, Test Shaft A. *Applied Foundation Testing*, AFT Project No. 109054, pp. 2-5.

47. Heady, J. Personal Communication. TxDOT Dallas District, Kaufman County Area Office, 2009.

48. Hetenyi, (1946). *Beams on Elastic Foundations*. Ann Arbor: University of Michigan Press.

49. Hibbeler, R.C. (2008). *Mechanics of Materials 7th edition*. New Jersey, USA: Pearson Prentice Hall, Pearson Education.

50. Holtz, R.D. and Kovacs, W. D. (1981). *An Introduction to Geotechnical Engineering*. Eaglewood Cliffs, NJ: Prentice Hall.

51. Hussein E.A. (2001). Viscoplastic Finite Element Model for Expansive Soils. *EJGE Paper 2001-0122*.

52. IBC-05-10. The Reinforced Earth Company, North Reading, MA.

53. Johnson, L.D., and Stroman, W.R. (1976). Analysis of Behavior of Expansive Soil Foundations. *U.S. Army Engineer Waterways Experiment Station Technical Report S-76-8*.

54. Johnson, Rebecca, Parsons, Robert L., Dapp, Steven, Brown, Dan, “Soil Characterization and PY Curve Development for LOESS, Report No. K-TRAN: KU 05-3,” Kansas Department of Transportation, February 2007.

55. Justo, J, Saura, J., Rodriguez, J, Delgado, A., Jaramillo, A. (1984). ”A finite element method to design and calculate pile foundations in expansive collapsing soils”. *Proceedings 5th International Expansive Soils Conference, Adelaide*, Volume 1, pp. 119–123.

56. Jones, D. E. and Holtz, W. G. (1973). Expansive Soils - the Hidden Disaster. *Civil Engineering (ASCE),* Volume 43(8), p. 49.

57. Kaplar, C. W. (1970). Pheonomenon and Mechanism of Frost Heaving. *Highway Research Record,* Volume 304, pp. 1–13.

58. KDOT "KDOT Project: RE-0446-01 Grading Cross Section", March 2007.

59. Klaiber, F. W., White, D. J., Wipf, T. J., Phares, B. M., and Robbins, V. W. (2004). *Development of Abutment Design Standards for Local Bridge Designs.* Final Report for Iowa DOT TR-486: Volume 1 of 3, August 2004, pp. 13–23.

60. Lu, N. and Likos, W. J. (2004). *Unsaturated Soil Mechanics.* John Wiley & Sons, New York, NY. 2004.

61. Marinho, F. A. M. and Oliveira, O. M. (2006). "The filter paper method revisited." *Geotechnical Testing Journal,* Volume 29(3), pp. 1–9.

62. Matlock, H. and Ripperger, E. A. (1958). Measurement of soil pressure on a laterally loaded pile. *Proceedings, American Society for Testing and Materials,* Volume 58, pp. 1245–1259.

63. Matlock, H. and Reese, L. C. (1961). Foundation Analysis of Offshore Pile-Supported Structures. *Proceedings, Fifth International Conference, International Society of Soil Mechanics and Foundation Engineering,* Paris, France, Volume 2, pp. 91–97.

64. Matlock, H. (1970). Correlations for design of laterally loaded piles in soft clay. *Proceedings, 2nd Offshore Technical Conference,* Volume 1, pp. 577–594.

65. McClelland, B. and Focht, Jr, J.A.. (1958). Soil modulus for laterally loaded piles. *Journal of Soil Mechanics Foundation Division,* ASCE, Volume 123, pp. 1049–1086.

66. McClelland, M. (1996). History of Drilled Shaft Construction in Texas. *Paper presented before the 7^{5th} Annual Meeting of the Transportation Research Board*, Washington, D.C.

67. McVay, C. M., (2003). Calibrating Resistance Factors for Load and Resistance Factor Design for Statnamic Load Testing, *Final Report BC354-42.* Florida Department of Transportation.

68. Meyerhof, G. G. and Adams, J. I. (1968). The ultimate uplift capacity of foundations. *Canadian Geotechnical Journal,* Volume 5**,** pp. 225–244.

69. Meyerhof, G. G. (1973a). The uplift capacity of foundations under oblique loads. *Canadian Geotechnical Journal,* Volume 10, pp. 64–70.

70. Meyerhof, G. G. (1973b). Uplift resistance of inclined anchors and piles. *Proceeding, 8th International Conference on Soil Mechanics and Foundation Engineering,* Moscow, Volume 2.1, pp. 167–172.

71. Meyerhof, G. G. (1980). The bearing capacity of rigid piles and pile groups under inclined loads in clay. *Canadian Geotechnical Journal,* Volume 18, pp. 297–300.

72. Meyerhof, G. G. et al. (1983). Uplift Pile Capacity for Eccentric Inclined Load. Journal of Geotechnical Engineering, Volume 109, No. 3, March 1983, pp. 408-423.

73. Minnesota Department of Transportation, “Noise Analysis: Guidelines for the Evaluation of Noise Barrier Designs” Office of Environmental Services.

74. Mitchell, J. K. (1976). *Fundamental of Soil Behavior*. NY: Wiley.

75. Mohamedzein, Y.E.A., Mohamed, M.G. and Shareif, A.M. (1999). ”Finite element analysis of short piles in expansive soils”. *Computers and Geotechnics*, Volume 24, pp. 231–243.

76. Nelson, J.D. and Miller, J.D. (1992). *Expansive Soils: Problems and Practice in Foundation and Pavement Engineering*. New York: Wiley.

77. Nuhfer E.B., Proctor R.J., and Moser N. (1993). *The Citizen’s Guide to Geologic Hazards*. Arvada, CO: AIPG Press.

78. O’Neill, M. W. and Poormoayed, N. (1980). Methodology for Foundations on Expansive Clays. *Journal of the Geotechnical Engineering Division,* ASCE, Volume 106, No. 12, December, 1980, pp. 1345–1367.

79. O’Neill, M. W. and Reese, L. C. (1999). Drilled shaft: Construction procedure and design methods. *Publication No. FHWA-IF-99-025,* Volume 2, pp. 1–21.

80. Penner, E. and Burn, K.N. (1970). Adfreezing and Frost Heaving of Foundations. *Canadian Building Digest,* National Research Council, Ottawa, Ontario: Institute for Research in Construction. Volume CBD-128, p. 8.

81. Petry, T. M. and Armstrong, J. C. (1989). Stabilization of Expansive Soils. *Transportation Research Record*, Volume 1219, pp. 103–112.

82. Pierson, M., Parsons, R. L., Han, J., Brown, D., Thompson, W. R. (2009). Capacity of Laterally Loaded Shafts Constructed Behind the Face of a Mechanically Stabilized Earth Block Wall. *Report No. K-TRAN: KU-07-6*. A Cooperative Transportation Research Program Between Kansas Department of Transportation, Kansas State University and the University of Kansas, March 2009.

83. Punthutaecha, K., Puppala, A. J., Vanapalli, S. K., and Inyang, H. (2006). “Volume change behaviors of expansive soils stabilized with recycled ashes and fibers.” *Journal of Materials in Civil Engineering*, Volume 18(2), pp. 295–306.

84. Puppala, A.J., Katha, B., and Hoyos, L.R. (2004). Volumetric Shrinkage Strain Measurements in Expansive Soils Using Digital Imaging Technology. *ASTM Geotechnical Testing Journal,* Volume 27, No. 6, 2004, pp. 547–556.

85. Reese, L. C. and Matlock, H. (1956). Nondimensional solutions for laterally loaded piles with soil modulus assumed proportional to depth. *Proceedings, 8th Texas Conference on Soil Mechanics and Foundation Engineering*. The University of Texas, Austin, Texas: Bureau of Engineering Research.

86. Reese, L. C , Cox, W. R., and Koop, R. D. (1975). Field testing and analysis of laterally loaded piles in stiff clay. *Proceedings, 7th Offshore Technical Conference,* Volume 2, pp. 473–483.

87. Reese, L. and Welch, R. (1975). Lateral Loading of Deep Foundations in Stiff Clay. *Journal of the Geotechnical Engineering Division,* ASCE, Volume 101, No. 7, July, 1975, pp. 633–649.

88. Reese, L. C. and Allen, J. D. (1977). Structural analysis and design for lateral loading. *Drilled Shaft Design and Construction Guidelines Manual*, Volume 2, U.S. Department of Transportation, FHWA, Office of Research and Development.

89. Robinson, B., Suarez, V., Robalino, P., Kowalsky, M., and Gabr, M. (2006). Pile Bent Design Criteria. *NCDOT Research Project 2005-19*. In Final Revision.

90. Rollins, M., K., Weaver, T. J., and Peterson, K. T. (1997). Statnamic lateral load testing of a full-scale fixed-head pile group, *Report*. UDOT, FHWA.

91. Ross, H.E. Jr., D.L. Sicking, R.A. Zimmer, and J. Michie. Recommended Procedures for the Safety Performance Evaluation of Highway Features. National Cooperative Highway Research Program Report 350. Transportation Research Board. Washington D.C., 1993.

92. Simms,T. Personal Communication. TxDOT Maintenance Division, Austin, TX, 2010.

93. Sinha, J. and Poulos, H. G. (1999). ”Piled raft systems and free standing pile groups in expansive soils”. *Proceedings, 8th Australia New Zealand Conference on Geomechanics*, Hobart, February, Volume 1, pp. 207–212.

94. Soil Moisture Equipment Corp., Soil Moisture Equipment Corp., 2003. TRASE Operating Instruction.

95. Sridharan, A., Sreepada R. A., Sivapullaiah, P. V. (1986). “Swelling Clays.” *Geotechnical Testing Journal*, Volume 9, No. 1, March 1986, pp. 24–33.

96. Tensar Earth Technologies. “Demonstration of Pile Driving through the HDPE Geogrid Reinforced Soil Fill of Full-Height Precast Concrete Panel Faced, Mechanically Stabilized Earth Wall,” 2001 Report, Colorado E-470 Project.

97. Tensar Earth Technologies, Inc. “Construction Drawings: I-435 and Leavenworth Rd. Interchange”, April 2007.

98. Terzaghi, K. (1955). Evaluation of coefficient of subgrade Reaction. *Geotechnique*, Volume 5, pp. 297–326.

99. Tex-107-E, (2002). “Determination the Bar Linear Shrinkage of Soils.” *Manual of Material Testing Procedure,* Texas Department of Transportation (TxDOT), Austin, Texas.

100. Texas Department of Transportation. *Cable Barrier System*. Special Specification 5367, 2004 Specifications, July 2006.

101. Ubanyionwu, G. I., (1985). Uplift Capacity of Rigid Piles in Clay under Inclined Pull, *Master Thesis*. Texas, USA: University of Texas at El Paso.

102. Unknown Author. “5 Finds Freeway Barrier Hazards”. KPHO CBS 5. Retrieved on October 24, 2008. http://www.kpho.com/news/10912699/detail.html

103. Welch, R.C. and Reese, L. C. (1972). Laterally Loaded Behavior of Drilled Shafts. *Research Report,* Volume (89-10). The University of Texas at Austin: Center for Highway Research.

104. Westman, E. C. (1993). *“Evaluation of pile uplift in expansive soils”*. *Master Thesis*, Department of Civil Engineering, University of Colorado at Denver.

105. Wikipedia®, Cable barrier, http://en.wikipedia.org/wiki/Cable_barrier, 2010.

106. Washington Department of Transportation. http://www.wsdot.wa.gov/publications/cablemedianbarrier/10_AppdxB_Reduced.pdf, 2007.

107. Wiseman, G., Komornik, A., and Greenstein, J. (1985). Experience with Roads and Buildings on Expansive Clays. *Transportation Research Record,* Volume 103, pp. 60–67.

108. Yong, R. N. and Warkentin, B. P. (1975). *Soil Properties and Behavior*. New York, NY: Elsevier.

BIOGRAPHICAL INFORMATION

Richard S. Williammee, Jr. graduated from Manheim Central High School, Pennsylvania in 1975. Shortly after graduation, he enlisted in the U.S. Air Force where he spent the next 4 years working as a Civil Engineering Technician performing drafting, surveying, and material testing duties. During this period, he started his college studies toward a degree in Civil Engineering. Upon separation from the Air Force, he enrolled at New Mexico State University full time where he completed his Bachelor of Science in Civil Engineering in 1983. He was hired by the Texas Department of Transportation (TxDOT) where he worked in the design, construction, and materials laboratory for the past 26 years. In 1988, his received his Texas Professional Engineer's license. From 1986 to 1989, he worked on his Master of Engineering Degree in Civil Engineering at the University of Texas at Arlington (UTA). The addition of their second daughter to the family reprioritized his commitments and stoppage of his degree pursuit until 2008 when he once again enrolled in the Master's Program at UTA. His 26 years of civil engineering experience allowed him to complete his studies and receive his Master of Science in Civil Engineering with an emphasis in Geotechnical Engineering in 2010.

From 2002 to 2010, he spent time on numerous pavement, recycled materials, and geotechnical related research and implementation projects for TxDOT as an advisor and/or director. He was awarded Outstanding Research Director of the Year in 2005. He has already accepted invitations to work on four additional research projects in 2010 – 2012 while developing new project statements for consideration of future research work with many different Texas universities.